Institute of Solid State Physics
University of Latvia

ANNUAL REPORT 2019

Riga 2020

Annual Report 2019, Institute of Solid State Physics, University of Latvia.
Editors: Dr.habil.phys. A.Šternbergs and Dr. phys A. Kuzmin
Set up at the Institute of Solid State Physics, University of Latvia, Kengaraga Str. 8, LV-1063 Riga, Latvia.

Riga, Institute of Solid State Physics, University of Latvia, 2020, 80 pages

Director: **Dr. phys. M.Rutkis**
Institute of Solid State Physics, University of Latvia
Kengaraga Str. 8, LV-1063 Riga, Latvia
***Tel.:** +371 67187816*
***Fax:** +371 67132778*
ISSP@cfi.lu.lv
http://www.cfi.lu.lv

Contents

Introduction

Institute of Solid State Physics (ISSP UL) of the University of Latvia is the main materials science institute in Latvia. It was founded in 1978 by amalgamation of the two largest physics research laboratories in University of Latvia: Laboratory of Semiconductor Research and Laboratory of Ferro- and Piezoelectric Research. Since 1986, the ISSP UL has the status of legally and fiscally independent organization of the University.

In 1990ies, after gaining independence and before joining EU, the funding of science in Latvia decreased/went in a free plunge, as the former sources disappeared and new funding channels were not yet established. Under these conditions, many research institutions collapsed, and only few strongest survived, ISSP UL among them. Four laboratories from the Institute of Physics of the Latvian Academy of Sciences joined ISSP UL in 1995. Twenty scientists of the former Nuclear Research Centre found shelter the ISSP UL in 1999 and established Laboratory of Radiation Physics. In 2004 scientists from the Institute of Physical Energetics joined ISSP UL and established Laboratory of Organic Materials.

To encourage more students to select material physics and chemistry, in mid-90ies ISSP UL stepped-up its teaching activities. A number of researchers were elected as professors of the University of Latvia. Post-graduate and graduate curricula were prepared. Presently they are offered in solid state physics, material physics, chemical physics, physics of condensed matter, semiconductor physics, and experimental methods and instruments.

In December 2000, the ISSP UL was awarded the **Centre of Excellence of the European Commission** (Centre of Excellence for Advanced Material Research and Technologies – **CAMART**). Together with the associated financial support of 0.7 M EUR for 3 years duration, this award boosted our research activities and allowed to extend the network of our research partners and scientists, who came to work to ISSP UL from the leading European research centres. In 2001, the Association EURATOM-University of Latvia was established and the ISSP UL became the coordinator of the Latvian Research Unit. The Institute is involved in theoretical modelling as well as in experimental characterization of fusion reactor construction and functional materials and has an expertise in material erosion and re-deposition diagnostics in Plasma-Facing Components using Laser-Induced Breakdown Spectroscopy. In 2014 EUROfusion

consortium agreement was signed, regulating European cooperation in thermonuclear synthesis research. A collaboration of 34 countries aims to solve the complex problems standing in the way to a practical electricity-generating fusion power plant.

In 2015, ISSP UL was awarded Horizon 2020 Teaming project: "**The Excellence Centre of Advanced Material Research and Technology Transfer – CAMART^2**". 169 proposals were submitted; 31 were selected to develop their Business Plans. The project scored 14.5 from 15 points; it was the only project from Latvia and Baltic countries. It was submitted in cooperation with Swedish partners from the Royal Institute of Technology (KTH) and Research Institute of Sweden (RISE). During 12 months of the Phase 1 a Business Plan for the future Centre of Excellence CAMART^2 was elaborated, demonstrating the long - term science and innovation development strategy. Its vision is to upgrade and further consolidate the ISSP UL as a key centre of excellence for education, science, innovation and technology transfer in the Baltic countries.

The Business Plan was highly estimated in the second phase of Horizon 2020 Teaming project, dedicated to the development of Centre of Excellence during 2017-2023.

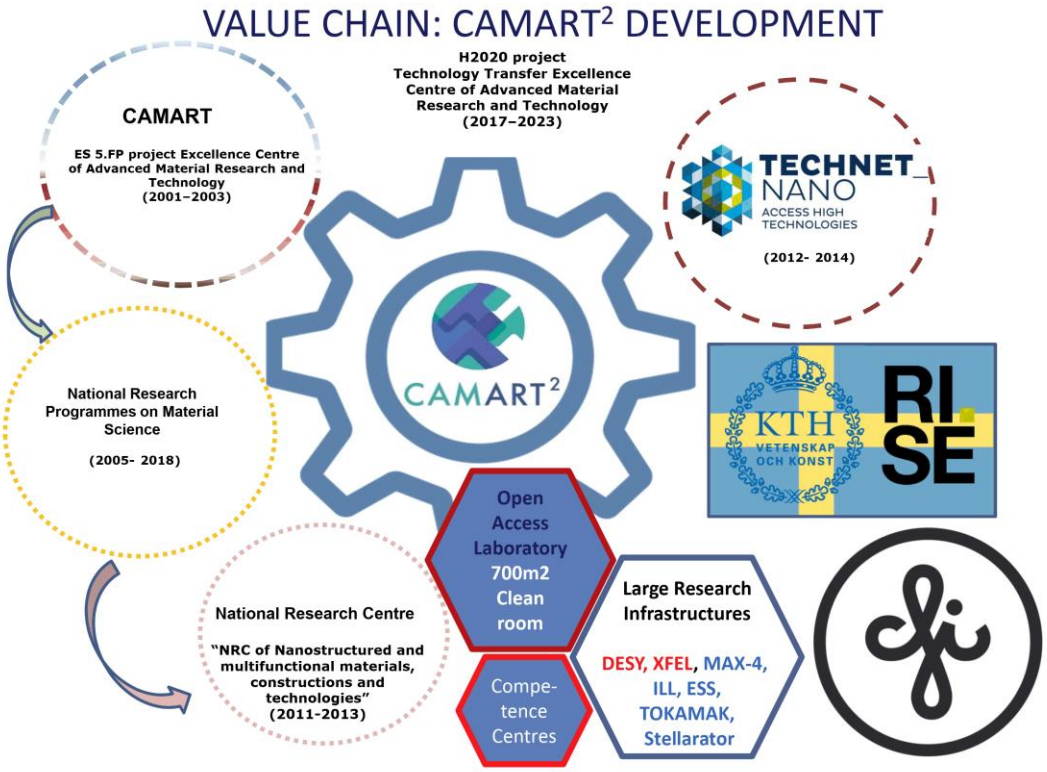

Figure 1: **Value chain: CAMART² development.**

ISSP UL has developed strong research and innovation ecosystem.

680 m^2 of ISO class 7-8 **cleanroom facility** is established, including equipment for:

- basic technological methods: thin film fabrication and parameter control, chemical synthesis, nano-structuring;
- analytical methods: XRD analysis, electron microscopy (SEM, TEM), X-ray photoelectron spectroscopy (XPS), morphology analysis, optical and EPR spectroscopy, spectral ellipsometry;
- prototyping of photonic and electronic devices. A new dedicated prototyping cleanroom laboratory was newly established.

In prototyping ISSP UL specializes in using methods of optical and e-beam lithography, cleaning and surface preparation, dry etching, bonding and packaging, thermal processes and

wet chemistry.

Presently, ISSP UL is further focusing on education. An overhaul of the University's master's programme in physics is in progress, to make it relevant to the projected industrial needs. Similar upgrades are also planned for the University's doctoral programme.

The ISSP UL's goal is to improve and enhance collaboration with industry in Latvia and abroad. To achieve this, it has set up a platform intended to serve as a single point of contact for scientists and companies. Named "Materize", the platform provides access to the ISSP UL's expertise and resources while also facilitating communication with companies for the purpose of realising projects based on industry-specific standards. Current case studies being undertaken include a cleanroom-based prototyping facility, organic light-emitting diodes, optical lithography, vacuum deposition of thin films and composite nanomaterials synthesis.

Every year "Materize" hosts events for idea creation, the Deep Science Hackathons. In year 2019 there were several Hackathons, including one for students. The Hackathon's goal is to identify high-tech ideas and find teams for their implementation, with a view to creating new products and companies that would contribute to the Baltic region's high-tech industry.

The Research Programme of ISSP UL puts emphasis on four Priority Directions:

I. Theoretical and experimental studies of materials structure and properties;
II. Nanotechnology, thin films, nanocomposites and ceramics;
III. Functional materials for photonics and electronics;
IV. Materials for energy harvesting and storage.

These Priority research Directions have been strategically established to increase international visibility of Institutes scientific capacity and will be further elaborated and implemented within interdisciplinary cross-laboratory collaboration. Research will be structured towards the application-driven Research & Innovation (R&I) domains where discoveries can make the change thus initiating and establishing the value chain. Realization of Priority Research Directions will be based on implementation of a number of measures and activities within Research & Innovation domains.

The Domains system is the basis of the new, advanced project applications development

concept, included in the ISSP UL Research Program. It is novel, well developed and step-by-step system for ensuring flow of promising project applications.

In year 2019 the Domain concept continued to show positive results, granting 7 out of 24 submitted projects in the third Fundamental and Applied Research Projects (FARP) contest of Latvian Science Council, ensuring 21% success rate instead of 13% success ratio, the average in this contest.

The structure of ISSP UL was reorganized and at the end of 2019 is as shown in Figure 2. The new structure promotes research and innovation by creating service-oriented environment, fostering openness and product-oriented research.

Figure 2:

Organizational structure of ISSP UL in 2019

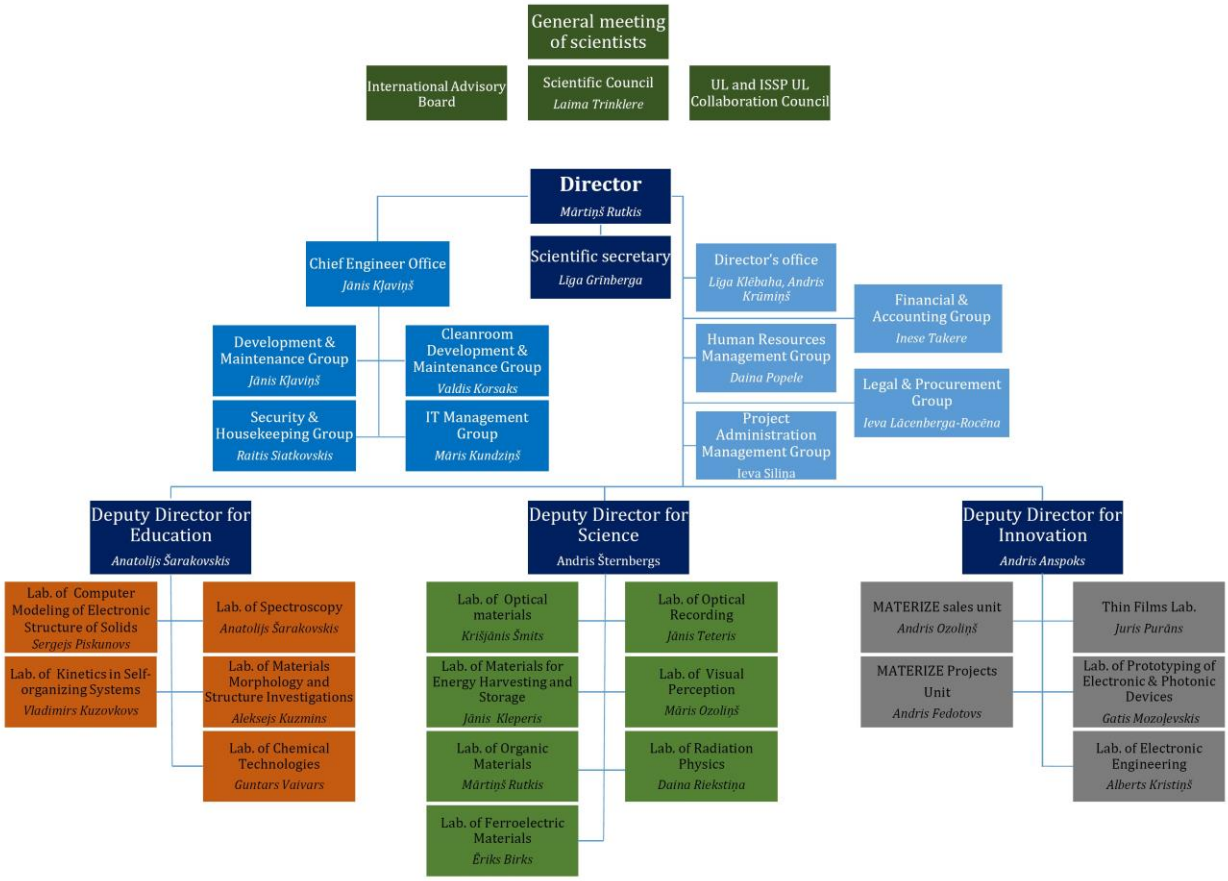

The highest decision-making body of ISSP UL is the **Scientific Council,** consisting of 15 members elected by the employees of the Institute (Table 1). Presently, Dr.phys. L.Trinklere is the chairperson of the ISSP UL Scientific Council. The Council appoints director and his/her deputies.

Table 1:

The Scientific Council of the Institute

1. Laima Trinklere, Dr.phys., Chair of the Scientific Council
2. Anatolijs Sarakovskis, Dr.phys., Vice-Chair of the Scientific Council and Deputy Director
3. Andris Anspoks, Dr.phys., Deputy Director
4. Guntars Kitenbergs, Dr.phys., University of Latvia
5. Gunars Bajars, Dr.chem.
6. Dmitrijs Bocarovs, Dr.phys.
7. Liga Grinberga, Dr.phys., Scientific Secretary
8. Janis Kleperis, Dr.phys.
9. Maris Knite, Dr.phys., Riga Technical University
10. Donats Millers, Dr.habil.phys.
11. Martins Rutkis, Dr.phys., Director
12. Andrejs Silins, Dr.habil.phys.
13. Andris Sternbergs, Dr.habil.phys., Deputy director
14. Anatolijs Truhins, Dr.habil.phys.
15. Jurgis Grube, Dr.phys.

To ensure an optimal alignment with global tendencies in material science, the ISSP UL performs consultations with the International Advisory Board (see Table 2) when making strategic decisions. Additionally, the International Advisory Board issues recommendations for commercialization of scientific results and for improving the management.

Table 2:

The International Advisory Board

1. Prof. Juras Banys, Vilnius University, Lithuania
2. Prof. Antonio Bianconi, Rome International Center for Materials Science Superstripes, Italy
3. Prof. Anette Bussmann-Holder, Max-Planck-Institute for Solid State Research, Germany
4. Prof. Ming-Chi Chou, Department of Materials and Optoelectronic Science, National Sun Yat-sen University, Taiwan
5. Prof. Niels E.Christensen, Aarhus University, Denmark
6. Prof. Robert Evarestov, St.Petersburg University, Russia
7. Prof. Claes-Goran Granqvist, Uppsala University, Sweden
8. Prof. Dag Høvik, The Research Council of Norway, Norway
9. Prof. Marco Kirm, University of Tartu, Estonia
10. Dr. Jiri Kulda, Institut Laue-Langevin, France
11. Prof. Toshio Ogawa, Shizuoka Institute of Science and Technology, Japan
12. Prof. Pauls Stradins, Colorado School of Mines, USA
13. Prof. Stefan Schweizer, South Westphalia University of Applied Sciences, Germany
14. Prof. Vladimir Shur, Institute of Natural Science, Ural Federal University, Russia
15. Prof. Andrejs Silins, Latvian Academy of Sciences, Latvia
16. Prof. Sergei Tuituinnikov, Joint Institute for Nuclear Research, Russia
17. Prof. Juris Upatnieks, Applied Optics, USA

The interdisciplinary research at the ISSP UL is performed by its highly qualified staff. At the end of 2019 there were 245 employees working at the Institute (226 employees at the end of 2018). ISSP UL Research personnel dynamics is shown in Figure 3. This Annual Report summarizes the research activities of the ISSP UL in 2019. The Table 3 below presents the key performance indicators of ISSP UL. The analysis of Key performance indicators (KPIs) is reported in the Action Plan for 2019.

Figure 3:

ISSP UL research staff dynamics 2009-2019

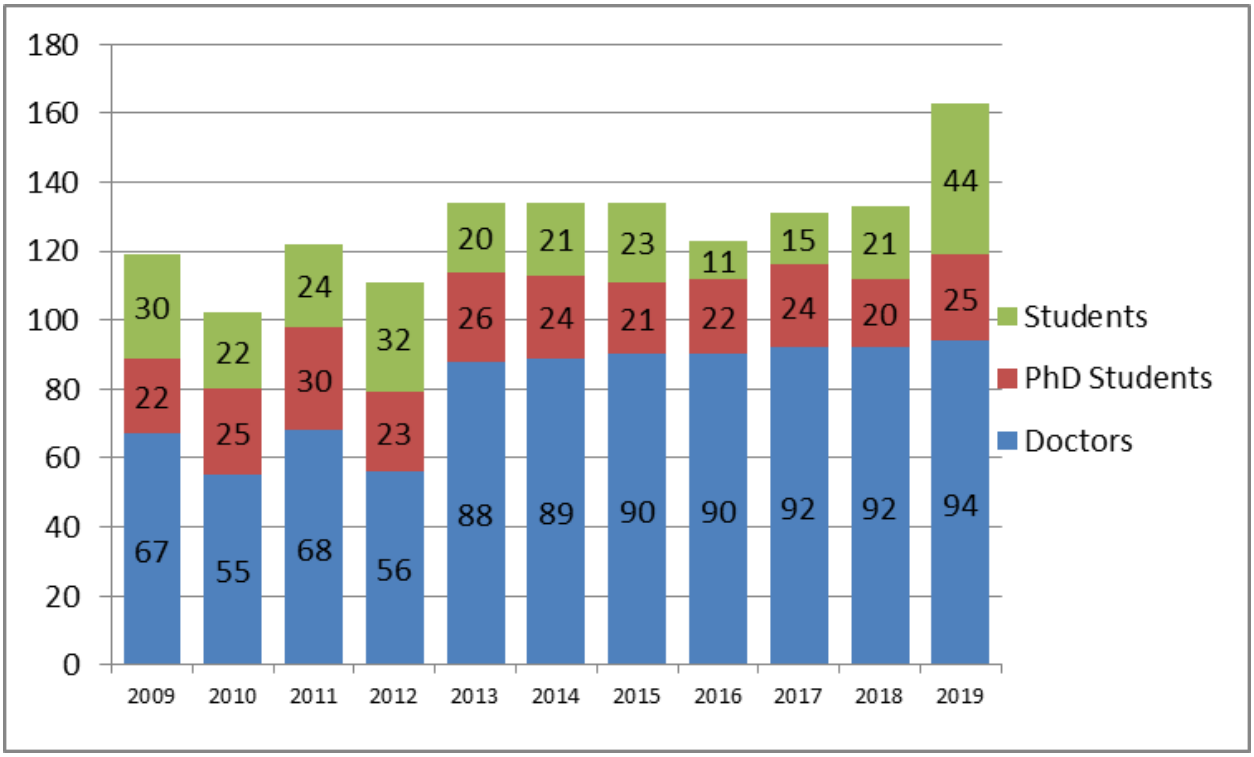

Table 3:

Key performance indicators

Key performance indicators for Research	3 years avrg.(2013-2015)	2016	2017	2018	2019	Goal for 2026
Number of scientific publications according to "Scopus"	119	140	100	129	129	400
Fraction of scientific publications in Int. Collaboration (%)	51	74	61	65.7	64.3	65
Number of citations/year according to "Scopus"	2043	2709	2253	2455	2606	5000
Average SNIP per publications	0.790	0.748	0.896	0.875	0.908	1.250
Number of scientific and technical personnel (FTE)	105	113	117	126	122	180
Publications/FTE	1.11	0.85	0.79	1.02	1.06	2.22
Gender balance of scientific and technical personnel (% female)	26	24.5	22.2	27.2	31	37

Scientific Highlights

I. Theoretical and experimental studies of materials structure and properties.

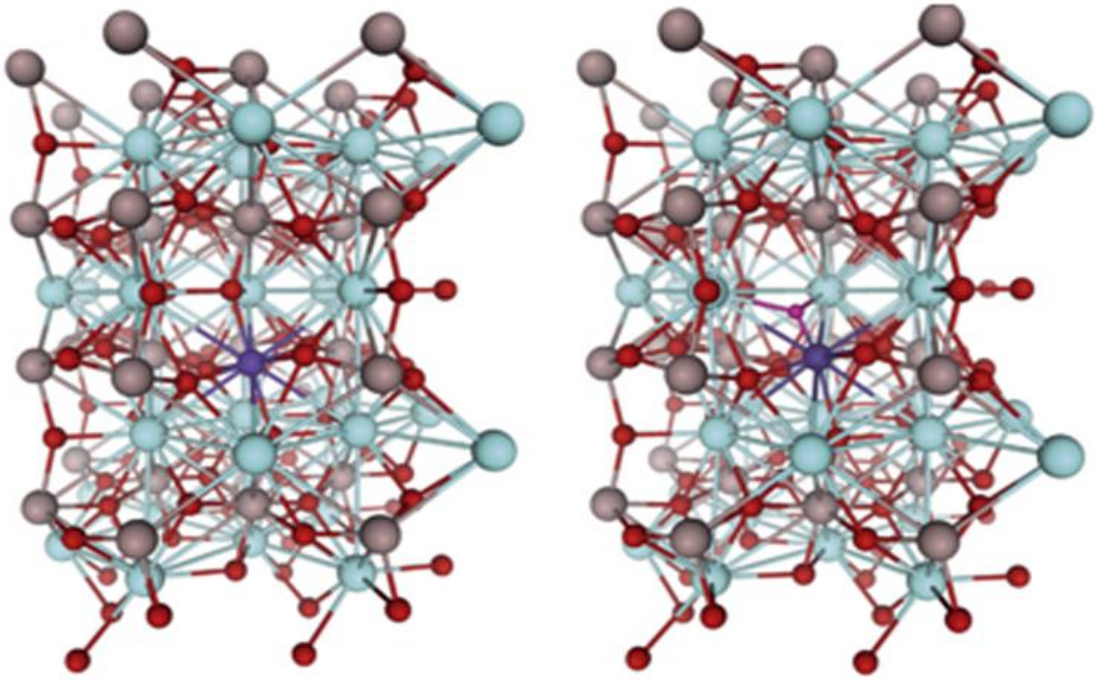

Theoretical calculations of new materials for energy production and storage

Roberts Eglitis[a], Juris Purans[a], Janis Kleperis[a], Anatolijs Popov[a], Ran Jia[b]

[a] *Institute of Solid State Physics, University of Latvia, Riga, Latvia*
[b] *Laboratory of Theoretical and Computational Chemistry, Institute of Theoretical Chemistry, Jilin University Changchun, People's Republic of China*

One of the winners of the 2019 Nobel Prize in Chemistry, John B. Goodenough (USA) discovered in 1980s materials for 4V voltage Li (lithium) ion batteries. The fact that 5V batteries are also possible was first discovered by team in the theoretical calculations of the cathode material $Li_2CoMn_3O_8$. Theoretical calculations have made it possible to explain how graphene increases the photovoltaic efficiency of organic materials in solar cells. In the series of calculations on the neutral (001) and polar (011) surfaces of the eight technologically most important ABO_3 perovskites, a theory is developed which explains the systematic tendencies in the behaviour of ABO_3 perovskites surfaces. By calculating from the first principles, the authors investigated the effect of boron (B) and nitrogen (N) impurities on 4,12,2-graphene, its atomic structure, mechanical and electrical properties, and discovered the piezoelectric effect due to B/N impurity atoms inducing a deformation of perfect graphene lattice.

Published in

1. R. Eglitis, *Ab initio* calculations of $Li_2(Co,Mn)O_8$ solid solutions for rechargeable batteries, International Journal of Modern Physics B 33, 1950151 (2019). (IF = 0.863, SNIP=0.413)
2. J.Y. Xi, R. Jia, W. Li, J. Wang, F.Q. Bai, R.I. Eglitis, H.X. Zhang, How does graphene enhance the photoelectric conversion efficiency in dye sensitized solar cells? An insight from a theoretical perspective, Journal of Materials Chemistry A 7, 2730-2740 (2019). (IF = 10.733, SNIP=1.575)
3. R. I. Eglitis and A.I. Popov, Systematic trends in (001) surface *ab initio* calculations of ABO_3 perovskites, Journal of Saudi Chemical Society 22, 459-468 (2018). (IF=2.759, SNIP=1.321)
4. R.I. Eglitis, J. Kleperis, J. Purans, A.I. Popov and R. Jia, *Ab initio* calculations of $CaZrO_3$ (011) surfaces: systematic trends in polar (011) surface calculations of ABO_3 perovskites, Journal of Materials Science 55, 203-217 (2020). (IF=3.442, SNIP=1.065)
5. R.I. Eglitis and A.I. Popov, *Ab initio* calculations for the polar (001) surfaces of $YAlO_3$, Nuclear Instruments and Methods B 434, 1-5 (2018). (IF= 1.210, SNIP=0.777)
6. R.I. Eglitis and A.I. Popov, Comparative *Ab initio* calculations for ABO_3 perovskite (001), (011) and (111) as well as $YAlO_3$ (001) surfaces and *F* centers, Journal of Nano- and Electronic Physics 11, 01001 (2019). (IF= 0.574, SNIP=0.461)
7. R. I. Eglitis, *Ab initio* calculations of $CaZrO_3$, $BaZrO_3$, $PbTiO_3$ and $SrTiO_3$ (001), (011) and (111) surfaces as well as their (001) interfaces, Integrated Ferroelectrics 196, 7-15 (2019). (IF= 0.486, SNIP=0.379)
8. R. Eglitis, J. Purans, A.I. Popov and Ran Jia, Systematic trends in $YAlO_3$, $SrTiO_3$, $BaTiO_3$ and $BaZrO_3$ (001) and (111) surface *ab initio* calculations, International Journal of Modern Physics B 2019, accepted (IF=0.863, SNIP=0.413)
9. D.-c. Yang, Z.-W. Tian, Y.-K. Chen, R.I. Eglitis, H.-X. Zhang, R. Jia, Giant piezoelectricity in B/N doped 4,12,2 – graphyne, Applied Surface Science 499, 143800 (2020). (IF= 5.155, SNIP=1.326)
10. J. Wang, M.Y. Wang, G. Yin, R. Jia, J. Wang, R.I. Eglitis, H.X. Zhang, Nickel-catalyzed carboxylation of aryl zinc reagent with CO_2: A theoretical and experimental study, Journal of CO_2 Utilization 29, 262-270 (2019). (IF= 5.503, SNIP=1.276)

This work was recognized by the Latvian Academy of Sciences as one of the ten most significant achievements in Latvian science of the year 2019.

Local structural investigation of hafnia-zirconia polymorphs in powders and thin films by X-ray absorption spectroscopy

T. Schenk[a], A. Anspoks[b], I. Jonane[b], R. Ignatans[c], B.S. Johnson[d], J.L. Jones[d], M. Tallarida[e], C. Marini[e], L. Simonelli[e], P. Hönicke[f], C. Richter[a], T. Mikolajick[a,g], U. Schroeder[a]

[a] *NaMLab gGmbH/TU Dresden, Noethnitzer Str. 64, D-01187 Dresden, Germany*
[b] *Institute of Solid State Physics, University of Latvia, Kengaraga Street 8, 1063, Riga, Latvia*
[c] *Institute of Materials, École Polytechnique Fédérale de Lausanne, CH-1015, Lausanne, Switzerland*
[d] *Department of Materials Science and Engineering, NC State University, Raleigh, NC, 27695-7907, USA*
[e] *ALBA Synchrotron, Carrer de la llum 2-20, 08290, Cerdanyola del Vallès, Barcelona, Spain*
[f] *Physikalisch-Technische Bundesanstalt (PTB), Abbestr. 2-12, 10587, Berlin, Germany*
[g] *Institute of Semiconductors and Microsystems, TU Dresden, D-01062, Dresden, Germany*

The polymorphism of hafnia and zirconia has been intensively studied, first as ceramics in the frame of refractories and solid electrolytes (oxygen conduction), transformation toughening ("ceramic steel") and later, in the quest for so-called "high-k dielectrics" (dielectrics with higher relative permittivity than 3.9) to replace SiO_2 in both transistors and capacitors of semiconductor industry.

In the present study, we employed extended X-ray absorption fine structure (EXAFS) method to probe the application relevant capacitor stacks of a dielectric film sandwiched between two electrodes as it is used in ferroelectric memories.

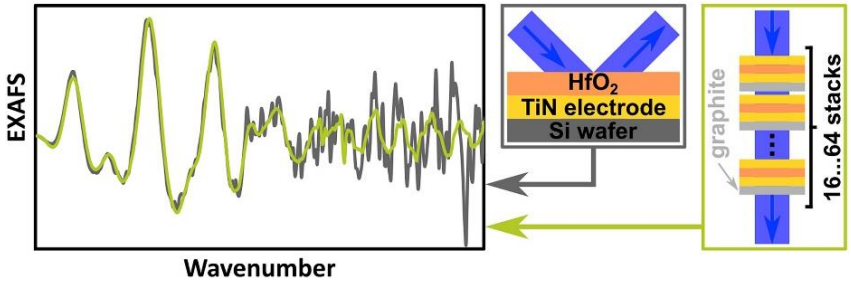

The Hf L_3-edge EXAFS spectra for a single HfO_2 thin film on silicon substrate in fluorescence mode (black) and for multiple stacks of a HfO_2 film on carbon substrate in transmission mode (green).

As a first step toward the analysis of thin films, we started with the analysis of bulk references. After that, we successfully demonstrated an approach that allowed us to extract high-quality spectra also for 20 nm thin films. Our analysis extends to the second coordination shell and includes effects created by chemical substitution of Hf with Zr to unambiguously discriminate the different polymorphs. The trends derived from X-ray absorption spectroscopy agree well with X-ray diffraction measurements. We clearly identified a gradual transformation from monoclinic to tetragonal phase as the Zr content of the films increases. We separated structural effects from effects created by chemical disorder when the ratio of Hf:Zr is varied and found differences for the incorporation of the substitute atoms between powders and thin films, which we attribute to the different fabrication routes.

This work opens the door for further in-depth structural studies to shine light into the chemistry and physics of these novel ferroelectric thin films that show high application relevance.

Published in:
T. Schenk, A. Anspoks, I. Jonane, R. Ignatans, B.S. Johnson, J.L. Jones, M. Tallarida, C. Marini, L. Simonelli, P. Hönicke, C. Richter, T. Mikolajick, U. Schroeder, Acta Mater. 180 (2019) 158-169. DOI: 10.1016/j.actamat.2017.02.074 (IF=7.293, SNIP=2.842)

Nickel-catalyzed carboxylation of aryl zinc reagent with CO_2: A theoretical and experimental study

Jing Wang[a], M.Y. Wang[a], G. Yin[b], Ran Jia[a], Jian Wang[a], F.Q. Bai[a], Roberts I. Eglitis[c], H.X. Zhang[a]

[a]*Laboratory of Theoretical and Computational Chemistry, Institute of Theoretical Chemistry, Jilin University, 130023 Changchun, PR China*
[b]*The Institute of Advanced studies, Wuhan University, PR China*
[c]*Institute of Solid State Physics, University of Latvia, 8 Kengaraga Str., Riga LV1063, Latvia*

Two Ni-complexes were tested for the Ni-catalyzed cross-coupling of aryl zinc reagent with CO_2 to form aryl carboxylic acid. Theoretical DFT study was performed in order to understand the detailed reaction mechanism.

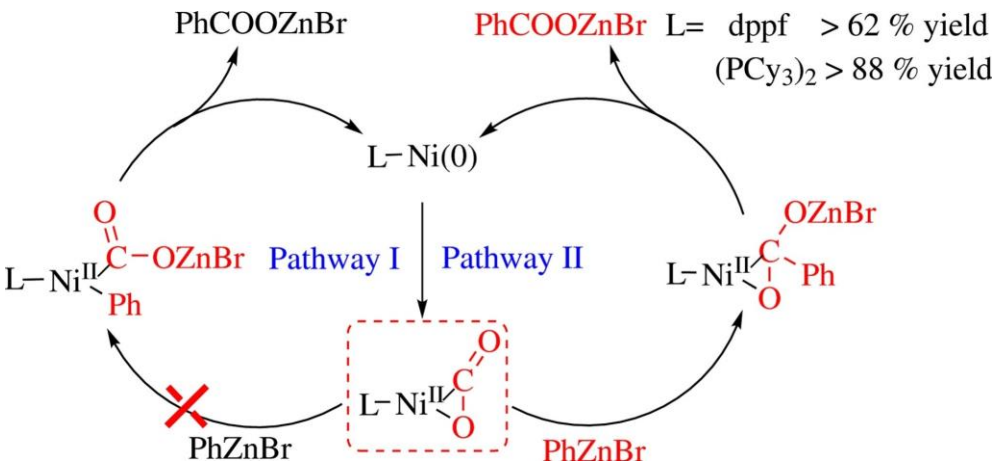

Catalytic cycle considering various mechanistic possibilities.
The Pathway I is named as “stepwise” mechanism,
and the Pathway II is the so-called “concerted” mechanism in this study.

The reasonable reaction pathway was deduced. However, our experiment provided unexpectedly low yield by using (dppf)Ni complex as the catalyst. Further theoretical study ascribed the shortage of the reaction to yield to the weak CO_2 capture ability of the (dppf)Ni complex.

Published in:
Jing Wang, M.Y. Wang, G. Yin, Ran Jia, Jian Wang, Roberts I. Eglitis, H.X. Zhang, Journal of CO_2 Utilization 29 (2019) 262-270. DOI: 10.1016/j.jcou.2018.12.007 (IF = 5.189, SNIP=1.276)

Identification of Active Sites for Oxygen Reduction Reaction on Nitrogen- and Sulfur-Codoped Carbon Catalysts

K. M. Villemson[a], K. Kaare [b], R. Raudsepp [b], T. Käämbre[c], K. Šmits[d], P. Wang[e], A. V. Kuzmin[f], A. Šutka[g], B. A. Shainyan[f], I. Kruusenberg[b].

[a] *Institute of Chemistry, University of Tartu, Ravila 14a, 50411 Tartu, Estonia*
[b] *National Institute of Chemical Physics and Biophysics, Akadeemia tee 23, 12618 Tallinn, Estonia*
[c] *Institute of Physics, University of Tartu, Wilhelm Ostwald Street 1, 50411 Tartu, Estonia*
[d] *Institute of Solid State Physics, University of Latvia, Kengaraga 8, 1063 Riga, Latvia*
[e] *Nanomaterials Laboratory, Institute of Systems, Information Technologies and Nanotechnologies, 819-0388 Fukuoka, Japan*
[f] *Siberian Branch of Russian Academy of Sciences, A. E. Favorsky Irkutsk Institute of Chemistry, 1 Favorsky Street, 664033 Irkutsk, Russian Federation*
[g] *Research Laboratory of Functional Materials Technologies, Faculty of Materials Science and Applied Chemistry, Riga Technical University, P. Valdena 3/7, 1048 Riga, Latvia*

Nitrogen- and sulfur-codoped carbon catalysts were prepared as electrocatalytic materials for the oxygen reduction reaction (ORR). Herein, we propose a novel and effective one-pot synthetic approach to prepare a NS-doped carbon catalyst by using the mixture of graphene oxide and multi-walled carbon nanotubes as a carbon support. Successful NS-doping of carbon and formation of the catalytically active sites were confirmed by X-ray photo-electron spectro-scopy and with energy dispersion spectroscopy. The ORR activity of NS-co-doped carbon was investigated by using a rotating disc electrode method. The NS-doped carbon shows superior ORR performance in alkaline media, and the electrocatalytic mechanism for the reduction of oxygen is explained well by density functional theory calculations of graphene sheets.

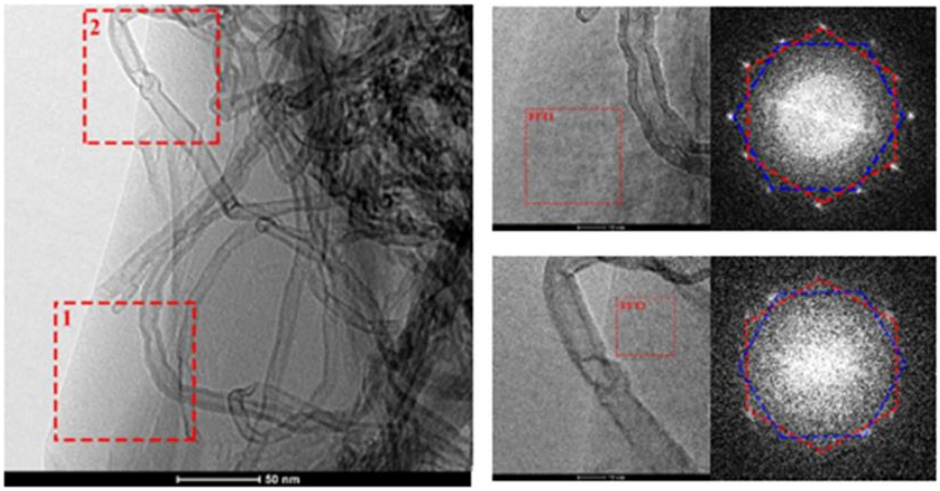

TEM image of the 1:5 C/oMUS catalyst material.

Published in:
K. M. Villemson, K. Kaare, R. Raudsepp, T. Käämbre, K. Šmits, P. Wang, A. V. Kuzmin, A. Šutka, B. A. Shainyan, I. Kruusenberg, J. Phys. Chem. C 123 (2019) 16065−16074. DOI: 10.1021/acs.jpcc.9b00117 (IF=4.3, SNIP=1.08)

Ab Initio Calculations on the Electronic Structure and Photocatalytic Properties of Two-Dimensional WS_2(0001) Nanolayers of Varying Thickness

Dmitry Bocharov[a], Sergei Piskunov[a], Yuri F. Zhukovskii[a], and Robert A. Evarestov[b]

[a] *Institute of Solid State Physics, University of Latvia, Kengaraga Street 8, LV-1063, Riga, Latvia*
[b] *St. Petersburg State University, 7/9 Universitetskaya nab., 199034 St. Petersburg, Russia*

The splitting of H_2O molecules on semiconducting electrodes under the irradiation of solar light is a clean and renewable way for the generation of hydrogen fuel. Efficiency of photocatalysis in the case of a defectless electrode depends on the relative position of the edges of the bandgap (the top of the valence band ε_{VB} and the bottom of the conduction band ε_{CB}), which should be properly aligned relatively to the oxidation and reduction potentials $\varepsilon_{O2/H2O}$ and $\varepsilon_{H+/H2}$ separated by 1.23 eV. It is known that the optimum band gap for water splitting under visible light should lie in the interval of 2.0 – 2.2 eV. After photon absorption electrons being excited migrate to a conduction band simultaneously creating holes in a valence band. Reaction centers for water splitting located on the surface of photocatalyst are found to be important to prevent recombination between electrons and holes. Creation of nanostructures is one of ways how to ensure the exit of recombination centers to the surface.

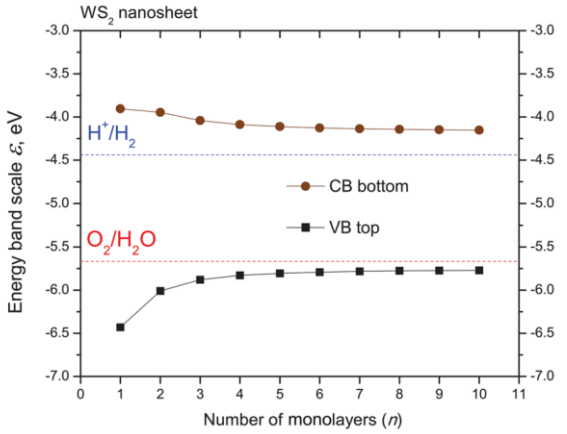

Dependence of calculated WS_2 band gap on nanosheet thickness and position of ε_{CB} and ε_{VB} edges with respect to O_2/H_2O and H^+/H_2 redox potentials.

In this study, we have performed hybrid DFT-LCAO calculations of WS_2 nanosheets possessing stable 2H*c* hexagonal phase with thickness between 1 and 40 ML using hybrid exchange-correlation functional HSE06 adopted for this purpose. Defect-less pristine WS_2 nanosheets have been found to be suitable for photocatalytic applications since widths of their band gaps correspond to the range of visible light between the red and violet edges (1.5 eV < $\Delta\varepsilon_{gap}$ < 2.7 eV) while the top of the valence band and the bottom of the conduction band are properly aligned relative to the oxidation and reduction potentials $\varepsilon_{O2/H2O}$ and $\varepsilon_{H+/H2}$. We found that the band gap of nanolayers decreases with growing the number of monolayers in layered WS_2 2D structure. The highest solar energy conversion efficiency (15–18%) usually achieved for $\Delta\varepsilon_{gap}$ = 2.0 – 2.2 eV (yellow range of the visible spectrum) has been found for the 2-monolayer thick stoichiometric WS_2(0001) nanosheet. WS_2 nanolayers as prospective material for photocatalysis demand no doping or formation of vacancies as in the case of nanostructures of transition metal oxides. Quite the contrary, presence of these defects can worsen the photocatalytic suitability of WS_2 nanolayers.

Published in:
D. Bocharov, S. Piskunov, Yu.F. Zhukovskii, R.A. Evarestov, Phys. Status Solidi RRL 13 (2019) 1800253.
DOI: 10.1002/pssr.201800253 (IF=3.729, SNIP=1.017)

Nitrogen substitutional defects in silicon: quantum mechanical investigation of the structural, electronic and vibrational properties

Alexander Platonenko,[a] Francesco Silvio Gentile,[b] Fabien Pascale,[c] Anna Maria Ferrari,[b] Maddalena D'Amore,[b] and Roberto Dovesi[b]

[a] *Institute of Solid State Physics, University of Latvia, Kengaraga Street 8, LV-1063, Riga, Latvia*
[b] *Dipartimento di Chimica, Università di Torino and NIS (Nanostructured Interfaces and Surfaces) Centre, Via P. Giuria 5, 10125 Torino, Italy*
[c] *Université de Lorraine – Nancy, CNRS, Laboratoire de Physique et Chimie Théoriques, UMR 7019. Vandoeuvre-lès-Nancy, 54506 France*

Nitrogen in silicon is known to improve material properties in various ways, increasing mechanical strength and greatly reducing the size and density of void defects. It was observed that nitrogen increases precipitation of oxygen by increasing the number of nucleation sites and retarding silicon self-interstitial migration. N impurities can pin dislocations and form electrically active defects such as the substitutional deep donor.

In the present paper, we have characterized seven N substitutional defects on the basis of the vibrational IR and Raman spectra. We underline that for the first time the IR and Raman intensities are presented, and that they are computed analytically.

Calculations have been performed by use of the B3LYP global hybrid functional, as implemented in the CRYSTAL17 code. As nitrogen, at variance of silicon, that is fourfold coordinated, is able to bind to only three neighbors, in many cases there are unpaired electrons in the unit cell. For these cases an open shell solution was looked for, by using the Spin Unrestricted Kohn-Sham DFT options available in CRYSTAL.

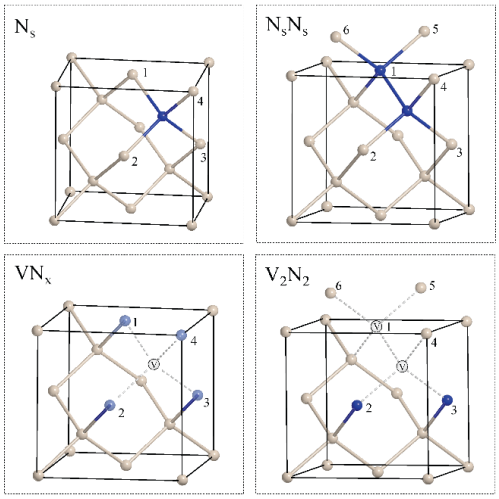

Schematic representation of the seven N substitutional defects here investigated.

It was shown that in all cases in which there are two or more possible spin states, the one with the lowest spin multiplicity is the most stable. All systems are characterized by a simple IR spectrum, in which a single peak has intensity at least 20 times larger than any other peak. In some cases, the single peak is in fact the superposition of two or three peaks, whose wavenumbers, however, are within a few cm^{-1}, so that they merge in a single peak. These peaks, that can be considered as fingerprints of the various defects, span the 645-712 cm^{-1} interval. The dominant peak is at 645 cm^{-1} for N_s, at 669 for VN_1, at 684 cm^{-1} for N_s-N_s, at about 688 cm^{-1} for VN_2, at 695 for VN_3 and at 712 cm^{-1} for VN_4. The multi-defect system V_2N_2, obtained by adding a second contiguous vacancy to VN_2, presents an IR spectrum that essentially coincides with the one of the simpler systems, confirming that the characterization of the defect is due to the presence of the N atoms and their position around the (first) vacancy.

Published in:
A.Platonenko, F.S. Gentile, F. Pascale, A.M. Ferrari, M. D'Amore, R. Dovesi, Phys. Chem. Chem. Phys. 21 (2019) 20939-20950. DOI: 10.1039/C9CP03185E (IF=3.567, SNIP=0.981)

Electronic and optical properties of pristine, N- and S-doped water-covered TiO_2 nanotube surfaces

Stephane Kenmoe[a], Oleg Lisovski[b], Sergei Piskunov[b], Yuri F. Zhukovskii[b], and Eckhard Spohr[c]

[a] *Department of Theoretical Chemistry, University of Duisburg-Essen, Universitätsstr. 2, D-45141 Essen, Germany*

[b] *Institute of Solid State Physics, University of Latvia, Kengaraga Street 8, LV-1063, Riga, Latvia*

For rational design and improvement of electronic and optical properties of water-splitting photocatalysts, the ability to control the band edge positions relative to the water redox potentials and the photoresponse as a function of environmental conditions is essential. In this work we have studied the influence of water and of doping with N and S atoms of a recently developed slab model for medium size titania nanotubes. Specifically, we have investigated the electronic and optical properties of neutral slab nanotube systems under acidic conditions equivalent to pH = 7 at the DFT+U and G_0W_0 levels of theory. Overall, among the systems considered in this study, the N+S co-doping appears to be the optimal system for photocatalytic water splitting in dry and humid conditions. However, the effect is rather moderate. Compared to pristine and N- and S- doping, it shows a more suitable alignment of band edges with respect to the redox potentials of water. Water simultaneously promotes and inhibits the oxygen and hydrogen evolution reactions, respectively. The inclusion of many body effects via the G_0W_0 calculations and solving the Bethe–Salpeter Equation yields the range of electronic and optical gaps in agreement with those measured in photoemission and optical absorption experiments. In dry and humid conditions, the electronic gap for all systems is found in the range of 6.0 – 6.2 eV and a redshift from electronic gap to optical gap is observed. The absorption spectra show an optical anisotropy and different absorption thresholds for in-plane and out-of-plane light polarizations. The photocatalytic activity can be tuned by choosing proper orientation of nanotubes.

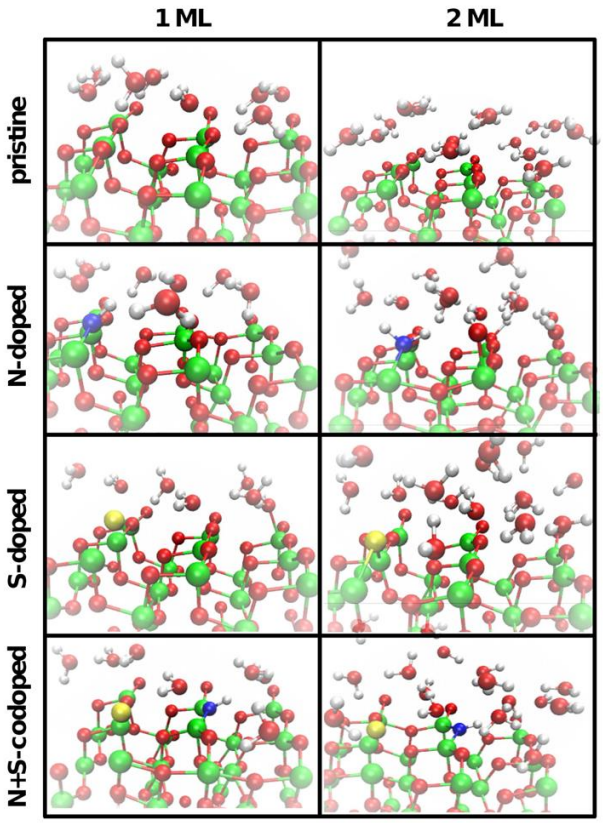

Snapshots of equilibrium trajectories for the pristine, N-doped, S-doped, and N+S-codoped nanotube surfaces covered with a single monolayer (left) or two monolayers (right) of water. Ti, O, H, N, and S are represented by green, red, white, blue, and yellow spheres.

Published in:
S. Kenmoe, O. Lisovski, S. Piskunov, Yu.F. Zhukovskii, E. Spohr, J. Chem. Phys. 150 (2019) 041714.
DOI: 10.1063/1.5050090 (IF=2.997, SNIP=0.969)

Ab initio simulations of $(Ba,Sr)TiO_3$ and $(Ba,Ca)TiO_3$ perovskite solid solutions

L.L. Rusevich, G. Zvejnieks, E.A. Kotomin
Institute of Solid State Physics, University of Latvia, 8 Kengaraga str., Riga LV-1063, Latvia

ABO_3-type crystalline compounds — so called *perovskites* — are interesting for materials science and important for many technological applications because of their ferroelectric and piezoelectric properties. So far, lead-zirconate-titanate is the most widely used piezoelectric material. Nowadays interest is increased in developing of "green" piezoelectric materials due to the lead toxicity. Development of new lead-free materials with good piezoelectric properties is a challenging problem. Chemical modification is one of the ways for tuning dielectric and electromechanical properties of ferroelectrics.

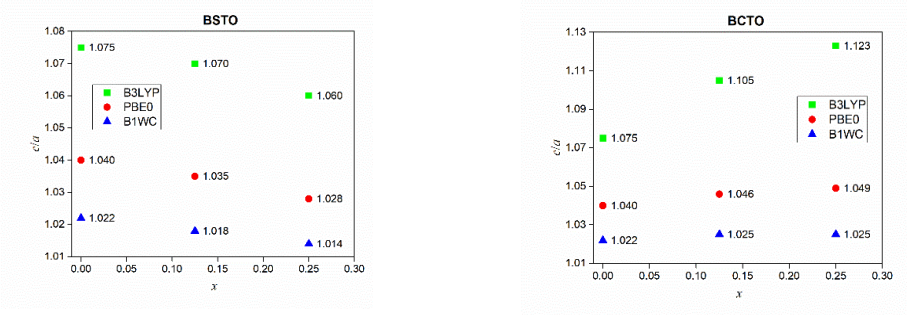

Dependences of tetragonal ratio *c*/*a* vs. chemical composition *x* for BSTO and BCTO solid solutions, calculated using 3 functionals.

In this study, we considered change of functional properties of $BaTiO_3$ (BTO) — typical ferroelectric material with a perovskite-type structure — upon the chemical substitution of Ba atoms by isovalent Sr or Ca atoms, i.e., $Ba_{(1-x)}Sr_xTiO_3$ (BSTO) and $Ba_{(1-x)}Ca_xTiO_3$ (BCTO) solid solutions. We investigated these compounds by means of first-principles calculations, with a focus on the structural, elastic and piezoelectric properties of tetragonal (room temperature) phases, ending with conclusions about similarities and differences in behaviour of these two systems. We performed computations within the approximation of linear combination of atomic orbitals (LCAO) of the density functional theory (DFT) by means of the computer code for quantum chemical *ab initio* simulations CRYSTAL14 combined with the supercell model.

We established that configurational disorder is important for BCTO simulations, while in BSTO this effect is rather small. It is interesting that BSTO and BCTO solid solutions reveal opposite behaviour of the tetragonal ratio *c*/*a* and elastic constants as the functions of chemical composition *x*. On the other hand, both BSTO and BCTO demonstrate significantly enhanced piezoelectric properties (direct and converse) in comparison with pure BTO. Indeed, direct piezoelectric constants e_{33} and e_{31} grow by more than 30% at x=0.25 in BSTO and BCTO, respectively. Due to the decrease of elastic constants, BCTO may be especially useful for improvement of converse piezoelectric constants of BTO — at x=0.25 the absolute values of converse piezoelectric constants d_{31} and d_{33} increase by ~55% in BCTO, and only by 17% in BSTO.

Published in:
L.L. Rusevich, G. Zvejnieks, E.A. Kotomin, Solid State Ionics 337 (2019) 76–81, DOI: 10.1016/j.ssi.2019.04.013. (IF=2.886, SNIP=0.939)

First-Principles Evaluation of the Morphology of WS_2 Nanotubes for Application as Visible-Light-Driven Water-Splitting Photocatalysts

Sergei Piskunov[a], Oleg Lisovski[a], Yuri F. Zhukovskii[a], Pavel N. D'yachkov[b], Robert A. Evarestov[c], Stephane Kenmoe[d], and Eckhard Spohr[d]

[a] *Institute of Solid State Physics, University of Latvia, Kengaraga 8, LV-1063 Riga, Latvia*
[b] *Institute of General and Inorganic Chemistry, Russian Academy of Science, Leninskii prosp. 31, 119991 Moscow, Russia*
[c] *Institute of Chemistry, Saint Petersburg State University, Universitetskaya nab. 7/9, 199034 Saint Petersburg, Russia*
[d] *Theoretical Chemistry Department, University of Duisburg-Essen, Universitätstr. 2, 45141 Essen, Germany*

Alternative nonoxide layered materials, in particular transition-metal chalcogenides, gained growing attention in the last years, since they possess significantly narrower band gaps than transition-metal oxides. One of them is tungsten disulfide WS2. The band gap of bulk WS_2 was measured to be ∼1.4 eV, corresponding to the near-infrared, invisible range of the light spectrum. In this work we have simulated by means of density functional theory the electronic structure of pristine single-walled WS_2 nanotubes of three different types of chirality as a function of nanotube diameter. The band edges depend in all of the cases only on the diameter d_{NT} (and not on the chirality indices of the nanotubes). For d_{NT} > 1.9 nm, the energy diagrams for WS_2 single-walled nanotubes (see Figure) support the potential ability of the NTs to serve as photocatalysts for water-splitting react-ions. In this diameter range, the necessary condition for the ordering of energies, $\varepsilon_{VB} < \varepsilon_{O2/H2O} < \varepsilon_{H2/H2O} < \varepsilon_{CB}$, is fulfilled. Thus, by choosing the nanotube diameter appropriately, the band gap can be tuned with high-energy resolution, which makes WS_2 single-walled nanotubes suitable for photocatalytic applications in the visible spectrum. In addition, we have computed the electronic structure of several selected double- and triple-walled WS_2 nanotubes with armchair-(n, n) and zigzag-type (n, 0) configurations which have not been simulated so far. It has been found that the value of the band gap is smaller than the corresponding values for each of its constituents caused by the influence of inter-wall interactions. This further increases the variability of possible energy ranges suitable for photocatalysis. Hence, in summary, for pristine WS_2 nanotubes with diameters in the range of 2−12 nm, the energies of the optical gaps, the positions of the top of the valence band and the bottom of the conduction band relative to the oxidation and reduction potentials of the H_2O medium are suitable for the photochemical splitting of water and hydrogen production under solar irradiation.

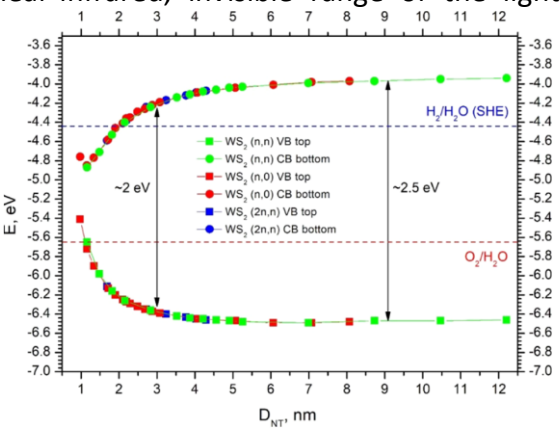

Dependence of valence band and conduction band edges on WS2 NT diameter for three different configurations: achiral (n, n) and (n, 0), as well as chiral (2n, n). Energy is referenced to a vacuum level.

Published in:
S. Piskunov, O. Lisovski, Yu.F. Zhukovskii, P.N. D'yachkov, R.A. Evarestov, S. Kenmoe, E. Spohr, ACS Omega 4 (2019) 1434-1442. DOI: 10.1021/acsomega.8b03121 (IF=2.584, SNIP=0.673)

Point defects in silicon dioxide: from crystalline- to amorphous-type defects

L.Skuja[a], N.Ollier[b], K.Kajihara[c], K.Smits[a]

[a] *Institute of Solid State Physics, University of Latvia, Kengaraga Street 8, LV-1063, Riga, Latvia*
[b] *Laboratoire des Solides Irradiés Ecole Polytechnique, Univ. of Paris-Saclay, 91128 Palaiseau, France*
[c] *Dept. of Applied Chemistry for Environment, Graduate School of Urban Environmental Sciences, Tokyo Metropolitan University, 1-1 Minami-Osawa, Hachioji, Tokyo 192-0397, Japan*

Amorphous or glassy silicon dioxide is the dominant material for optical fiber waveguides, ultraviolet-transmitting optics, high laser power-resistant or radiation-resistant optical devices. Mechanisms of point defect creation and their optical properties in glassy SiO_2 are therefore of considerable interest. The properties of defects are advantageous to study in ordered crystalline environment compared to amorphous state, characterized by the lack of orientational order and large site-to-site variations, giving rise to inhomogeneous broadening.

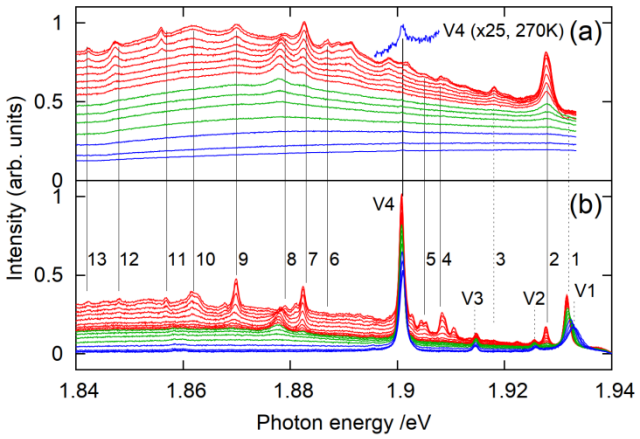

Photoluminescence spectra (exc.=632.8nm) of 10^{19}n/cm^2 neutron-irradiated (a) and 1.4 ×10^{19}e$^-$/cm^2 2.5 MeV electron-irradiated (b) high-purity α-quartz obtained at temperatures between 14 K (top-most trace) and 300K (lower-most) trace in (a,b). Raman (vibrational) lines are denoted by V, the enumerated lines are zero-phonon line of oxygen-dangling bonds and their vibronic sidebands.

However, the point defects in crystal SiO_2 are totally different from ones in amorphous SiO_2, where they have mostly dangling bond character. This problem was overcome by using electron irradiation at high doses just below the amorphization threshold, where dangling bonds, projecting into local nano-sized internal voids in the structure of α-quartz, start to form. This was compared to the case of neutron-irradiation, where dangling bonds are created into amorphized particle tracks. The presence of dangling oxygen bonds ("NBOHC") in non-amorphized quartz was proved for the first time. Their concentration was <100× lower and their inhomogeneous broadening was much less compared to neutron-irradiated quartz. Another practically important disorder-characteristic defect, divalent silicon ("SiODC", silicon oxygen-deficiency center) was observed only in neutron-irradiated quartz. While e$^-$ irradiation created many oxygen vacancies, contrary to the case of irradiated glassy SiO_2, or neutron-irradiated quartz, interstitial O_2 molecules were not detected, indicating that the structural voids in an intact structure of α-quartz are of insufficient size to host O_2 molecules.

Published in:
L. Skuja, N. Ollier, K. Kajihara, K. Smits, Creation of glass-characteristic point defects in crystalline SiO2 by 2.5 MeV electrons and by fast neutrons, J. Non-Crystal. Solids 505 (2019) 252–259. doi:10.1016/j.jnoncrysol.2018.11.014 (IF=2.56, SNIP=1.18)

II. Nanotechnology, thin films, nanocomposites and ceramics.

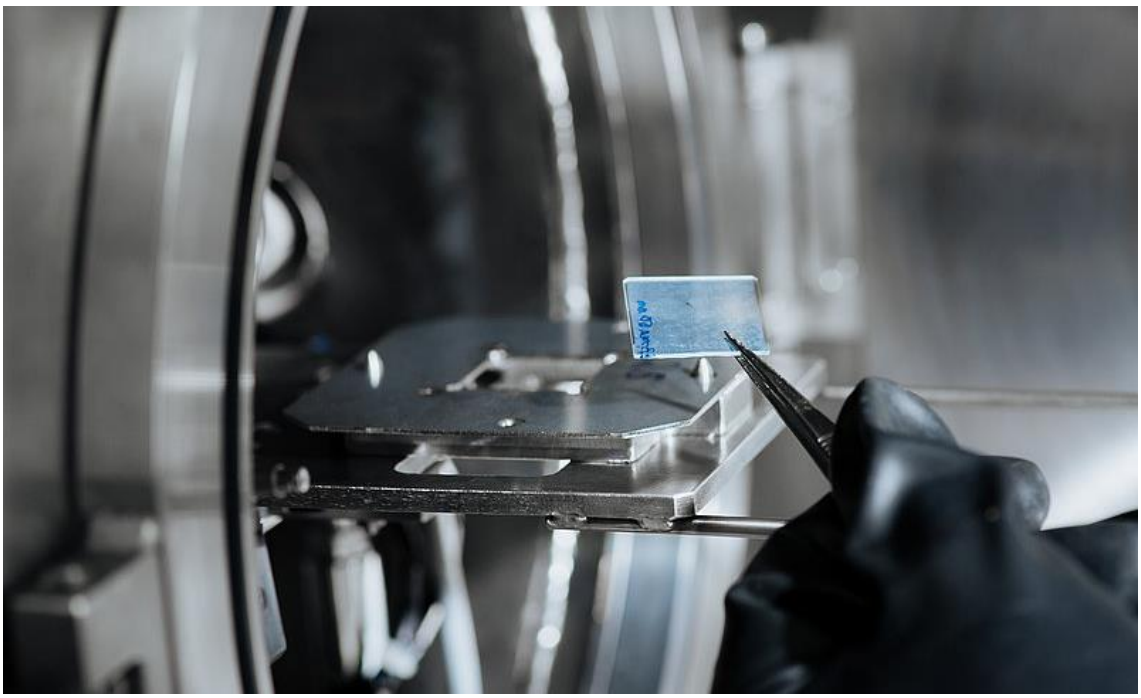

Manifestation of dipole-induced disorder in self-assembly of ferroelectric and ferromagnetic nanocubes

D. Zablotsky[a,b], L.L. Rusevich[a], G. Zvejnieks[a], V. Kuzovkov[a], E. Kotomin[a,c]

[a] *Institute of Solid State Physics, Kengaraga str. 8, LV-1063 Riga, Latvia*
[b] *University of Latvia, Raina bulv. 19, LV-1586 Riga, Latvia*
[c] *Max Planck Institute for Solid State Research, Heisenbergstr. 1, 70569 Stuttgart*

Ferroelectric perovskite-type metal oxides, e.g. $BaTiO_3$, and their solid solutions with $SrTiO_3$ are high-performance dielectrics widely used in a broad variety of electronic, electro-optic, photovoltaic, electro-chemical, and microelectromechanical components. The colloidal processing of nearly monodisperse and highly crystalline single-domain ferroelectric or ferromagnetic nanocubes is a promising route to produce superlattice structures for integration into next-generation devices, whereas controlling the local behaviour of nanocrystals is imperative for fabricating highly-ordered assemblies. The current picture of nanoscale polarization in individual nanocrystals suggests a potential presence of a significant dipolar interaction, but its role in the condensation of nanocubes is unknown.

We simulated the self-assembly of colloidal dipolar nanocubes under osmotic compression and performed the microstructural characterization of their densified ensembles.

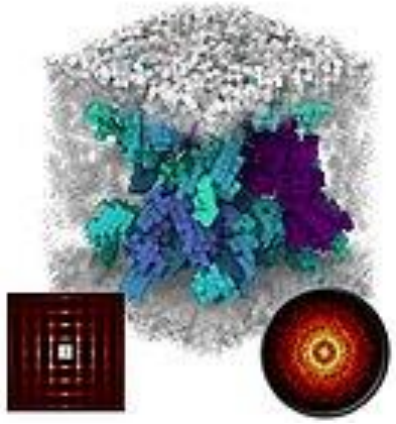

Crystallite size analysis in the assembled solids. Figure illustrates a few (50) of the largest clusters.

The microstructural characterization of osmotically densified ensembles of ferroelectric nanocubes was obtained *via* numerical simulations exploiting discrete element method coupled with particle-particle particle-mesh approach for computing long-range dipolar interactions. Our results indicate that the long-range positional and orientational correlations seem to be highly sensitive to the presence of dipoles, which could be a challenge to produce ordered assemblies of nanoperovskites. Exploring the features of mesoscale disorder we find characteristically similar behavior in a wide array of systems. We show that in fact for solubilized $BaTiO_3$ nanocubes the polarization screening must be complete without appreciable dipole moment (below a few ~ kT), whereas stray interactions from incompletely screened surface charges are the likely major sources of disorder in self-assembled architectures of some nanoscale perovskites, most specifically $SrTiO_3$.

Published in:
D. Zablotsky, L.L. Rusevich, G. Zvejnieks, V. Kuzovkov, E.Kotomin, Nanoscale 11 (2017) 7293-7303. DOI: 10.1039/C9NR00708C (IF=6.970, SNIP=1.338)

Upconversion luminescence in transparent oxyfluoride glass ceramics containing hexagonal $NaErF_4$

G. Krieke, A. Antuzevics, M. Springis, U. Rogulis.

Institute of Solid State Physics, University of Latvia, Kengaraga Street 8, LV-1063, Riga, Latvia

Oxyfluoride glass ceramics are composite materials, which typically consist of a fluoride crystalline phase distributed in an oxide glass. These composites combine excellent spectroscopic properties of fluoride crystals with transparency characteristic of glasses which can be maintained in glass ceramics by careful control of precipitated nanostructures. In oxyfluoride glass ceramics rare earth ions are manly incorporated in fluoride phase making these materials suitable for use in optics. Due to various practical applications, particular interest is dedicated to Er^{3+} upconversion luminescence – anti-Stokes process in which infrared photons are converted to visible emission.

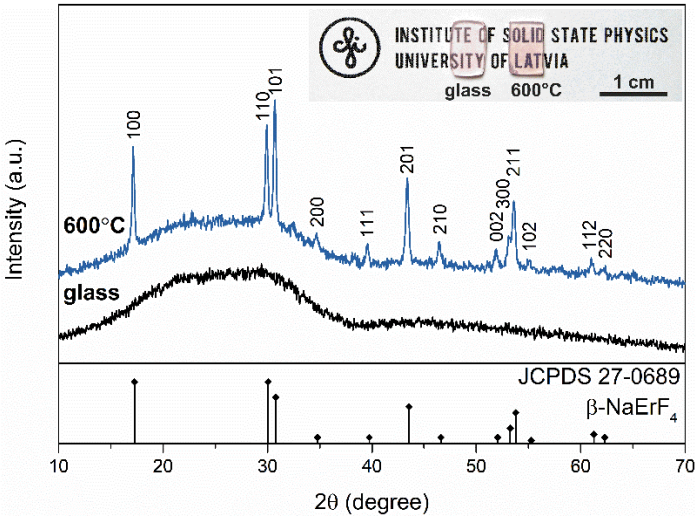

XRD patterns of precursor glass and glass ceramics heat treated at 600°C for 10 h. Inset: photograph of glass and transparent glass ceramic samples.

In this study crystallization and spectroscopic properties of novel transparent glass ceramics containing β-$NaErF_4$ was reported.

In the prepared glass ceramics intense red upconversion luminescence was detected and it was approximately one order of magnitude higher in comparison to precursor glass. Splitting of upconversion luminescence bands and abrupt increase of their intensities indicated that Er^{3+} ions partially incorporate the crystalline phase of the nanocomposite. The dominant energy transfer processes were identified using the rate equation formalism.

Time-resolved site-selective spectroscopy studies at low temperatures were employed to elucidate the local structure of Er^{3+} ions in the glass ceramics and microcrystalline β-$NaErF_4$. Incorporation of Er^{3+} ions in three distinct sites were detected in crystalline phases. In crystal structure β-$NaErF_4$ there are only two Er^{3+} sites. We suggest that the third Er^{3+} site originates from crystal field variations at the erbium ion positions, which could be caused by the alternating occupation of the half-filled Na^+ position.

Published in:
G. Krieke, A. Antuzevics, M. Springis, U. Rogulis, J. Alloys Comp. (2019), 326-332, DOI: 10.1016/j.jallcom.2019.05.276 (IF=4.175, SNIP=1.386)

Afterglow, TL and OSL properties of Mn^{2+}-doped $ZnGa_2O_4$ phosphor

A.Luchechko[a], Y.Zhydachevskyy[b,c], S. Ubizskii[b], O. Kravets[a], A.I Popov[d], U.Rogulis[d], E. Elsts[d], E.Bulur[e], Suchocki[c]

[a] *Ivan Franko National University of Lviv, 107 Tarnavskogo St., Lviv, 79017, Ukraine*

[b] *Lviv Polytechnic National University, 12 Bandera St., Lviv, 79646, Ukraine*

[c] *Institute of Physics, Polish Academy of Sciences, Al. Lotnikow 32/46, Warsaw, 02-668, Poland*

[d] *Institute of Solid State Physics, University of Latvia, Kengaraga Street 8, LV-1063, Riga, Latvia*

[e] *Physics Department, Middle East Technical University, 06800, Ankara, Turkey*

Phosphors activated with Mn^{2+} ions are of high importance among others spinel phosphors for various kinds of applications. Mn^{2+} ($3d^5$) ions, in particular in $ZnGa_2O_4$ spinel, produces a bright green color emission under the excitation by UV light or electron beam that can be applicable for vacuum fluorescent displays, field emission displays and thin-film electroluminescent devices. Despite a considerable potential of spinel compounds to exhibit optically stimulated luminescence as well as a long persistent luminescence, the materials with spinel structure activated with Mn^{2+} ions in this context remain scanty studied. Therefore this work's aim is to study the afterglow, TSL and OSL properties of $ZnGa_2O_4$: Mn^{2+} in order to understand the ability to manage the properties of the material to fill better the requirements necessary for practical applications.

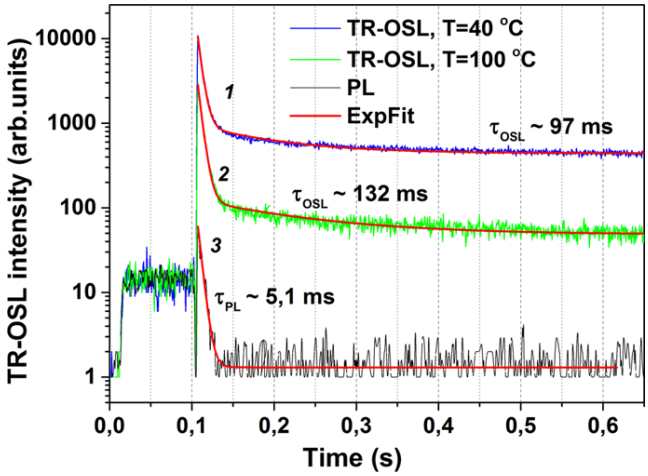

Typical TR-OSL decay curves obtained for $ZnGa_2O_4$: Mn^{2+} ceramics at room temperature after 10Gy β–irradiation and next preheating during 2 min at 40 °C (1) and 100 °C (2), as well as an analog of PL decay for the non-irradiated sample (3).

In this work, $ZnGa_2O_4$ spinel ceramics doped with Mn^{2+} ions was prepared by a solid-state reaction at 1200 °C in air. Manganese concentration was equal to 0.05 mol.% of MnO with respect to ZnO. Ceramics produced in this way show an efficient green emission at about 505 nm under UV or X-ray excitations, which is caused by Mn^{2+} ions. Time profiles of the beginning of glow and afterglow have been studied together with thermally stimulated (TSL) and optically stimulated (OSL) luminescence. Experimental results demonstrate a presence of few types of shallow and deep traps responsible for the observed afterglow and TSL/OSL emission of the material. The possibility of pulsed optical stimulation and time-resolved OSL characteristics of $ZnGa_2O_4$: Mn^{2+} has been reported for the first time. The presented results suggest the $ZnGa_2O_4$: Mn^{2+} spinel as a promising material for further fundamental research and possibility of application as a green long-lasting phosphor or storage phosphor for TSL/OSL radiation dosimetry.

Published in:

A. Luchechko, Y Zhydachevskyy, S Ubizskii, O Kravets, A.I.Popov, U Rogulis, E Elsts, E Bulur & A. Suchocki, Scientific Reports 9 (2019) 9544. DOI: 10.1038/s41598-019-45869-7 *(IF=4.011, SNIP=1.589)*

Effect of Mn doping on the low-temperature synthesis of tricalcium phosphate (TCP) polymorphs

L. Sinusaite[a], A. Renner[b], M. Schutz[b], A. Antuzevics[c], U. Rogulis[c], I. Grigoraviciute-Puroniene[a], S. Mathur[b], A. Kareiva[a], S. L. Stoll[d], A. Zarkov[a,d]

[a] *Institute of Chemistry, Vilnius University, Naugarduko 24, LT-03225 Vilnius, Lithuania*
[b] *Institute of Inorganic Chemistry, University of Cologne, Greinstrasse 6, 50939 Cologne, Germany*
[c] *Institute of Solid State Physics, University of Latvia, Kengaraga 8, LV-1063 Riga, Latvia*
[d] *Department of Chemistry, Georgetown University, Washington, DC 20057, United States*

Calcium phosphates (CPs) are the main constituents of bones and teeth and play an essential role in human life. Tricalcium phosphate ($Ca_3(PO_4)_2$, TCP) is one of the representative biomaterials, which finds an application in bone cements and bone implants due to its excellent resorbability and osteoconductivity.

In the present work the influence of manganese (Mn) doping on the low-temperature synthesis of both α and β-TCP polymorphs is reported. Formation of both crystalline phases under identical processing conditions can be controlled by the level of doping.

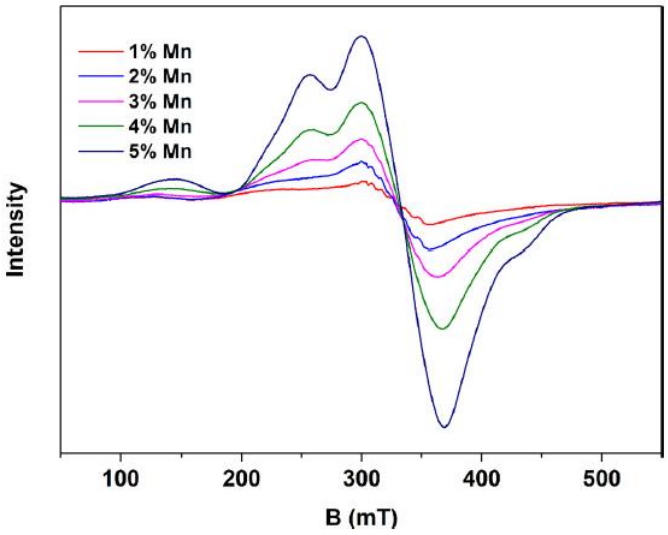

Electron paramagnetic resonance spectra of CP precipitates with different amount of Mn annealed at 700 °C.

Formation of the desired polymorph can be ensured by varying Mn content in the as-prepared precipitates. Calcium phosphates with Mn doping level in the range from 1 to 5 mol% have been studied. Although Mn content does not affect the structure of as-prepared precipitates, we have shown that after annealing procedure an increase in Mn concentration leads to the formation of β-TCP, while pure α-TCP was obtained without Mn doping and a mixture of two polymorphs was obtained for intermediate Mn concentrations. Moreover, it was found that doping with Mn ions allows to obtain single-phase β TCP at lower temperatures – 700 °C. Cytotoxicity tests have not revealed any toxic effects of Mn ions even for the samples with the highest Mn concentration.

Published in:
L. Sinusaite, A.M. Renner, M.B. Schütz, A. Antuzevics, U. Rogulis, I. Grigoraviciute-Puroniene, S. Mathur, A. Zarkov, Effect of Mn doping on the low-temperature synthesis of tricalcium phosphate (TCP) polymorphs, J. Eur. Ceram. Soc. 39 (2019) 3257–3263. DOI: 10.1016/j.jeurceramsoc.2019.03.057 (IF=4.029, SNIP=1.710)

Black carbon-doped TiO_2 films: Synthesis, characterization and photocatalysis

S. Varnagiris[a], A. Medvids[b], M. Lelis[a], D. Milcius[a], A. Antuzevics[c]

[a] *Lithuanian Energy Institute, 3 Breslaujos Str., LT-4 4403 Kaunas, Lithuania*
[b] *Technical Physics Institute, Riga Technical University, 3/7 Paula Valdena Str., LV-1048 Riga, Latvia*
[c] *Institute of Solid State Physics, University of Latvia, 8 Kengaraga Str., LV-1063 Riga, Latvia*

Energy depletion and environmental pollution related problems have become one of the most important areas across the globe in recent decades. Titanium dioxide (TiO_2) is recognized as a leading photocatalyst for environment purification due to its strong oxidizing power under ultraviolet irradiation, high chemical stability, low cost and other properties.

The present report describes the experimental investigation of the photocatalytically active black colour TiO_2 formation by using a magnetron sputtering technique.

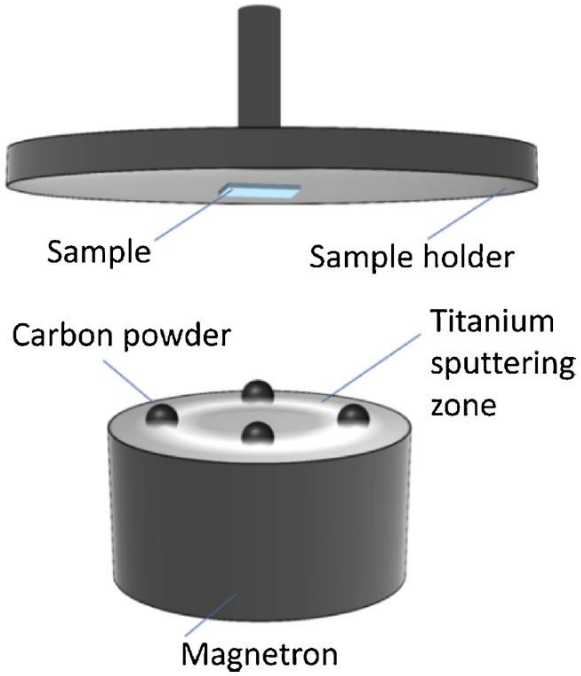

Scheme of experimental set-up during carbon-doped TiO_2 formation.

Analysis of the films showed that TiO_2 film thickness, surface roughness and crystalline size increase with longer deposition time. XPS analysis confirmed carbon incorporation into the TiO_2 film. Electron paramagnetic resonance spectroscopy demonstrated generation of oxygen vacancies where unpaired electrons were trapped. Analysis of the optical properties of the carbon-doped TiO_2 films revealed that incorporation of carbon during deposition process can reduce the optical band gap of TiO_2 from approximately 3.3 eV to 2.2–2.4 eV. Additionally, Methylene Blue bleaching experiment showed that black colour TiO_2 films exhibit significant photocatalytic activity under both UV-A (365 nm) and visible light (455 nm) irradiation.

The results show that the present black coloured TiO_2 formation technique has promising characteristics for further photocatalytically active TiO_2 formation.

Published in:
S. Varnagiris, A. Medvids, M. Lelis, D. Milcius, A. Antuzevics, Black carbon-doped TiO_2 films: Synthesis, characterization and photocatalysis, J. Photochem. Photobiol. A Chem. 382 (2019) 111941. DOI: 10.1016/j.jphotochem.2019.111941 (IF=3.261, SNIP=0.851)

High power impulse magnetron sputtering of Zn/Al target in an Ar and Ar/O_2 atmosphere: The study of sputtering process and AZO films

M. Zubkins, H. Arslan, L. Bikse, J. Purans

Institute of Solid State Physics, University of Latvia, Kengaraga Street 8, LV-1063, Riga, Latvia

Reactive high power impulse magnetron sputtering (R-HiPIMS) has been demonstrated as a promising technique for the ZnO:Al (AZO) thin film deposition at low temperature with improved electrical properties compared to the reactive direct current magnetron sputtering (R-dcMS). However, there are not enough studies about the HiPIMS process using Zn/Al target itself. Additionally, AZO films have not been deposited with the pulse duration times long enough to allow the discharge to develop into the self-sputtering (SS) mode.

C-V-t characteristics and the time average plasma optical emission spectra (OES) of the metallic (Ar) and reactive (Ar+O_2) HiPIMS of Zn/Al target have been studied as a function of different sputtering parameters, such as frequency, average power, pulse duration time, and oxygen flow rate. AZO films were deposited on glass substrates without intentional heating by R-HiPIMS using 500 µs long pulses. Structural, electrical and optical properties of the AZO films were studied as a function of peak current.

Due to the high sputter yield of Zn, strong Ar gas rarefaction has been observed and lower peak power densities compared to other metals were obtained. Nevertheless, the HiPIMS regime can be achieved by increasing the time between pulses or increasing the average power. When the peak power density of 500 µs pulses is above 0.3 kW/cm^2, the sustained self-sputtering discharge develops.

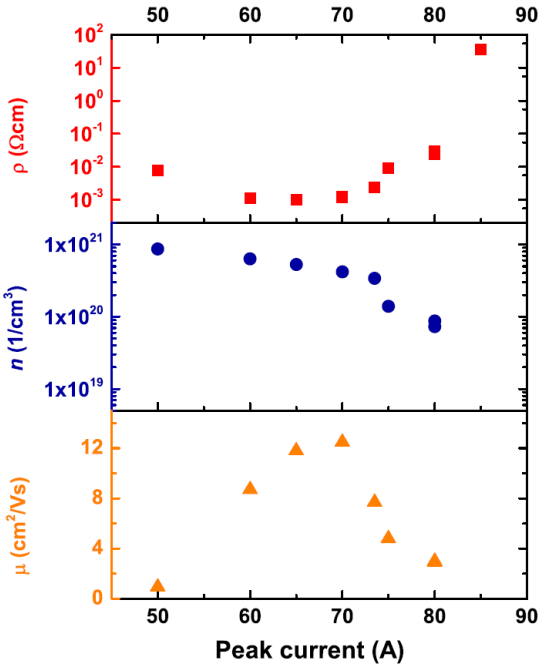

Resistivity, electron concentration and mobility of the HiPIMS (t_{On}=500 µs, t_{Off}=40'000 µs) deposited AZO films as a function of peak current.

The changes in electrical and optical properties of the AZO films showed that the peak current can be used as a control parameter in the reactive sputtering. A higher oxygen flow rate is necessary to achieve transparent AZO films by R-HiPIMS compared to R-dcMS. A slight improvement in electrical conductivity was achieved when depositing AZO films at low temperature by R-HiPIMS; however, the film properties are still moderate suggesting that the SS is not an optimal mode to achieve high quality AZO films. From the XRD, there is the indication of existing zincblende structural phase in the AZO films deposited at high oxygen partial pressure. However, further research is necessary to prove this fact.

Published in:
M. Zubkins, H. Arslan, L. Bikse, J. Purans, Surface & Coatings Technology 369 (2019) 156–164. DOI: 10.1016/j.surfcoat.2019.04.044 (IF=3.192, SNIP=1.435)

III. Functional materials for photonics and electronics.

Tuning the photoresponse of nano-heterojunction: Pressure-induced inverse photoconductance in functionalized WO_3 nanocuboids

S. Rahman[a], S. Samanta[a], A. Kuzmin[b], D. Errandonea[c], H. Saqib[a], D.L. Brewe[d], J. Kim[e], J. Lu[f], L. Wang[a]

[a] *Center for High Pressure Science and Technology Advanced Research, Shanghai 201203, China*
[b] *Institute of Solid State Physics, University of Latvia, LV-1063, Riga, Latvia*
[c] *Departamento de Física Aplicada-ICMUV, MALTA Consolider Team, Universidad de Valencia, Edificio de Investigación, 46100 Valencia, Spain*
[d] *X-Ray Science Division, Advanced Photon Source, Argonne National Laboratory, Argonne, IL 60439, USA*
[e] *Department of Chemical Physics, University of Science and Technology of China, Hefei 230026, China*
[f] *HYU-HPSTAR-CIS High Pressure Research Center, Department of Physics, Hanyang University, Seoul 04763, Republic of Korea*

Inverse photoconductivity (IPC) is a unique photoresponse behavior that exists in few photoconductors in which electrical conductivity decreases with irradiation, and has great potential applications in the development of photonic devices and non-volatile memories with low power consumption. However, it is still challenging to design and achieve IPC in most materials of interest.

In this study, pressure-driven photoconductivity has been investigated in n-type WO_3 nanocuboids functionalized with p-type CuO nanoparticles under visible illumination and an interesting pressure-induced IPC accompanying a structural phase transition has been observed.

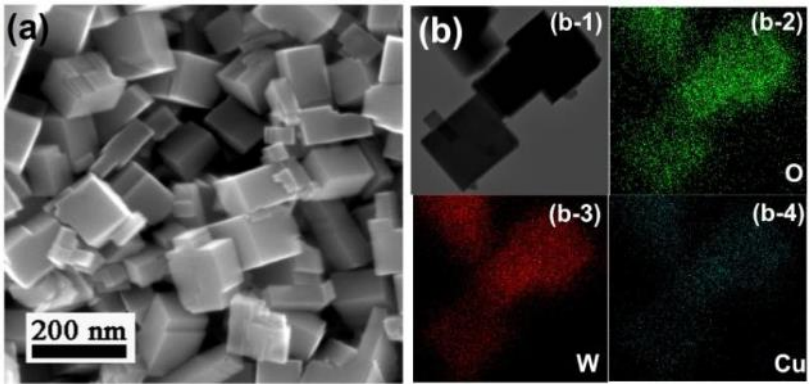

(a) SEM image and (b) multi-elemental mapping images of CuO/WO_3 hybrids.

Native and structural distortion induced oxygen vacancies assist the charge carrier trapping and favor the persistent positive photoconductivity beyond 6.4 GPa. The change in photoconductivity is mainly related to a phase transition and the associated changes in the bandgap, the trapping of charge carriers, the WO_6 octahedral distortion, and the electron–hole pair recombination process. A unique reversible transition from positive to inverse photoconductivity is observed during compression and decompression. The origin of the IPC is intimately connected to the depletion of the conduction channels by electron trapping and the chromic property of WO_3. This synergistic rationale may afford a simple and powerful method to improve the optomechanical performance of any hybrid material.

Published in:
S. Rahman, S. Samanta, A. Kuzmin, D. Errandonea, H. Saqib, D.L. Brewe, J. Kim, J. Lu, L. Wang, Adv. Sci. (2019) 1901132:1-9., DOI: 10.1002/advs.201901132 (IF=15.804, SNIP=2.100)

High-temperature X-ray absorption spectroscopy study of thermochromic copper molybdate

I. Jonane[a], A. Anspoks[a], G. Aquilanti[b], A. Kuzmin[a]

[a] *Institute of Solid State Physics, University of Latvia, LV-1063, Riga, Latvia*
[c] *Elettra-Sincrotrone Trieste, 34149, Basovizza, Trieste, Italy*

Transition metal molybdates are well-known materials having a wide range of technological applications. In particular, copper molybdate ($CuMoO_4$) has been intensively studied due to its diverse functional properties, including thermochromism, piezochromism, and photoluminescence. It is also known as an efficient oxidation catalyst, photocatalyst and n-type photoanode in water splitting photoelectrochemical cells. Furthermore, the properties of the molybdate can be tailored by reducing the particle size or by doping and producing solid solutions.

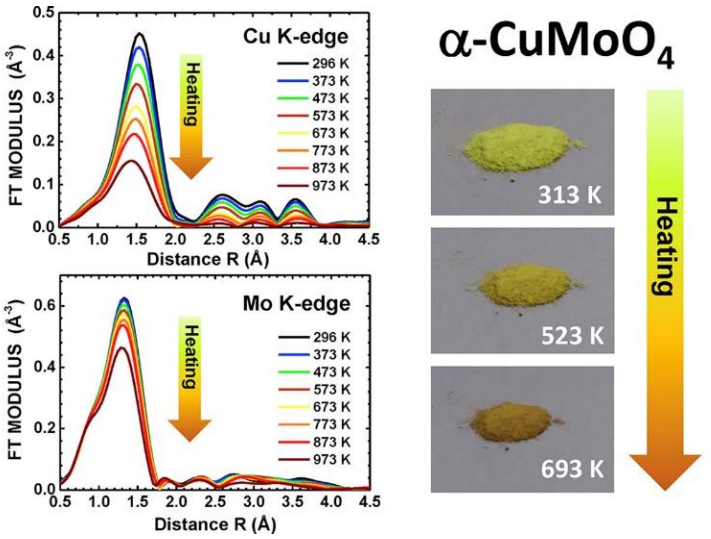

Left panel: temperature dependence of the Fourier transforms of the experimental Cu and Mo K-edges EXAFS spectra in $CuMoO_4$. Middle panel: change of the copper molybdate color upon heating.

X-ray absorption spectroscopy at the Cu and Mo K-edges was used to study the effect of heating on the local atomic structure and dynamics in copper molybdate (α-$CuMoO_4$) in the temperature range from 296 to 973 K. The reverse Monte-Carlo (RMC) method was successfully employed to perform accurate simulations of EXAFS spectra at both absorption edges simultaneously. The method allowed us to determine structural models of α-$CuMoO_4$ being consistent with the experimental EXAFS data. These models were further used to follow temperature dependencies of the local environment of copper and molybdenum atoms and to obtain the mean-square relative displacements for Cu–O and Mo–O atom pairs. Moreover, the same models were able to interpret strong temperature-dependence of the Cu K-edge XANES spectra. We found that the local environment of copper atoms is more affected by thermal disorder than that of molybdenum atoms. While the MoO_4 tetrahedra behave mostly as the rigid units, a reduction of correlation in atomic motion between copper and axial oxygen atoms occurs upon heating. This dynamic effect seems to be the main responsible for the temperature-induced changes in the $O^{2-} \rightarrow Cu^{2+}$ charge transfer processes and, thus, is the origin of the thermochromic properties of α-$CuMoO_4$ upon heating above room temperature.

Published in:
I. Jonane, A. Anspoks, G. Aquilanti, A. Kuzmin, Acta Mater. 179 (2019) 26-35.DOI: 10.1016/j.actamat.2019.06.034 (IF=7.293, SNIP=2.842)

Emission Enhancement by Intramolecular Stacking between Heteroleptic Iridium(III) Complex and Flexibly Bridged Aromatic Pendant Group

Kaspars Traskovskis,[a] Valdis Kokars,[a] Sergey Belyakov,[b] Natalija Lesina,[c] Igors Mihailovs,[a,c] and Aivars Vembris[c]

[a]*Institute of Applied Chemistry, Riga Technical University, 3/7 Paula Valdena Street, Riga LV-1048, Latvia*
[b]*Latvian Institute of Organic Synthesis, 21 Aizkraukles Street, Riga LV-1006, Latvia*
[c]*Institute of Solid State Physics, University of Latvia, 8 Kengaraga Street, Riga LV-1063, Latvia*

Phosphorescent iridium(III) complexes suffer from a strong aggregation quenching, limiting their use in solution-processed or crystalline organic light-emitting diodes. Here we report how an intramolecular stacking between a flexibly bridged bulky aromatic pendant group and the core of nonionic heteroleptic complex can be exploited to minimize the negative effects of this drawback. The stacked conformation provides a rigid sterical shielding of the polar molecular surface, improving photoluminescence quantum yield of the complex both in solution and crystalline state.

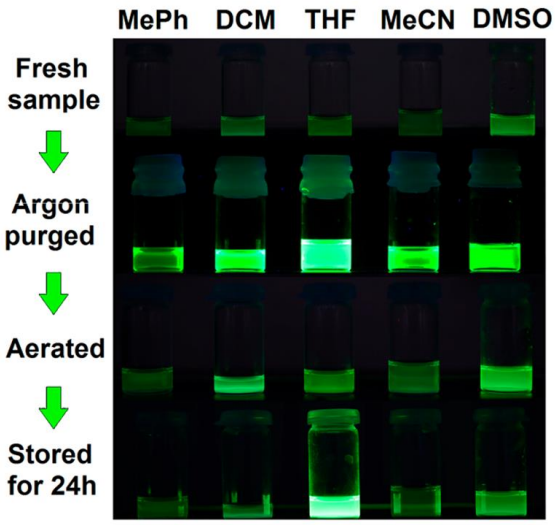

Emission of UV (360 nm) irradiated solutions of $(trppy)_2Ir(pic)$ ($c = 1 \times 10^{-3}$ mol L^{-1}) in different polarity solvents. Note the most intense PL in deoxygenated THF. The emission once again turns on in previously aerated THF solution after 24 h storage due to a precipitation of microcrystallites.

In summary, on the basis of $(trppy)_2Ir(pic)$, we have presented the first structural example where intramolecular stacking between a nonionic heteroleptic iridium(III) complex core and a flexibly bridged bulky aromatic substituent takes place. The main application direction of this effect can be proposed toward the development of efficient solid-state emissive materials. A potential acquisition of phosphorescent crystals with limited emission quenching for OLED applications can be named as the most promising perspective, as, to the best of our knowledge, $(trppy)_2Ir(pic)$ exhibits the highest reported Φ_{PL} value among non-ionic iridium(III) complexes in their crystalline state. Additionally, minimal PL band transformations between solid and dissolved states are observed. Further investigations are being performed to modify the existing molecule and to apply the principle to other structurally similar iridium(III)-based emitters.

Published in:
K. Traskovskis, V. Kokars, S. Belyakov, N. Lesina, I. Mihailovs, A. Vembris, Inorganic Chemistry 2019 58 (7), 4214-4222. DOI: 10.1021/acs.inorgchem.8b03273. (IF=4.850, SNIP=1.09)

Eu^{3+} ternary and tetrakis complexes with carbazole and methyl group substituted dibenzoylmethane derivatives: Induction of aggregation-enhanced emission

Ilze Malina[a], Kaspars Traskovskis[a], Natalija Lesina[b], Aivars Vembris[b]

[a] *Institute of Applied Chemistry, Riga Technical University, Paula Valdena Str. 3, Riga, LV-1048, Latvia*

[b] *Institute of Solid State Physics, University of Latvia, Kengaraga Str. 8, Riga, LV-1063, Latvia*

Two β-diketones with methyl and carbazole substituents attached to dibenzoylmethane (Me-DBM, CBZ-DBM) and their corresponding novel Eu^{3+} ternary (Eu(Me-DBM)3PHEN C1, Eu(CBZ-DBM)3PHEN C2) and tetrakis ([Eu(Me-DBM)4]N+(Et)4 C3, Eu(CBZ-DBM)4]N+(Et)4 C4) complexes were synthesized, fully characterized with 1H NMR, 13C NMR, FT-IR spectroscopy methods, elemental analysis and thermogravimetric analysis. The photophysical properties of the compounds were investigated in solution and solid-state. The acquired results show that the complexes based on Me-DBM ligand exhibit strong AEE behavior, with very low emission efficiency in solutions and moderately high PLQY values of 0.53 and 0.57 in powders. CBZ-DBM based complexes in solution show either dual Eu^{3+} and ligand centered emission (C3) or only ligand emission (C4), while in the solid state only Eu3+ emission is detected. At the same time the measured solid-state PLQY values of CBZ-DBM based compounds are notably lower (0.09 and 0.10). The results of quantum chemical modeling show that this decrease in luminescence efficiency is mainly attributed to the close situated S1 and T1 energy levels of CBZDBM that obstruct the intersystem crossing process. Additionally, no AEE behavior was observed for C3 and C4 due to CT nature of CBZ-DBM that reduces the conformational freedom of the molecule. Taking into account the practical application aspects of the synthesized compounds, the molecular design of Me-DBM based complexes can be considered as more promising, due to increased emission efficiency. AEE characteristics of these compounds can be exploited towards the development of environment-sensitive luminescent probes. The potential use of these compounds in OLEDs is limited due to the fact that the dispersion in charge transporting host reduces emission efficiency through the obstructed aggregation ability of the molecules.

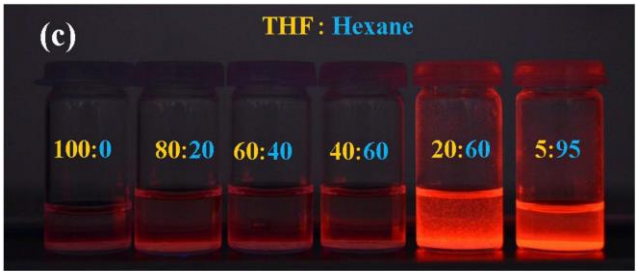

Aggregation enhanced emission of the compound C2, illustrated by UV irradiated solutions with different THF:hexane volume fractions

Published in:
I.Malina, K. Traskovskis, N. Lesina, A. Vembris, Dyes and Pigments 163 (2019) 257-266.
DOI: 10.1016/j.dyepig.2018.11.060 (IF=4.018, SNIP=0.91)

Dendronized azochromophores with aromatic and perfluoroaromatic fragments: Synthesis and properties demonstrating Ar-Ar^F interactions

Lauma Laipniece[a], Valdis Kampars[a], Sergey Belyakov[a,b], Andrejs Tokmakovs[c], Edgars Nitiss[c], Martins Rutkis[c]

[a] *Faculty of Materials Science and Applied Chemistry, Riga Technical University, P. Valdena 3/7, Riga, LV-1048, Latvia*
[b] *Latvian Institute of Organic Synthesis, Aizkraukles 21, Riga, LV-1006, Latvia*
[c] *Institute of Solid State Physics, University of Latvia, Kengaraga 8, Riga, LV-1063, Latvia*

We have synthesized four new dendronized azochromophores using push-pull azobenzene as active chromophore moiety and adding benzyl and/or (pentafluorophenyl)methyl fragments containing dendrons to it. We demonstrated for the first time AreArF interactions in crystal of large dendronized NLO active chromophore. AreArF interactions are clearly present in crystal of compound 14: both dendron fragments of two molecules are stacking and one pentafluorophenyl fragment is interacting with azobenzene moiety. The unexpected aspect was that interaction of pentafluorophenyl ring occurred with the acceptor part of azobenzene moiety, and not with the donor part, as could be expected considering electron density of the molecule. It is possible that some of these stable interactions are present in glassy state or in solution. Connection of benzyl and pentafluorophenyl fragments containing dendrons to azobenzene chromophore donor or acceptor part gave very interesting and different results. In these chromophore series, the connection of pentafluorophenyl dendron fragment to donor part of azochromophore is most successful: compounds 14 and 17 both demonstrate high Tg, and TSHI50, which is possibly due to Ar-Ar^F interactions, stabilizing overall conformation of molecular glass molecules in amorphous thin film. Connection of benzyl dendron fragment to donor part of azochromophore leads to lower Tg, and TSHI50. The type of dendron connected to acceptor part of azochromophore has little influence on material properties. Formation of complementary blends of chromophores did not give expected enhancement of thermal and NLO properties. We explain this with intermolecular interactions, but these interactions may be in such a way to favor centrosymmetric ordering of chromophores leading to decreased NLO coefficients.

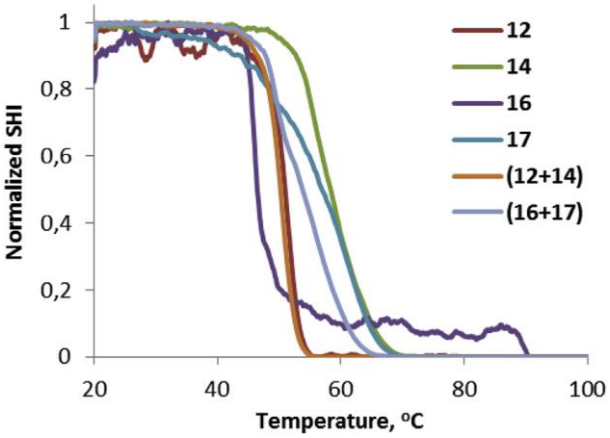

Heat induced decay of SHI in poled amorphous films

Published in:
L. Laipniece, V. Kampars, S. Belyakov, A. Tokmakovs, E. Nitiss, M. Rutkis, Dyes and Pigments 162 (2019) 394-404.
DOI: 10.1016/j.dyepig.2018.10.035 (IF=4.018, SNIP=0.91)

Thiphenylmethane based structural fragments as building blocks towards solution-processable heteroleptic iridium(III) complexes for OLED use

Kaspars Traskovskis,[a] Armands Ruduss,[a] Valdis Kokars,[a] Igors Mihailovs,[ab] Natalija Lesina[b] and Aivars Vembris[b]

[a] *Riga Technical University, Faculty of Materials Science and Applied Chemistry, 3/7 Paula Valdena Street, Riga LV-1048, Latvia.*
[b] *Institute of Solid State Physics, University of Latvia, 8 Kengaraga Street, Riga LV-1063, Latvia*

A novel structural approach to the synthesis of solution-processable yellow and orange light emitting heteroleptic iridium(III) complexes is presented. The materials can be acquired based on O and N functionalized 2-arylbenzo[d]thiazole cyclometalating ligands by an introduction of phase-behavior modifying 1,1,1-triphenylpentyl substituents in a simple 4 to 5 step-reaction sequence. According to the results of DSC analysis the acquired compounds do not possess inherent crystallinity and form a stable amorphous phase, at the same time showing an excellent solubility in a wide range of organic solvents. The presence of the modifying groups does not affect the emission efficiency, as large FPL values in the range of 0.64 to 0.90 were measured for the synthesized complexes. Amongst the investigated compounds a clear improvement in solid-state emissive properties is observed if picolinic acid ancillary ligand is used instead of acetylacetone. Additionally, the presented materials show a distinctive preference for molecular charge transporting host materials in comparison to the polymeric alternatives. The compounds can be successfully used to produce solution-processed OLEDs and the best obtained device showed an external quantum efficiency of 7.9%, current efficiency of 12.4 cd A^{-1} and power efficiency of 7.8 lm W^{-1} at luminance 6000 cd m^{-2}, with the highest measured luminance of 17 451 cd m^{-2}. According to the observed volt-ampere characteristics, a further device optimization is possible, with the use of more appropriate electron or hole transport layers, in order to improve the charge balance. Despite this, the achieved performance parameters of the solution-processed OLEDs already exceed those reported for their close structural analogues, highlighting the viability of the presented material design.

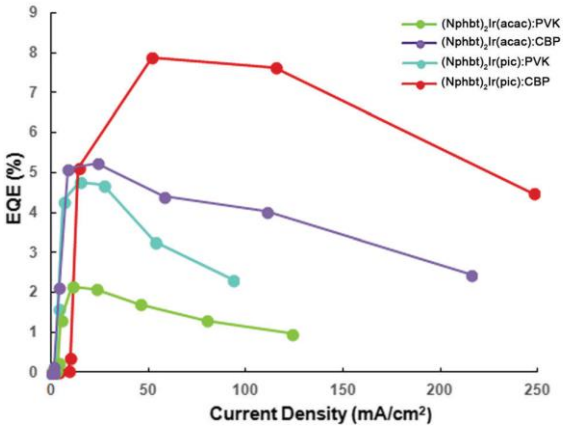

Characteristics of (Cbzbt)2Ir(acac) and (Cbzbt)2Ir(pic) based OLEDsexternal quantum efficiency versus current density

Published in:
K. Traskovskis, A. Ruduss, V. Kokars, I.Mihailovs, N. Lesina, A. Vembris, New J. Chem. 43 (2019) 37-47. DOI: 10.1039/c8nj04484h (IF=3.069, SNIP=0.72)

Luminescence of natural α-quartz crystal with aluminum, alkali and noble ions impurities

A.N. Trukhin

Institute of Solid State Physics, University of Latvia, Kengaraga Street 8, LV-1063, Riga, Latvia

Many samples of natural crystalline α-quartz at low temperatures (77 K) exhibit the intense blue photoluminescence excited in the range of 6 eV. Recent studies show that this luminescence appears in aluminum-containing quartz and is attributed to a certain complex of aluminum and alkali ions. Substitution of alkali ions for noble ions for the case of copper and for silver in quartz, supports Al, O-, Me+ (Me+ alkali or noble ion) model of the luminescence center. After the substitution, the initial luminescence of natural quartz disappeared and a new luminescence of the luminescence centers of copper and silver appeared. Thermal quenching of PL of the original quartz crystal is observed in the temperature range above 200 K similarly to the self-trapped exciton (STE) luminescence. Luminescence centers related to alkali ions and noble ions have not been studied yet at higher temperatures. The task of this work is to understand why the defects of natural quartz provide luminescence at high temperature and to explain the role of those defects in recombination processes. Quenching almost completely occurs at 700 K for centers with alkali ions on the one hand and noble ions on the other. Different values of the activation energy of quenching are obtained. For the alkali related center, it is about 0.2 eV, and for the center of noble ions it is about ~0.7 eV. Possible reasons for this may be related to the differences between alkali ions and noble ions. Let us consider the possible models of the luminescence center. Generation of STE-like structure near the aluminum defect is proposed. For the alkali related center of blue luminescence, two factors are assumed: the strength of STE-like oxygen-oxygen bond at low temperatures and the presence of the alkali atom in the interstitial position at high temperatures. The process of thermal quenching in different temperature regions can be explained by different intersection of adiabatic surfaces of ground and excited states. In the case of a center with noble ions, the intra-ionic transitions take place without creation of STE-like structure.

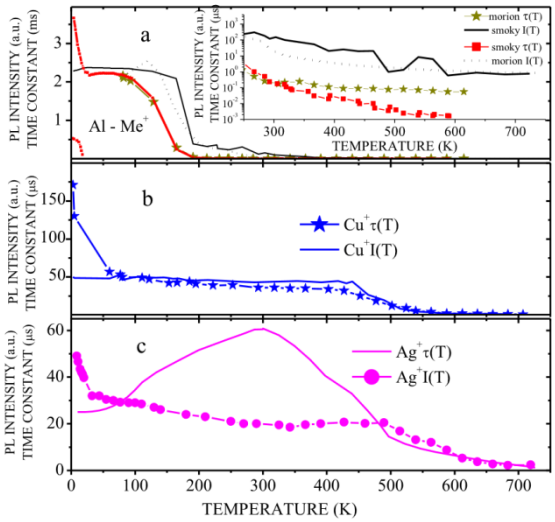

Temperature dependences of PL intensity (lines) and time constant (points) of natural quartz morion (dashes) and smoky (lines) (part a). Temperature dependences of PL intensity (lines) and decay time constant (points) of copper (360 nm, part b, Cu+ I(T) τ(T)) and silver (260 nm, part c, labeled Ag+ I(T) τ(T)) doped natural quartz. Excitation –ArF excimer laser (193 nm).

Published in:
A.N. Trukhin, J. Luminescence 214 (2019) 116602. DOI: 10.1016/j.jlumin.2019.116602 (IF=2.961, SNIP=1.048)

Spectral and kinetic characteristics of pyroelectric luminescence in $LiGaO_2$

L.Trinkler[a], A.Trukhin[a], J.Cipa[a], B.Berzina[a], V.Korsaks[a], Mitch M.C. Chou[b], Chu-An Li[b]

[b] *Institute of Solid State Physics, University of Latvia, Kengaraga Street 8, LV-1063, Riga, Latvia*
[c] *Center of Crystal Research, Department of Materials and Optoelectronic Science, National Sun Yat-sen University, Kaohsiung, Taiwan*

Pyroelectricity is observed in certain organic and inorganic dielectric and semiconductor crystals with non-centrosymmetrical lattice as change of electric polarization giving rise to electrical fields inside the sample under changes of temperature. Excess polarization of such crystals is compensated by free charge carriers gathering on a sample surface; after temperature stabilizing leakage current gradually eliminates pyroelectric field. In the case of rapid temperature changes charge distribution fails to attain equilibrium, electric field in a crystal rises up to several tents to hundreds of V/cm, causing dielectric discharge on the crystal surface. Charge emission can occur both outside and inside a crystal, causing spontaneous light emission, called pyroelectric luminescence (PEL).

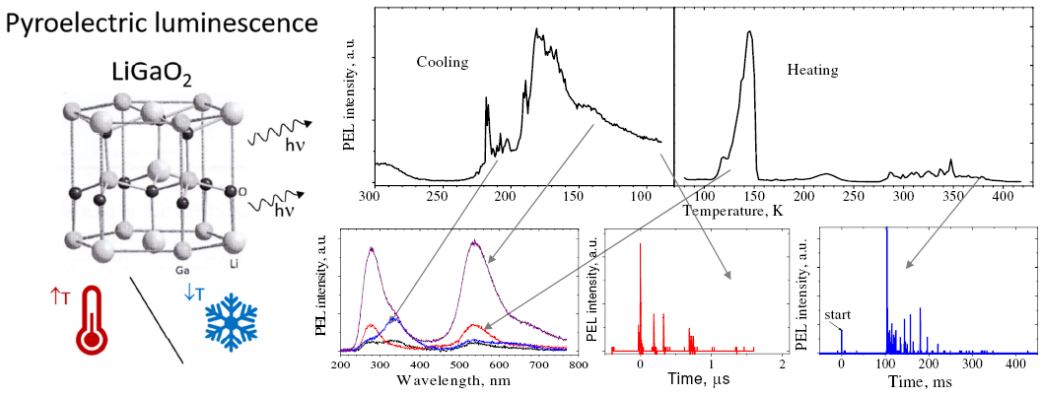

Most important properties of pyroelectric luminescence in $LiGaO_2$: PEL during cooling and heating run, PEL spectrum and PEL kinetics during cooling and heating run.

In the present study for the first time pyroelectric luminescence is observed in lithium metagallate crystal $LiGaO_2$; at sample cooling and heating the PEL temperature curves contain the spiky and smooth signal regions. For the first time the spectral and kinetic characteristics of PEL are obtained. Structure of the PEL emission spectra, containing solely intrinsic luminescence bands, is similar for spiky and smooth signal and is identical to the UV light-induced PL emission spectrum peaks. Thi is in favour of the PEL process occurrence in the bulk of the crystal. Similar temporal structure of the spiky and smooth PEL signals containing successive pulses in millisecond and microsecond timescale, respectively, and identical emission spectra allow a suggestion that the same luminescence mechanism takes place in both PEL types. The obtained duration of a single free-standing PEL pulse, which is equal to or shorter than several nanoseconds, is consistent with the proposed PEL mechanism as radiative recombination of electrons with positively charged intrinsic luminescence centres.

Published in:
L. Trinkler, A. Trukhin, J. Cipa, B. Berzina, V. Korsaks, Mitch M.C. Chou, Chu-An Li, Optical Materials 94 (2019) 15-20.
DOI: 10.1016/j.optmat.2019.05.014 (IF=2.687, SNIP=1.009)

Time-resolved cathodoluminescence spectroscopy of YAG and YAG:Ce^{3+} phosphors

E.Polisadova[a], D.Valiev[a], V.Vaganov[a], V.Oleshko[a], Tao Han[b], C.Zhang[b], A.Burachenko[c], A.I.Popov[d]

[a] *National Research Tomsk Polytechnic University, Lenin Avenue 30, 634050, Tomsk, Russia*
[b] *Research Institute for New Materials Technology, Chongqing University of Arts and Sciences, Chongqing, 402160, People's Republic of China*
[c] *Institute of High Current Electronics, Siberian Branch, Russian Academy of Sciences, 2/3 Akademichesky Avenue, 634055, Tomsk, Russia*
[d] *Institute of Solid State Physics, University of Latvia, Kengaraga Street 8, LV-1063, Riga, Latvia*

Complex oxides with the garnet structure of the composition $A_3B_2C_3O_{12}$ are widely used as hosts for doping with different rare-earth ions for different applications such as laser crystals, fast scintillators, and ionizing radiation dosimeters. In particular, yttrium aluminum garnet doped with Ce^{3+} ions (YAG:Ce^{3+}) phosphors are of great interest because of their application as luminescent converters in white light-emitting diodes (w-LEDs). However, the luminescence mechanisms, models of luminescent centers, and energy transfer processes in garnets with different morphologies and dopants are still unclear. Therefore, the study of the processes responsible for the luminescence mechanisms and the influence on the light yield of the phosphors under different excitation is so far important.

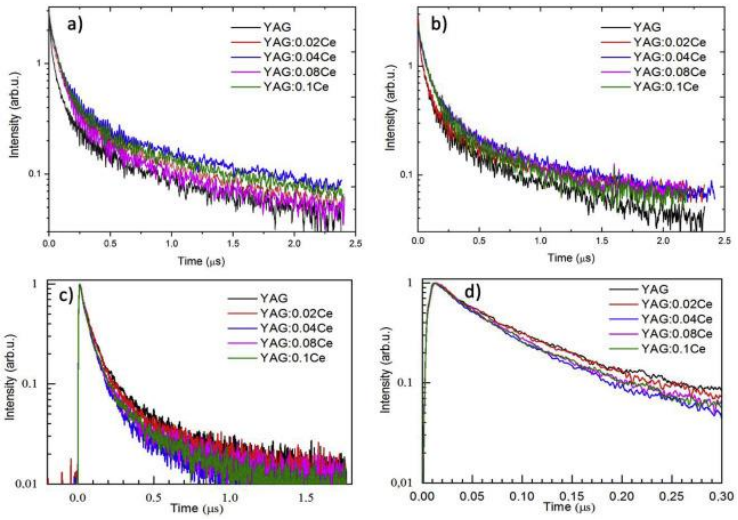

Luminescence decay kinetics YAG:*x*Ce under e-beam excitation with nanosecond (a, b) and picoseconds pulse duration (c, d) for wavelengths at (a) 2.4 eV, (b) 2.19 eV, (c, d) 2.25 eV.

In this work, the application of the time-resolved spectroscopy technique and the high-current electron beam for luminescence excitation allows us to study fast processes of energy dissipation solids, including creation and relaxation processes of the electronic excitations.

This paper aims to study the cathodoluminescent properties (CL) of YAG powders under electron beam excitation with different pulse durations and electron energies (250 keV, pulse duration at FWHM ~ 15 ns and E_e = 55 keV, pulse duration at FWHM ~ 100 ps . A comparative analysis of CL properties of undoped YAG and YAG:Ce^{3+} phosphor powders is performed. The effect of excitation conditions, e.g. the energy of electrons, the electron pulse duration are shown to be important for understanding the luminescence mechanisms.

Published in:
E.Polisadova, D.Valiev, V.Vaganov, V.Oleshko, Tao Han, C.Zhang, A.Burachenko, A.I.Popov, Optical Mater. 96 (2019) 109289, DOI: 10.1016/j.optmat.2019.109289 (IF=2.687, SNIP=1.009)

The search for defects in undoped $SrAl_2O_4$ material

Virginija Vitola[a], Donats Millers[a,b], Krisjanis Smits[a], Ivita Bite[a], Aleksejs Zolotarjovs[a]

[a] *Institute of Solid State Physics, University of Latvia, Riga, Latvia*
[b] *ElGoo Tech*

$SrAl_2O_4$:Eu,Dy is a very efficient long afterglow phosphor with wide range of possible applications. The luminescence properties and the possible luminescence mechanism of this material have been studied extensively, but there is almost no information available about the undoped material. Therefore, this article deals with the luminescence and thermally stimulated luminescence of an undoped $SrAl_2O_4$, revealing the possible defects that might be involved in the creation of the long afterglow in doped material.

The analysis of luminescence is a helpful tool to understand the long lasting luminescence processes in Eu and Dy doped material. We report a clearly distinguishable luminescence of undoped $SrAl_2O_4$ material under X-ray excitation up to RT. The luminescence of undoped $SrAl_2O_4$ consists of two main parts – trace impurity metals, namely, Mn^{4+} and Cr^{3+} luminescence, and intrinsic defects luminescence – F - centers and F_2 - centers. The intensities of broad bands of this luminescence are low at RT due to partial quenching and narrow luminescence bands of Cr^{3+} became dominant. There is a strong possibility, that in the rare earth doped $SrAl_2O_4$ material these defects might be present as well and we propose that the presence of these defects is stimulating the Eu^{3+} ion incorporation.

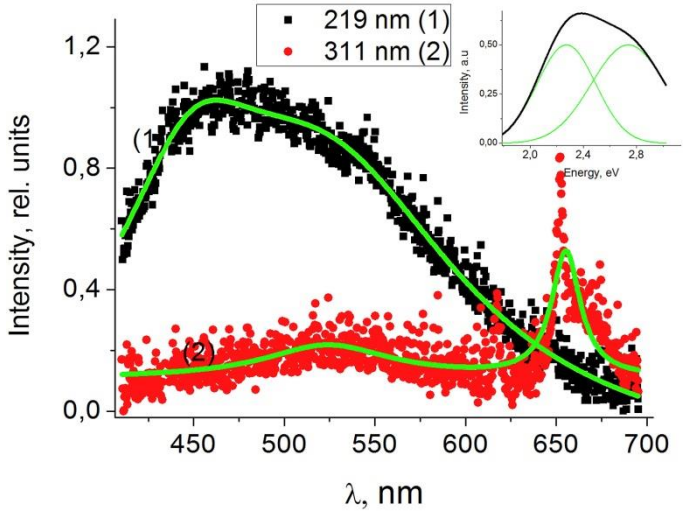

Photoluminescence spectra at 10 K under different excitation wavelengths.

The analysis of thermally stimulated luminescence glow peak shows two strong glow peaks – a peak under RT at ≈ 100 K, emerging from intrinsic defects of the $SrAl_2O_4$ crystal – it is important to note that this peak also is present in the doped materials, as well as a peak above RT at ~420 K that might be attributed to the defects perturbed by trace impurities; and it is also present in the doped material, but its position depends on the dopant incorporation.

Published in:
V. Vitola, D. Millers, K. Smits, I. Bite, A. Zolotarjovs, Optical Materials 87 (2019) 48-52.
DOI: 10.1016/j.optmat.2018.06.004 (IF=2.687, SNIP=1.009)

Photoconductivity & photoelectron emission of $LiGaO_2$ crystal excited in intrinsic absorption range

A.Trukhin, L.Trinkler

Institute of Solid State Physics, University of Latvia, Kengaraga Street 8, LV-1063, Riga, Latvia

$LiGaO_2$ (LGO) crystal is a material belonging to class of crystals with high degree of bond ionicity. This is a wide-band material (E_g around 6 eV) with yet insufficiently experimentally studied electronic structure. The electronic structure of wide-band dielectric materials can be studied using a comparison of photoelectric effects and photoluminescence excited in the intrinsic absorption region. When a dielectric is illuminated with light, two electrical effects may be observed - external photoelectron emission and photoconductivity.

The photoelectric response spectra were studied in a $LiGaO_2$ crystal. The obtained spectra were interpreted as the release and diffusion of charge carriers, as well as external photoemission of electrons. The charge carrier release starts from excitation with a photon with energy greater than the optical gap of the $LiGaO_2$ crystal (~6 eV). The efficiency of generation of charge carriers exponentially increases up to 8 eV with saturation beginning from 9 eV. The nature of the photoelectric response is attributed to the Dember effect corresponding to the higher mobility of electrons compared to the holes. The low yield of the internal photoeffect in the range of the intrinsic absorption band at 6 eV is associated with its exciton nature. Above 9.5 - 10 eV, an additional response was revealed, which was interpreted as external photoelectron emission with a threshold of about E_{th} = 10.1 ± 0.2 eV. The relative emission yield of electrons increases as $(h\nu - E_{th})^{1/3}$, which corresponds to indirect transitions between the valence and conductivity bands. The emission of photoelectrons for the direct band-to-band transitions increases linearly with the photon energy and the corresponding threshold is defined as 12.7 ± 0.2 eV. The affinity of electrons is estimated as 2.5 eV.

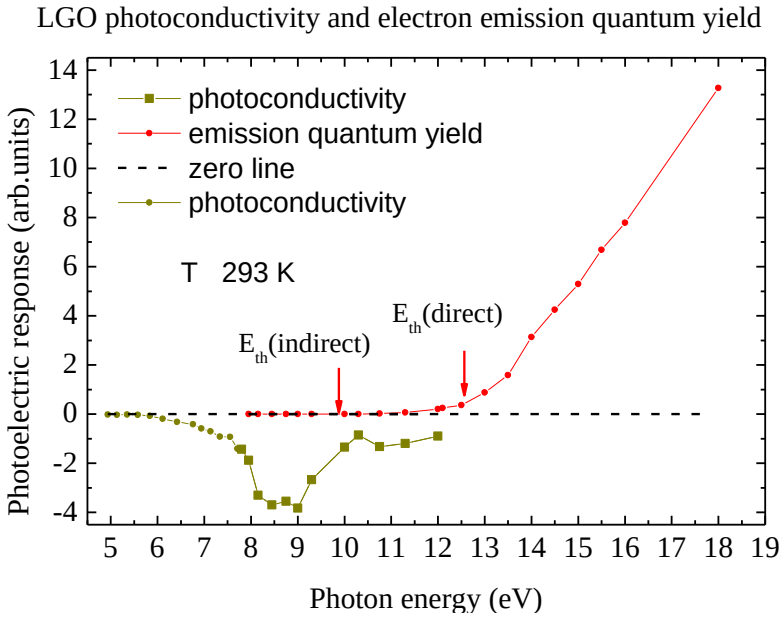

Spectra of photoelectric response of $LiGaO_2$ crystal sample.

Published in:
A.Trukhin, L. Trinkler, Optical Materials 93 (2019) 11-14. DOI: 10.1016/j.optmat.2019.05.005 (IF=2.687, SNIP=1.009)

Eu^{3+} ion distribution in oxyfluoride glass nanocomposites

A. Antuzevics, G. Krieke, E. Pavlovska, U. Rogulis

Institute of Solid State Physics, University of Latvia, 8 Kengaraga Str., LV-1063 Riga, Latvia

Assessment of activator distribution in lanthanide doped nanocomposites is an important and challenging task. In this work oxyfluoride glass ceramics have been chosen as a model system to characterize incorporation efficiency of Eu^{3+} ions in CaF_2 nanocrystals using a combination of X-ray diffraction (XRD) and electron paramagnetic resonance (EPR) techniques.

The linear dependence of CaF_2 lattice parameter on Eu^{3+} dopant concentration has been used to determine the distribution of activators in glass ceramics. For the investigations of non-magnetic Eu^{3+} ions via EPR spectroscopy, paramagnetic probe ions can be introduced to glass ceramics. Gd^{3+} probe local structure is modified by the addition of Eu^{3+} in CaF_2. At low concentration range of europium, the ratio of tetragonal-to-cubic CaF_2:Gd^{3+} EPR signals proved to be more sensitive towards changes of the concentration, while at higher concentrations of europium the broadening of the spectrum seems to be more appropriate for the evaluation of Eu^{3+} content. Both effects can be applied to evaluate the content of Eu^{3+} in the nanocrystals present in glass ceramics and up to 5 mol% are in a good agreement with the estimations from XRD.

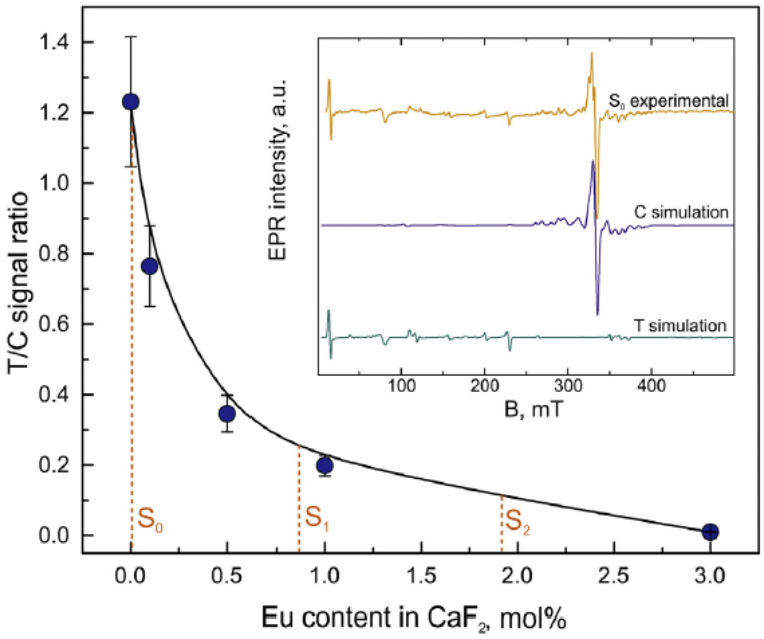

Analysis of Eu^{3+} concentration in the CaF_2 phase of glass ceramics based on Gd^{3+} probe EPR spectra.

The proposed method based on EPR spectroscopy is an excellent alternative for the investigation of materials in cases when typical methods cannot be applied, such as crystals with similar activator and host matrix ionic radii implying insignificant changes of lattice parameters.

Published in:
A. Antuzevics, G. Krieke, E. Pavlovska, U. Rogulis, Eu^{3+} ion distribution in oxyfluoride glass nanocomposites, J. Non-Cryst. Solids 522 (2019) 119548. DOI: 10.1016/j.jnoncrysol.2019.119548 (IF=2.600, SNIP=1.177)

Luminescence of localized states in oxidized and fluorinated silica

A.N. Trukhin

Institute of Solid State Physics, University of Latvia, Kengaraga Street 8, LV-1063, Riga, Latvia

Localized states are a specific property of a disordered system. We can say that in the case of optical glasses, localized states are defects (traps) of the basic structure of glass. The value of the category "defect" should be wider than a point defect. Mott stated that there is no transport between these traps (defects), despite overlapping wave functions. Currently, the problem lies in the fact that localized states and intrinsic point defects are still not well distinguished, and there are several models for them. Thus, in the energy band model, localized states are described as traps located below the conduction band and above the valence band, having an increased density of states near the bottom of the conduction band and at the top of the valence band. A point defect in this approach is a single level in the band gap. Localized states were studied in silica samples with a strong oxygen deficiency and, accordingly, high optical absorption in the optical gap. The main conclusion of these studies is the excitation of recombination luminescence of an electron trapped at oxygen-deficiency centers (ODC) and a self-trapped hole (STH).

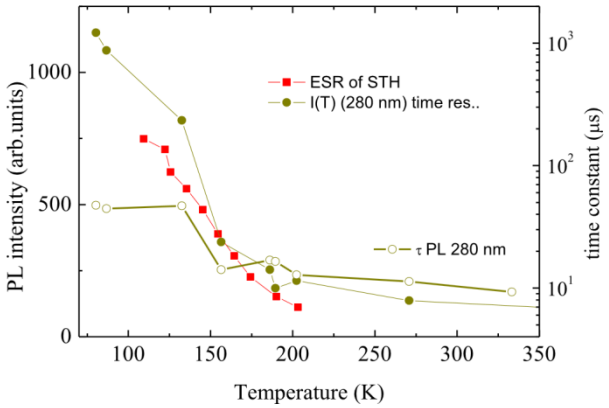

Correlation of temperature dependences of STH signal and PL intensity & time constant for UV luminescence of KC4B silica type IV under F_2 laser. The PL band at 280 nm is due to singlet-singlet transitions in ODC.

The problem lies in the properties of localized states in pure silica obtained under normal or oxidized conditions. There may be traces of states located below the optical gap, and the search and study of these states is the task of this work. Such low density states can play a crucial role in the elementary processes responsible for initiating many photostimulated reactions. For example, solarization of optical fibers produced from silicon dioxide. In the samples studied the ODC luminescence exhibits decay kinetics that differs from those of an ODC (II) point defect or two-coordinated silicon.

Recombination luminescence is associated with recombination between a STH and an electron trapped at an ODC defect. The thermally stimulated luminescence curve is in the range of STH release. The thermally released hole moves and recombines with an electron trapped at ODC.

Therefore, despite the reduced optical absorption of samples with a high content of oxygen or fluorine, the same processes of release, capture and recombination of electrons and holes are observed, as in silica with a high oxygen deficiency. The hole is mostly self-trapped, and electrons are trapped in oxygen-deficient centers.

Published in:
A.N.Trukhin, J. Non-Cryst. Solids. 521 (2019) 119525. DOI: 10.1016/j.jnoncrysol.2019.119525 (IF=2.600, SNIP=1.177)

Photoelectric response of localized states in silica glass

A.N. Trukhin

Institute of Solid State Physics, University of Latvia, Kengaraga Street 8, LV-1063, Riga, Latvia

The localized states of silica glass have been proved only in recent decades, but their existence is predicted by the general properties of disordered materials. It was found that when the localized states of silicon dioxide are excited, the holes appear as self-trapped, and the electrons are trapped in the so-called oxygen deficient center (I) or ODC(I). Earlier it was noted that the concentration of self-trapped hole centers increases with increasing oxygen deficiency. Recombination of a hole with an electron on the ODC (I) provides luminescence of the modified oxygen deficient center. Thus, the excitation of localized states predicts some electrical activity associated with the possible release of charge carriers. Then, it is necessary to study the photoelectric response of the insulator.

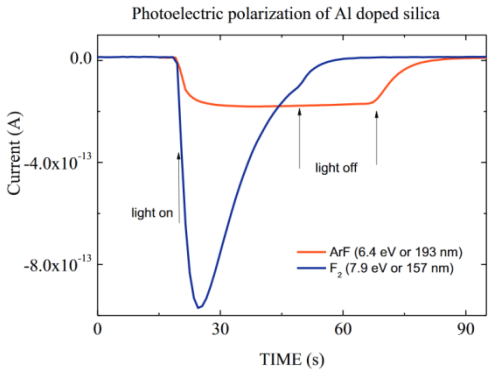

Photoelectric polarization of Al doped silica at 293 K. The sign of the photoelectric response is defined as charge carriers with a higher diffusion capacity. It depends on the nature of the traps. Aluminum in silica effectively absorbs holes, and then the sign of the signal is negative because of the prevailing diffusion of the electron.

When the insulator is illuminated with light, two electrical effects can be observed - external photoelectron emission and photoconductivity. Photoconductivity is associated with the release of charge carriers and their movement in the volume of materials. Typically, the current in the external circuit is provided by shifting the carriers a distance to recombination or capture. The main processes that determine the internal photoelectric effect are the diffusion of charge carriers and their trapping in traps. In the case of a strong difference in the values of the diffusion coefficient of electrons relative to the hole, their separation occurs in space, and as a result, an electric field appears in the bulk of the insulator (Dember field). The trapping of carriers on traps induces a space charge. The space charge field prevents the carriers from moving. The space charge can stop the current in the external circuit. Then, on the light pulse of the Π-form, we obtain a damped photoelectric response during the light pulse.

Now experiments are conducted with pure silica samples. The main attention was paid to samples with a small optical absorption below the optical gap (~ 8 eV It is found that, despite the low absorption coefficient of samples of pure silica glass, excitation by means of excimer lasers ensures the release of charge carriers. Electron and holes are released, diffused and trapped in all studied samples. Trapping leads to space charge creation limiting mobility of the released electrons and holes. Therefore, excited localized states of silica provide mobile charge carriers upon excitation.

Published in:
A.N.Trukhin, J. Non-Cryst. Solids. 511 (2019) 161-165. DOI: 10.1016/j.jnoncrysol.2019.02.002 (IF=2.600, SNIP=1.177)

Glass-forming non-symmetric bis-styryl-DWK-type dyes for infra-red radiation amplification systems

Elmars Zarins[a], Julija Pervenecka[b], Aivars Vembris[b], Valdis Kokars[a]

[a] *Institute of Applied Chemistry, Riga Technical University, 3/7 Paul Walden Str., LV, 1048, Riga, Latvia*

[b] *Institute of Solid State Physics, University of Latvia, 8 Kengaraga Str., LV, 1063, Riga, Latvia*

Thermal and optical properties and their relations with chemical structures of a series of glass-forming non-symmetric DWK-type dyes have been investigated. Incorporating a substituent with an electron donor, electron acceptor and neutral electron affinities in 4-position within the 6-styryl-fragment considerably affected DWK dye optical properties while thermal characteristics were influenced mostly by the electron acceptor at 4-position in 4H-pyrane ring. Thermal stability of dyes with malononitrile (DWK) and indene-1,3-dione (ZWK) electron acceptors was by about 20–30 °C higher in comparison with barbituric acid (JWK) containing compounds (T_d from 237 to 286 °C), however, no clear relation between compound chemical structure and glass transition temperature could be established. Introducing substituents with stronger electron withdrawing properties in 4-position within the 6- styryl-fragment in non-symmetric bis-styryl DWK dyes leads to a bathochromic shift of photoluminescence and ASE maxima in their neat films reaching the IR region (λ_{PL}=700 nm and λ_{ASE}=743 nm for DWK-8) in addition to reducing their ASE excitation threshold values (E_{th}) up to 180 μJ/cm^2 for DWK-8. More physical property studies are required, but some of the investigated non-symmetric bis-styryl-DWK-dyes show potential as promising low-cost solution processable materials for IR radiation amplification.

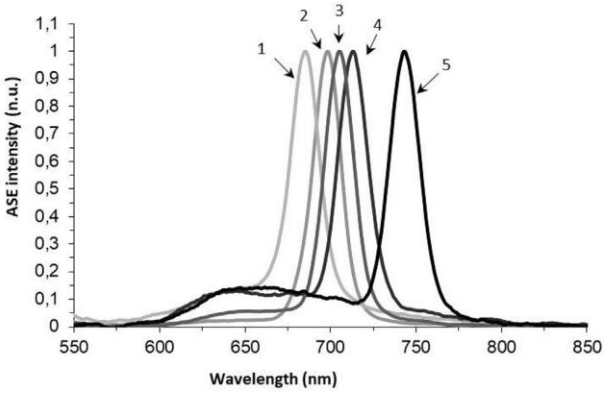

Amplified spontaneous emission of investigated dyes. 1 – DWK-4 ; 2 – DWK-3; 3 – DWK-6; 4 – DWK-5; 5 – DWK-8.

Published in:
E. Zarins, J. Pervenecka, A. Vembris, V. Kokars, Optical Materials 93 (2019) 85-92. DOI: 10.1016/j.optmat.2019.05.002. (IF=2.023, SNIP=1.01)

IV. Materials for energy harvesting and storage, clean energy transformation.

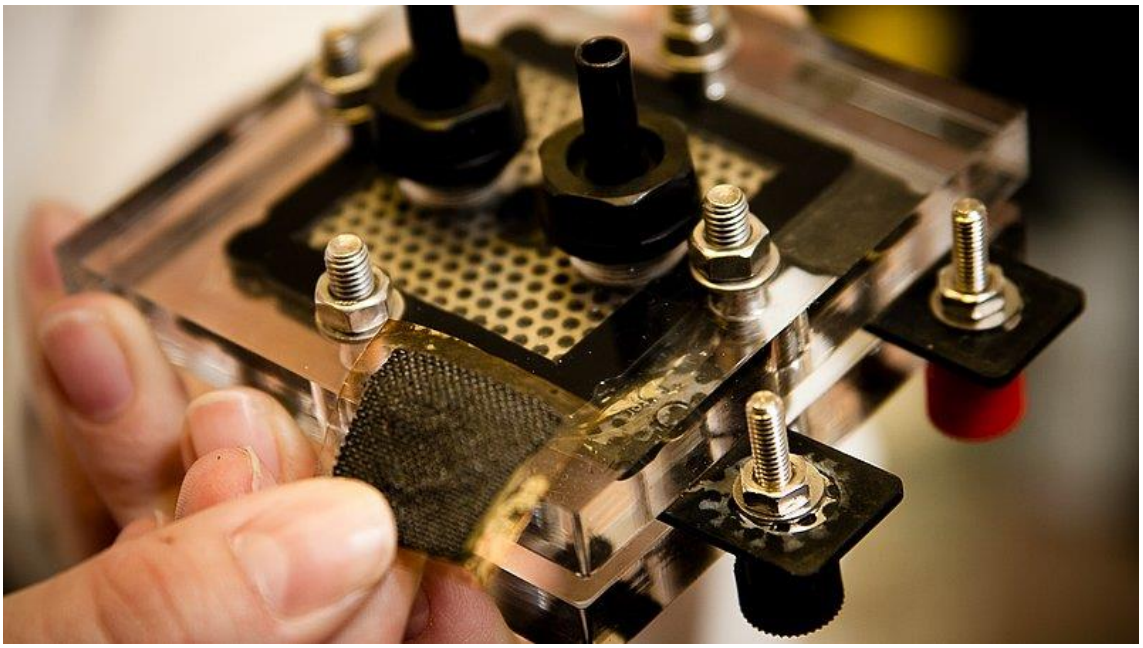

How does graphene enhance the photoelectric conversion efficiency of dye sensitized solar cells? An insight from a theoretical perspective

J.Y. Xi[a], Ran Jia[a], W. Li[a], J. Wang[a], F.Q. Bai[a], Roberts I. Eglitis[b], H.X. Zhang[a]

[a]*Laboratory of Theoretical and Computational Chemistry, Institute of Theoretical Chemistry, Jilin University, 130023 Changchun, PR China*
[b]*Institute of Solid State Physics, University of Latvia, 8 Kengaraga Str., Riga LV1063, Latvia*

The main goal of this work is to clearly answer the question from a theoretical perspective: how does graphene enhance the photoelectric conversion efficiency in the semiconducting layer of a dye sensitized solar cell? Several arrangements of the graphene layer between the dye molecule and the TiO_2 (101) surface are carefully studied and discussed.

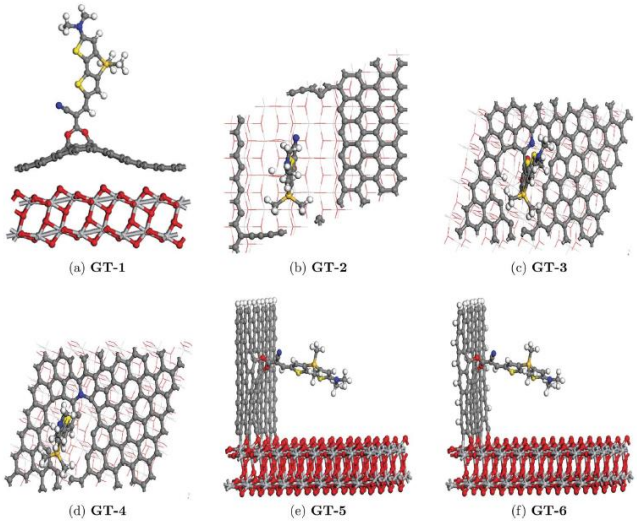

Sketches of the simulation models.

The dynamic interfacial electron propagations are simulated with consideration of the underlying nuclear motion effect. Theoretical investigation shows that graphene can speed up the electron injection from the dye molecules to the semiconductor layer, only when the graphene sheet is bonded to the TiO_2 surface via C–Ti bonds. The excited electrons of the dye molecules on the graphene sheet will be rapidly injected into the semiconducting layer. Additionally, if the graphene sheet is parallel to the TiO_2 surface, the free electrons on graphene can only hop onto the TiO_2 surface in a relatively long tunneling period. Therefore, graphene in this case mainly plays the role of a shielding layer for preventing the recombination of the electrons injected into TiO_2 and the electron holes remaining on the dye molecules or in the electrolyte. The combination of these two mechanisms indicates that graphene layers in the proper conformation can effectively improve the photoelectric conversion efficiency of a dye sensitized solar cell.

Published in:
J.Y. Xi, Ran Jia, W. Li, J. Wang, F.Q. Bai, Roberts I. Eglitis, H.X. Zhang, J. Mater. Chem. A 7 (2019) 2730-2740. DOI: 10.1039/c8ta06872k (IF = 10.737, SNIP=1.621)

Theoretical and Experimental Study of $(Ba,Sr)TiO_3$ Perovskite Solid Solutions and $BaTiO_3/SrTiO_3$ Heterostructures

L.L. Rusevich[a], G. Zvejnieks[a], E.A. Kotomin[a], M. Maček Kržmanc[b], A. Meden[c], Š. Kunej[b], I.D. Vlaicu[d]

[a] *Institute of Solid State Physics, University of Latvia, 8 Kengaraga str., Riga LV-1063, Latvia*
[b] *Advanced Materials Department, Jožef Stefan Institute, Jamova 39, 1000 Ljubljana, Slovenia*
[c] *Faculty of Chemistry and Chemical Technology, University of Ljubljana, Večna pot 113, Ljubljana 1001, Slovenia*
[d] *National Institute of Materials Physics, 405A Atomistilor Street, Magurele-Ilfov, 077125-Romania*

Nowadays development of devices for energy storage applications, for the harvesting and mutual transformations of mechanical and electrical energies is of great interest. In this respect, the utilizing of piezoelectricity is the efficient way, and, therefore, ferroelectric perovskites are important materials for many technological applications.

In this study, the results of joint experimental and theoretical study of structural and piezoelectric properties of $(Ba,Sr)TiO_3$ perovskite solid solutions are discussed and compared. Experimentally, complex perovskite plate-like $(Ba,Sr)TiO_3$ particles were synthesized by the topochemical conversion in the molten salt from $Bi_4Ti_3O_{12}$ template plates. All dimensions (side length ≈ 1 µm, thickness ≈ 200–400 nm) were well above the critical size necessary for observation of piezo- and ferroelectricity. The first-principles computations of the structural and electromechanical properties of solid solutions were performed with CRYSTAL14 computer code within the linear combination of atomic orbitals (LCAO) approximation, using three advanced hybrid functionals of the density-functional-theory (DFT). Different chemical compositions are considered for the ferroelectric and paraelectric phases.

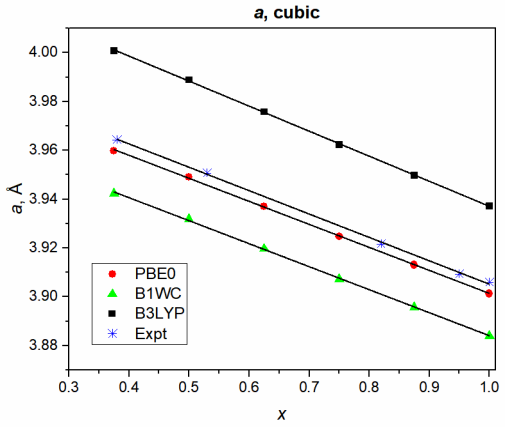

Theoretical and experimental dependences of lattice constant a vs chemical compositions x for the cubic phase of BSTO. The lines demonstrate linear fitting.

The calculated structural properties of solid solutions in tetragonal and cubic phases are in a very good agreement with experimental data. Experimentally obtained and calculated band gaps are compared for cubic $SrTiO_3$ and tetragonal $BaTiO_3$. $BaTiO_3/SrTiO_3$ heterostructures were considered theoretically for different chemical compositions. The calculated piezoelectric properties of solid solutions and heterostructures in ferroelectric phase are compared. It is predicted that both solid solution and heterostructure improve the piezoelectric properties of the bulk $BaTiO_3$, but solid solution is more preferable for equal Sr concentrations.

Published in:
L.L. Rusevich, G. Zvejnieks, E.A. Kotomin, M. Maček Kržmanc, A. Meden, Š. Kunej, I.D. Vlaicu, J. Phys. Chem. C 123 (2019) 2031-2036. DOI: 10.1021/acs.jpcc.8b09750 (IF=4.309, SNIP=1.083)

First-principles comparative study of perfect and defective halide perovskite crystals

E. A. Kotomin[a,b], R. A. Evarestov[c], A. Senocrate[b], J.Maier[b]

[a] *Institute of Solid State Physics, Kengaraga str. 8, LV-1063 Riga, Latvia*
[b] *Max Planck Institute for Solid State Research, Stuttgart, Germany*
[c] *Institute of Chemistry, St.Petersburg State University, Petrodvorets, Russia*

Halide perovskites have attracted great interest as light absorbers for photovoltaic applications. Among these materials, hybrid organic-inorganic systems based on methylammonium and/or formamidinium lead iodide have shown the highest performances in solar cell devices. Such hybrid compositions, however, suffer from high instability under operation. One currently explored alternative is to move to the fully inorganic $CsPbX_3$ (with X=I, Br), as these compounds could potentially fulfill both performance and stability criteria.

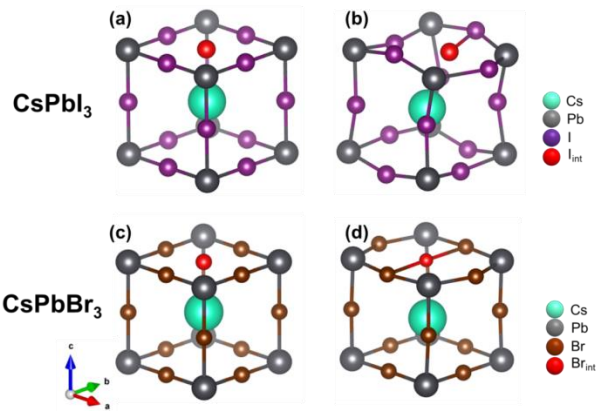

Comparison between the structure of $CsPbI_3$ and $CsPbBr_3$ with the addition of an interstitial halide atom. Structure **(a), (c)** before and **(b), (d)** after optimizing geometry.

However, many aspects regarding the stability of these inorganic materials, as well as the influence of ionic defects on their properties have yet to be thoroughly investigated experimentally and theoretically. Indeed, so far most of theoretical studies on the atomic and electronic structure of halide perovskites were focused of defect-free materials, inorganic as well as hybrid organic-inorganic compositions. However, due to the low temperature fabrication, and also the fact that these materials are mixed ionic-electronic conductors, one could expect a considerable concentration of ionic defects in these systems. However, despite their potential role in influencing electronic transport and device performance, there are only a few investigations of point defects in Cs compounds.

First principles DFT hybrid functional PBESOL0 calculations of the atomic and electronic structure of perfect $CsPbI_3$, $CsPbBr_3$ and $CsPbCl_3$ crystals, as well as defective $CsPbI_3$ and $CsPbBr_3$ crystals were performed and discussed. For the perfect structure, decomposition energy into binary compounds (CsX and PbX_2) are calculated, and a stability trend $CsPbBr_3$>$CsPbI_3$>$CsPbCl_3$ is found. In addition, calculations of the temperature-dependent heat capacity are performed and shown to be in good agreement with experimental data. As for as the defect structure is considered, it is shown that interstitial halide atoms in $CsPbBr_3$ do not tend to form di-halide dumbbells Br_2- while such dimers are energetically favoured in $CsPbI_3$, analogous to the well-known H-centers in alkali halides. In the case of $CsPbBr_3$, a loose trimer configuration Br_3(2-) seems to be energetically preferred. The effects of crystalline symmetry and covalency are discussed as well as the role of defects in recombination process.

Published in:
R.A. Evarestov, A. Senocrate, E.A. Kotomin, J. Maier, Phys. Chem. Chem. Phys. 21 (2019) 7841-7846.
DOI: 10.1039/c9cp00414a (IF=3.567, SNIP=0.981)

Interface-induced enhancement of piezoelectricity in the $(SrTiO_3)_m/(BaTiO_3)_{M-m}$ superlattice for energy harvesting applications

G. Zvejnieks, L. L. Rusevich, D. Gryaznov, E. A. Kotomin

Institute of Solid State Physics, University of Latvia, Kengaraga Street 8, LV-1063, Riga, Latvia

The interplay between ferroelectric and anti-ferrodistortive displacements is carefully analyzed for the $(SrTiO_3)_m/(BaTiO_3)_{M-m}$ heterostructure using the 3D STO_m/BTO_{M-m} superlattice model. Thus, impact of such displacements on the piezoelectric properties is determined. Based on group theoretical analysis and density functional calculations, we deduce two possible space groups of tetragonal symmetry which allow us to reproduce the experimentally known pure STO and BTO bulk phases and to model corresponding intermediate superlattices. The density functional calculations are due to the method of linear combination of atomic orbitals and hybrid (B1WC) exchange correlation functional as implemented in CRYSTAL computer code. The characteristic feature of the space group P4mm (#99) is atomic displacement in the [001] direction which allows us to simulate the ferroelectric (FE) displacement (figure). The space group P4 (#75), besides the FE displacement, permits also oxygen octahedral antiphase rotations around the [001] direction and, thus, the anti-ferrodistortive (AFD) atomic displacement observed in STO at low temperatures.

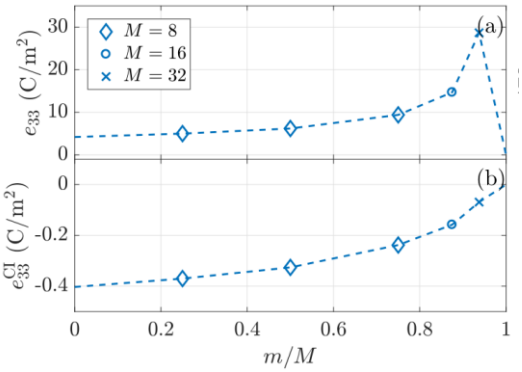

Figure. Direct piezoelectric constant for the P4 model calculated with atomic position relaxation e_{33} (a) and without atomic position

Our hybrid density functional calculations demonstrate that for $m/M \leq 0.75$ both the tetragonal models show similar geometries and piezoelectric constants. Moreover, both the models predict an approximately 6-fold increase of the piezoelectric constant e_{33} (figure) compare to the BTO bulk value. The obtained calculation results clearly demonstrate that piezoelectricity arises due to the coordinated collective FE displacements of atoms in both STO and BTO slabs and interface. The piezoelectric constant is at its maximum value when the superlattice consists of even a single or double layer of BTO which is sufficient to trigger FE displacement in the STO slab, in P4mm and P4 models, respectively. The purely electronic contribution to the piezoelectric constant e_{33}^{CI} (without atomic relaxation) is calculated using the "clamped-ion" approximation (figure). It is negative and by almost an order of magnitude smaller than e_{33} of bulk BTO phase. It tends to zero with an increase of the number of STO layers. Thus, the electronic contribution alone cannot explain an enhancement of e_{33} in the STO/BTO heterostructure with the number of STO layers.

Published in:
G. Zvejnieks, L. L. Rusevich, D. Gryaznov, E. A. Kotomin, Phys. Chem. Chem. Phys. 21 (2019) 23541-23551, DOI: 10.1039/c9cp04086b (IF=3.561, SNIP=0.981)

First-principles calculations on CeO_2 doped with Tb^{3+} ions

A. Chesnokov, D. Gryaznov, E. A. Kotomin

Institute of Solid State Physics, University of Latvia, Kengaraga Street 8, LV-1063, Riga, Latvia

Ceria (CeO_2) is important technological material with numerous applications, e.g. in fuel cells. The atomic and electronic structure of CeO_2 doped with Tb has been calculated from first principles with inclusion of the strong electron correlation effects on the basis of Hubbard model (DFT+U) as implemented in VASP code. The supercell model with 96 atoms was used. If one Tb atom replaces Ce and one oxygen atom removed, it leads to the concentration of Tb ~3% and oxygen stoichiometry deviation δ = 0.03. The two values of Hubbard U-parameter were applied separately on Ce and Tb ions, in order to treat correctly two oxidation states of Tb (3+ and 4+). Calculations with and without oxygen vacancies were performed. The corresponding total energy difference between the 3+ and 4+ states is very small in the absence of oxygen vacancy and, thus, these states can co-exist without oxygen vacancy formation (unlike Gd doping). Moreover, the presence of the electronic holes was observed and associated with the increased density of O 2p states at the Fermi energy for Tb^{3+} in comparison with Tb^{4+}.

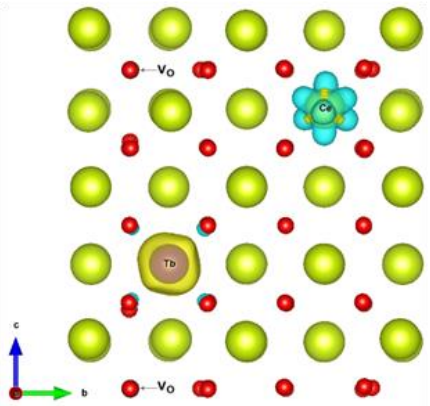

Figure. Spin density map for two electrons from a missing oxygen atom localized on two cations.

The oxygen vacancy in CeO_2 doped with Tb ions leads to multiple configurations with localization of electrons left from a missing oxygen atom on different number of cations. This is why we performed a careful site symmetry analysis to identify the ground state configuration with respect to the spin projection. In order to reach this goal, the Gibbs formation energy of oxygen vacancy due to Tb doping was calculated as well. The dependence of Gibbs formation energy on the temperature and oxygen partial pressure was obtained. The Gibbs formation energy is reduced, by almost a factor of four, at standard pressure and 400 K for the ground state configuration, in a comparison with the undoped CeO_2. It is the configuration with the localization on two cations as shown in Figure and, thus, shows the formation of small polarons. The lowest formation energy for the small polaron occurs when the Ce^{3+} is the third nearest neighbor whereas Tb^{3+} ion is the first nearest neighbors to oxygen vacancy. Spin density map in Figure clearly shows the effect of localization on 4f orbitals of Tb^{3+} and Ce^{3+}. The formation energy changes from 0.66 eV to 2.58 eV for different defect configurations, depending on the degree of localization and number of cations.

Published in:
A. Chesnokov, D. Gryaznov, E. A. Kotomin, Optical Materials 90 (2019) 76-83. DOI: 10.1016/j.optmat.2019.02.016 (IF=2.687, SNIP=1.009)

Fast-neutron-induced and as-grown structural defects in magnesium aluminate spinel crystals with different stoichiometry

V.Seeman[a], E.Feldbach[a], T.Kärner[a], A.Maaroos[a], N.Mironova-Ulmane[b], A.I.Popov[b], E.Shablonin[a]. E.Vasil'chenko[a], A.Lushchik[a]

[a] *Institute of Physics, University of Tartu, W. Ostwald Str. 1, 50411, Tartu, Estonia*

[b] *Institute of Solid State Physics, University of Latvia, Kengaraga Street 8, LV-1063, Riga, Latvia*

Magnesium aluminate spinel is a fascinating material used for various applications in science and technology. Of particular interest is a high resistance of $MgAl_2O_4$ against prolonged and dense irradiation. In particular, there is practically no swelling of Mg-Al spinel even after heavy irradiation with fast neutrons, and, therefore, $MgAl_2O_4$ can be used in the environment of the future fusion reactors. Presently, the search for materials with diagnostics window capabilities in fusion devices is an urgent task within the research programs of the EUROfusion consortium. Several oxides, in particular MgO, Al_2O_3 and their equimolar mixture – $MgAl_2O_4$ single crystals and transparent ceramics have been considered as attractive candidates for diagnostics/optical windows in future fusion.

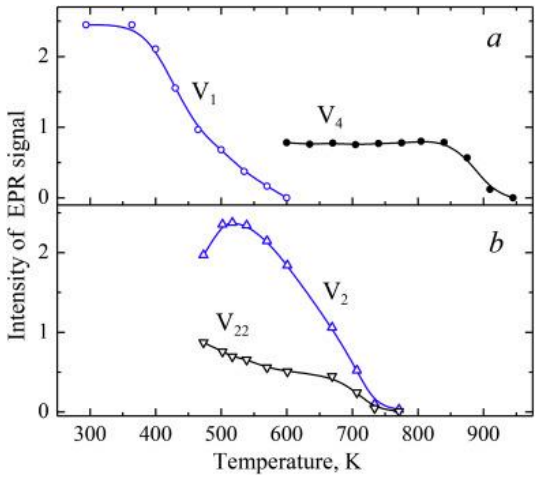

Pulse annealing of the EPR signal of the V_1 and V_4 as well as V_2 and V_{22} centers in neutron-irradiated $MgO{\cdot}2.5Al_2O_3$ (*a*) and $MgAl_2O_4$ (*b*) single crystals.

The present study was devoted to the correlation between novel paramagnetic intrinsic radiation defects and relevant radiation-induced absorption bands in stoichiometric $MgAl_2O_4$ single crystals irradiated with fast fission neutrons. A special attention is paid to the investigation of intrinsic structural defects and their thermal annealing in fast-neutron-irradiated nonstoichiometric $MgO{\cdot}2.5Al_2O_3$ single crystals using the methods of EPR, optical absorption and cathodoluminescence. Several hole-type paramagnetic defects (a hole localized at a regular oxygen ion near charged structural defect/defects) have been revealed in fast-neutron-irradiated $MgO{\cdot}2.5Al_2O_3$ single crystals using the EPR method. Three of them (a dominant V_1 and small amount of V_2 and V_{22}) were recently revealed in a neutron-irradiated stoichiometric $MgAl_2O_4$, while a novel V_4 center, ascribed to a hole in a form of O^- ion nearby a complex of a magnesium vacancy and a positively charged antisite defect ($V_4 \equiv O^-$-V_{Mg}-$Al|_{Mg}$), was created by fast neutrons only in a nonstoichiometric single crystal. The pulse annealing of the EPR signal of these centers was compared to that of radiation induced optical absorption in the same crystals. The EPR and optical characteristics of the holes localized near as-grown structural defects in X-ray irradiated 1:1 and 1:2.5 Mg-Al spinel crystals were compared as well. The tentative scenario of the thermal annealing process of neutron-induced defects (hole-type and complementary electron F-type ones) in $MgO{\cdot}2.5Al_2O_3$ was considered.

Published in:

V.Seeman, E.Feldbach, T.Kärner, A.Maaroos, N.Mironova-Ulmane, A.I.Popov, E.Shablonin. E.Vasil'chenko, A.Lushchik, Optical Mater. 91 (2019) 41-49, DOI: 10.1016/j.optmat.2019.03.008 (IF=2.687, SNIP=1.009)

Interaction of carbon with microstructural defects in a W-Re matrix: An ab initio assessment

A. Bakaev[a,b], A. Zinovev[a,c], D. Terentyev[a], G. Bonny[a], C. Yin[a], N. Castin[a], Yu. A. Mastrikov[d], E. E. Zhurkin[b]

[a] *SCK•CEN, Nuclear Materials Science Institute, Boeretang 200, Mol B-2400, Belgium*
[b] *Peter the Great St. Petersburg Polytechnic University (SPbPU), Polytechnicheskaya 29, St.Petersburg 195251, Russia*
[c] *Institute of Mechanics, Materials and Civil Engineering (iMMC), Université catholique de Louvain, av. Georges Lemaître 4, B-1348 Louvain-la-Neuve, Belgium*
[d] *Institute of Solid State Physics, University of Latvia, Kengaraga str. 8, LV-1063 Riga, Latvia*

The interaction of carbon atoms with point defects and the core of edge and screw dislocations with Burgers vector $a_0/2<111>$ in W and a W-Re matrix is studied by means of ab initio calculations. The structure and energetics of the ground-state atomic configurations are presented and rationalized. It is found that di-vacancies, which are thermally unstable in pure W according to the state-of-the-art *ab initio* calculations, can nucleate at C and Re-C complexes, which fill the gap in the explanation of the emergence of nanovoids observed experimentally under irradiation. Also, on the basis of the recent experimental evidence and our calculations, the temperature ranges for the manifestation of the yield drop phenomenon, which is related to the obstruction of dislocation motion due to their decoration by impurities such as carbon, are revealed.

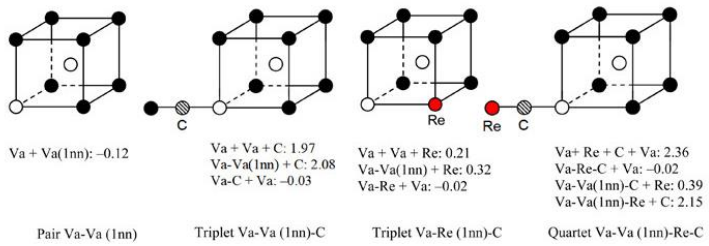

Selected configurations of divacancy (white) as 1NN in a combination with rhenium (red) and carbon (dashed) solute atoms in tungsten (black) host matrix.

While the DFT calculations predict the repulsion of the di-vacancy complexes in pure W, the experimental analysis of the thermal annealing of electron-irradiated tungsten samples has shown the nucleation of vacancy clusters at about 600–700 K, which dissolve at the temperatures of about 1000-1150 K as revealed by the analysis of the annealed up to 1900K tungsten samples after the irradiation by 30 keV 1×10^{20} D_2^+ m^{-2} ions. Our *ab initio* simulations explain this experimental data by proposing a mechanism, which can glue the di-vacancies together and allow further growth of the larger vacancy clusters. The obtained sets of binding energies for C atoms with edge and screw dislocations in W were also used to estimate the temperature ranges for C de-trapping from dislocations.

The exact values of interaction strength for C at point defects and dislocations, calculated in this work, are essential to parameterize reliable Object Kinetic Monte Carlo (OKMC) models of the evolution of microstructure in W under neutron- or ion irradiation.

Published in:
A. Bakaev, A. Zinovev, D. Terentyev, G. Bonny, C. Yin, N. Castin, Yu. A. Mastrikov, E. E. Zhurkin, J. Appl. Phys. 126 (2019) 075110. DOI: 10.1063/1.509444 (IF=2.328, SNIP=0.815)

Synthesis and investigation of charge transport properties in adducts of hole transporting carbazole derivatives and push-pull azobenzenes

Armands Ruduss[a], Kaspars Traskovskis[a], Aivars Vembris[b], Raitis Grzibovskis[b], Kaspars Pudzs[b], Marcis Lielbardis[b], Valdis Kokars[a]

[a] *Institute of Applied Chemistry, Riga Technical University, 3/7 Paula Valdena Str., Riga, LV-1048, Latvia*

[b] *Institute of Solid State Physics, University of Latvia, 8 Kengaraga Str., Riga, LV-1063, Latvia*

Novel 3-(diphenylamino)carbazolyl-functionalized derivatives of DMAAzi (DZC-1, DZC-2 and DZC-3) were synthesized. Thermal and photoelectrical properties of the synthesized compounds were compared to a trityl-functionalized DMAAzi chromophore (DZTr). All of the synthesized compounds exhibit an intensive absorption in the visible part of the spectra, a sufficient thermal stability and form thin amorphous films from volatile solvents. The obtained results show that with the introduction of bulky carbazole groups glass transition temperatures of materials were slightly increased compared to the trityl-functionalized DZTr. A significant effect of the 3-(diphenylamino)carbazolyl-groups on the molecule energy level structure and charge transporting properties was observed. With the introduction of electron-rich carbazole moieties a decrease of molecular ionization energy by 0.16–0.20 eV compared to DZTr was measured. Contrary, electron affinity level is destabilized with the introduction of these groups. Although, a positive effect on the hole transporting properties thereby would be anticipated, results show no improvement of hole drift mobility compared DZTr. The hole mobilities of the investigated carbazole functionalized compounds vary in range from 1.2×10−6 to 4.4×10−7 cm2/V s at an electric field of 8.1×105 V/cm. The characterization of charge carrier local trapping states revealed a formation of deep trap levels for DZC-1, DZC-2 and DZC-3 with local energy states at approximately 0.78 eV; 0.72 eV and 0.60 eV, respectively. It was concluded, that hole transporting 3-(diphenylamino) carbazolyl-groups in the bulk of the material are relatively isolated therefore obstructing hole transport via hopping mechanism and forming deep trap levels. The electron mobilities of the carbazole functionalized compounds vary in a larger range from the order of 10−5 to 10−8 cm2/V s at an electric field of 8.1×105 V/cm, with a considerable decrease observed after the introduction of additional 3-(diphenylamino)carbazolyl-group. The investigated materials exhibit suitable thermal and light absorption properties, but the low hole mobility severely hinders the potential application of synthesized compounds as donor materials in BHJ solar cells. Although, the holes are stabilized at the carbazole moiety, a charge transporting ability is obstructed by the low hole mobility of these materials.

Published in:
A. Ruduss, K. Traskovskis, A. Vembris, R. Grzibovskis, K. Pudzs, M. Lielbardis, V. Kokars, J. Phys. Chem. Solids 127 (2019) 178-185. DOI: 10.1016/j.jpcs.2018.12.019 (IF=2.048, SNIP=0.95)

Publications 2019
with authorship of ISSP UL in
Web of Science and Scopus Databases

1. **Manika, I., Maniks, J., Zabels, R., Grants, R., Kuzmin, A**., Schwartz, K.
Depth profiles of damage creation and hardening in MgO irradiated with GeV heavy ions
(2019) Nuclear Instruments and Methods in Physics Research, Section B: Beam Interactions with Materials and Atoms, 461, pp. 77-82.
DOI: 10.1016/j.nimb.2019.09.026
SNIP (2018)= 0,777

2. **Nitiss, E., Bundulis, A., Tokmakovs, A., Busenbergs, J., Rutkis, M.**
All-Organic Waveguide Sensor for Volatile Solvent Sensing
(2019) Photonic Sensors, 9 (4), pp. 356-366.
DOI: 10.1007/s13320-019-0543-z
SNIP (2018)= 0,884

3. **Platonenko, A.,** Gentile, F.S., Maul, J., Pascale, F., **Kotomin, E.A.,** Dovesi, R.
Nitrogen interstitial defects in silicon. A quantum mechanical investigation of the structural, electronic and vibrational properties
(2019) Materials Today Communications, 21, art. no. 100616.
DOI: 10.1016/j.mtcomm.2019.100616
SNIP (2018)= 0,686

4. Schenk, T., **Anspoks, A., Jonane, I., Ignatans, R.,** Johnson, B.S., Jones, J.L., Tallarida, M., Marini, C., Simonelli, L., Hönicke, P., Richter, C., Mikolajick, T., Schroeder, U.
Local structural investigation of hafnia-zirconia polymorphs in powders and thin films by X-ray absorption spectroscopy
(2019) Acta Materialia, 180, pp. 158-169.
DOI: 10.1016/j.actamat.2019.09.003
SNIP (2018)= 2,842

5. **Antuzevics, A., Krieke, G., Pavlovska, E., Rogulis, U.**
Eu^{3+} ion distribution in oxyfluoride glass nanocomposites
(2019) Journal of Non-Crystalline Solids, 522, art. no. 119548.
DOI: 10.1016/j.jnoncrysol.2019.119548
SNIP (2018)= 1,177

6. **Jonane, I., Anspoks, A.,** Aquilanti, G., Kuzmin, A.
High-temperature X-ray absorption spectroscopy study of thermochromic copper molybdate
(2019) Acta Materialia, 179, pp. 26-35.
DOI: 10.1016/j.actamat.2019.06.034
SNIP (2018)= 2,842

7. **Trukhin, A.N.**
Luminescence of natural α-quartz crystal with aluminum, alkali and noble ions impurities
(2019) Journal of Luminescence, 214, art. no. 116602.
DOI: 10.1016/j.jlumin.2019.116602
SNIP (2018)= 1,048

8. **Trukhin, A.N.**
Luminescence of localized states in oxidized and fluorinated silica glass
(2019) Journal of Non-Crystalline Solids, 521, art. no. 119525.
DOI: 10.1016/j.jnoncrysol.2019.119525
SNIP (2018)= 1,177

9. Macutkevic, J., Kamba, S., Glemza, K., Banys, J., **Bormanis, K., Sternberg, A.**
High Temperature Dielectric Properties of PMN-PSN-PZN Relaxors
(2019) Physica Status Solidi (B) Basic Research, 256 (10), art. no. 1900050.
DOI: 10.1002/pssb.201900050
SNIP (2018)= 0,66

10. Polisadova, E., Valiev, D., Vaganov, V., Oleshko, V., Han, T., Zhang, C., Burachenko, A., **Popov, A.I.**
Time-resolved cathodoluminescence spectroscopy of YAG and YAG:Ce^{3+} phosphors
(2019) Optical Materials, 96, art. no. 109289.
DOI: 10.1016/j.optmat.2019.109289
SNIP (2018)= 1,009

11. Rahman, S., Samanta, S., **Kuzmin, A.,** Errandonea, D., Saqib, H., Brewe, D.L., Kim, J., Lu, J., Wang, L.
Tuning the Photoresponse of Nano-Heterojunction: Pressure-Induced Inverse Photoconductance in Functionalized WO_3 Nanocuboids
(2019) Advanced Science, 6 (19), art. no. 1901132.
DOI: 10.1002/advs.201901132
SNIP (2018)= 2,1

12. Burkhanov, A.I., Dikov, R.V., **Bormanis, K., Kalvane, A.**
Processes of Low-Frequency and Infra-Low-Frequency Polarization in Ferroelectric Ceramics $(1 – x)Ba0.95Pb0.05TiO_3 + xCo_2O_3$
(2019) Bulletin of the Russian Academy of Sciences: Physics, 83 (9), pp. 1094-1099.
DOI: 10.3103/S106287381909003X
SNIP (2018)= 0,509

13. **Rusevich, L.L., Zvejnieks, G., Kotomin, E.A.**
Ab initio simulation of $(Ba,Sr)TiO_3$ and $(Ba,Ca)TiO_3$ perovskite solid solutions
(2019) Solid State Ionics, 337, pp. 76-81.
DOI: 10.1016/j.ssi.2019.04.013
SNIP (2018)= 0,939

14. Varnagiris, S., Medvids, A., Lelis, M., Milcius, D., **Antuzevics, A.**
Black carbon-doped TiO_2 films: Synthesis, characterization and photocatalysis
(2019) Journal of Photochemistry and Photobiology A: Chemistry, 382, art. no. 111941.
DOI: 10.1016/j.jphotochem.2019.111941
SNIP (2018)= 0,851

15. Antsov, M., **Polyakov, B.,** Zadin, V., Mets, M., Oras, S., Vahtrus, M., Lõhmus, R., Dorogin, L., Vlassov, S.
Mechanical characterization of pentagonal gold nanowires in three different test configurations: A comparative study
(2019) Micron, 124, art. no. 102686.
DOI: 10.1016/j.micron.2019.102686
SNIP (2018)= 0,797

16. Bohacek, P., Krasnikov, A., Nikl, M., Zazubovich, S., **Zolotarjovs, A.**
On low-temperature luminescence quenching in $Gd_3(Ga,Al)_5O_{12}$:Ce crystals
(2019) Optical Materials, 95, art. no. 109252.
DOI: 10.1016/j.optmat.2019.109252
SNIP (2018)= 1,009

17. **Krieke, G., Antuzevics, A., Springis, M., Rogulis, U.**
Upconversion luminescence in transparent oxyfluoride glass ceramics containing hexagonal NaErF4
(2019) Journal of Alloys and Compounds, 798, pp. 326-332.
DOI: 10.1016/j.jallcom.2019.05.276
SNIP (2018)= 1,386

18. Bakaev, A., Zinovev, A., Terentyev, D., Bonny, G., Yin, C., Castin, N., **Mastrikov, Yu.A**., Zhurkin, E.E.
Interaction of carbon with microstructural defects in a W-Re matrix: An ab initio assessment
(2019) Journal of Applied Physics, 126 (7), art. no. 075110.
DOI: 10.1063/1.5094441
SNIP (2018)= 1,047

19. Šutka, A., Malnieks, K., Lapčinskis, L., Kaufelde, P., Linarts, A., Berzina, A., **Zabels, R.,** Jurkans, V., Gorņevs, I., Blums, J., Knite, M.
The role of intermolecular forces in contact electrification on polymer surfaces and triboelectric nanogenerators
(2019) Energy and Environmental Science, 12 (8), pp. 2417-2421.
DOI: 10.1039/c9ee01078e
SNIP (2018)= 4,622

20. Trinkler, L.**,** Trukhin, A., Cipa, J., Berzina, B., Korsaks, V., Chou, M.M.C., Li, C.-A.
Spectral and kinetic characteristics of pyroelectric luminescence in $LiGaO_2$
(2019) Optical Materials, 94, pp. 15-20.
DOI: 10.1016/j.optmat.2019.05.014
SNIP (2018)= 1,009

21. Myasnikova, L.N., Istlyaup, A.S., Sergeyev, D.M., Zhanturina, N.N., Shunkeyev, K.S., **Popov, A.I.**
Computer Simulations of the Band Structure and Density of States of the Linear Chains of NaCl Ions
(2019) Latvian Journal of Physics and Technical Sciences, 56 (4), pp. 49-56.
DOI: 10.2478/lpts-2019-0024
SNIP (2018)= 0,325

22. Sinusaite, L., Renner, A.M., Schütz, M.B., **Antuzevics, A., Rogulis, U.,** Grigoraviciute-Puroniene, I., Mathur, S., Zarkov, A.
Effect of Mn doping on the low-temperature synthesis of tricalcium phosphate (TCP) polymorphs
(2019) Journal of the European Ceramic Society, 39 (10), pp. 3257-3263.
DOI: 10.1016/j.jeurceramsoc.2019.03.057
SNIP (2018)= 1,71

23. **Vanags, M**., Spule, A., Gruškeviča, K., Vihodceva, S., Tamm, A., Vlassov, S., Šutka, A.
Sol-gel auto-combustion synthesis of $Ca_2Fe_2O_5$ brownmillerite nanopowders and thin films for advanced oxidation photoelectrochemical water treatment in visible light
(2019) Journal of Environmental Chemical Engineering, 7 (4), art. no. 103224.
DOI: 10.1016/j.jece.2019.103224
SNIP (2018)= 1,198

24. **Zubkins, M., Arslan, H., Bikse, L., Purans, J.**
High power impulse magnetron sputtering of Zn/Al target in an Ar and Ar/O_2 atmosphere: The study of sputtering process and AZO films
(2019) Surface and Coatings Technology, 369, pp. 156-164.
DOI: 10.1016/j.surfcoat.2019.04.044
SNIP (2018)= 1,435

25. **Trukhin, A., Trinkler, L.**
Photoconductivity & photoelectron emission of $LiGaO_2$ crystal excited in intrinsic absorption range
(2019) Optical Materials, 93, pp. 11-14.
DOI: 10.1016/j.optmat.2019.05.005
SNIP (2018)= 1,009

26. **Karitans, V., Nitiss, E., Tokmakovs, A., Ozolinsh, M.,** Logina, S.
Optical phase retrieval using four rotated versions of a single binary amplitude modulating mask
(2019) Journal of Astronomical Telescopes, Instruments, and Systems, 5 (3), art. no. 039004.
DOI: 10.1117/1.JATIS.5.3.039004
SNIP (2018)= 1,827

27. Wang, P., Xiao, H., Li, L., **Dumbrajs, O.**
Functional Analysis Method for Nonlinear Theory of Gyrotrons
(2019) IEEE Transactions on Plasma Science, 47 (7), art. no. 8732591, pp. 3141-3147.
DOI: 10.1109/TPS.2019.2917040
SNIP (2018)= 0,962

28. Zarins, E., **Pervenecka, J., Vembris, A.,** Kokars, V.
Glass-forming non-symmetric bis-styryl-DWK-type dyes for infra-red radiation amplification systems
(2019) Optical Materials, 93, pp. 85-92.
DOI: 10.1016/j.optmat.2019.05.002
SNIP (2018)= 1,009

29. Lapčinskis, L., Malnieks, K., Linarts, A., Blums, J., **Šmits, K.N**., Järvekülg, M., Knite, M.R., Šutka, A.
Hybrid Tribo-Piezo-Electric Nanogenerator with Unprecedented Performance Based on Ferroelectric Composite Contacting Layers
(2019) ACS Applied Energy Materials, 2 (6), pp. 4027-4032.
DOI: 10.1021/acsaem.9b00836

30. **Eglitis, R.**
Ab initio calculations of Li2(Co, Mn)O8 solid solutions for rechargeable batteries
(2019) International Journal of Modern Physics B, 33 (15), art. no. 1950151.
DOI: 10.1142/S0217979219501510
SNIP (2018)= 0,413

31. **Kucinskis, G., Bajars, G., Bikova, K., Kaprans, K., Kleperis, J.**
Microstructural Influence on Electrochemical Properties of $LiFePO_4$/C/Reduced Graphene Oxide Composite Cathode
(2019) Russian Journal of Electrochemistry, 55 (6), pp. 517-523.
DOI: 10.1134/S1023193519060120
SNIP (2018)= 0,517

32. Cipa, J., Zarins, A., Supe, A., Kizane, G., Zolotarjovs, A., Baumane, L., **Trinkler, L.,** Leys, O., Knitter, R.
X-ray induced defects in advanced lithium orthosilicate pebbles with additions of lithium metatitanate
(2019) Fusion Engineering and Design, 143, pp. 10-15.
DOI: 10.1016/j.fusengdes.2019.03.096
SNIP (2018)= 1,063

33. Villemson, K.M., Kaare, K., Raudsepp, R., Käämbre, T., Šmits, K.N., Wang, P., **Kuzmin, A.V**., Šutka, A., Shainyan, B.A., Kruusenberg, I.
Identification of Active Sites for Oxygen Reduction Reaction on Nitrogen- and Sulfur-Codoped Carbon Catalysts
(2019) Journal of Physical Chemistry C, 123 (26), pp. 16065-16074.
DOI: 10.1021/acs.jpcc.9b00117
SNIP (2018)= 1,083

34. **Zolotarjovs, A., Smits, K., Laganovska, K., Bite, I., Grigorjeva, L., Auzins, K., Millers, D., Skuja, L.**
Thermostimulated luminescence of plasma electrolytic oxidation coatings on 6082 aluminium surface
(2019) Radiation Measurements, 124, pp. 29-34.
DOI: 10.1016/j.radmeas.2019.02.020
SNIP (2018)= 1,099

35. **Trukhin, A.N.**
Photoelectric response of localized states in silica glass
(2019) Journal of Non-Crystalline Solids, 511, pp. 161-165.
DOI: 10.1016/j.jnoncrysol.2019.02.002
SNIP (2018)= 1,177

36. **Platonenko, A., Gryaznov, D., Zhukovskii, Y.F., Kotomin, E.A.**
First Principles Simulations on Migration Paths of Oxygen Interstitials in $MgAl_2O_4$
(2019) Physica Status Solidi (B) Basic Research, 256 (5), art. no. 1800282.
DOI: 10.1002/pssb.201800282
SNIP (2018)= 0,66

37. **Mastrikov, Y.A.,** Sokolov, M.N., **Kotomin, E.A., Gopejenko, A., Zhukovskii, Y.F.**
Ab Initio Modeling of Y and O Solute Atom Interaction in Small Clusters within the bcc Iron Lattice
(2019) Physica Status Solidi (B) Basic Research, 256 (5), art. no. 1800346.
DOI: 10.1002/pssb.201800346
SNIP (2018)= 0,66

38. Seeman, V., Feldbach, E., Kärner, T., Maaroos, A., **Mironova-Ulmane, N., Popov,** A.I., Shablonin, E., Vasil'chenko, E., Lushchik, A.
Fast-neutron-induced and as-grown structural defects in magnesium aluminate spinel crystals with different stoichiometry
(2019) Optical Materials, 91, pp. 42-49.
DOI: 10.1016/j.optmat.2019.03.008
SNIP (2018)= 1,009

39. Zaporina, N.A., Doynikova, O.A., Krumina, A.P., Bocharov, D.V., Grabis, J.P.
Erratum to: Methods of Electron Microdiffraction and X-Ray Analysis in Structure Study of Nanodisperse Partially Stabilized ZrO_2 Powders (Journal of Surface Investigation. X-ray, Synchrotron and Neutron Techniques, (2009), 3, 3, (464-467), 10.1134/S1027451009030227)
(2019) Journal of Surface Investigation, 13 (3), p. 566.
DOI: 10.1134/S1027451019030376
SNIP (2018)= 0,569

40. Sobolev, N., Djurabekova, F., **Kotomin, E.**
Defect-Induced Effects in Nanomaterials
(2019) Physica Status Solidi (B) Basic Research, 256 (5), art. no. 1900181.
DOI: 10.1002/pssb.201900181
SNIP (2018)= 0,66

41. Hu, F., Liu, X.-T., Zhang, J.-L., Zheng, Q.-C., **Eglitis, R.I.,** Zhang, H.-X.
MD Simulation Investigation on the Binding Process of Smoke-Derived Germination Stimulants to Its Receptor
(2019) Journal of Chemical Information and Modeling, 59 (4), pp. 1554-1562.
DOI: 10.1021/acs.jcim.8b00844
SNIP (2018)= 1,163

42. **Zablotsky, D., Rusevich, L.L., Zvejnieks, G., Kuzovkov, V., Kotomin, E.**
Manifestation of dipole-induced disorder in self-assembly of ferroelectric and ferromagnetic nanocubes
(2019) Nanoscale, 11 (15), pp. 7293-7303.
DOI: 10.1039/c9nr00708c
SNIP (2018)= 1,338

43. Lapčinskis, L., Cirulis, I., **Lesničenoks,** P., Abele, A., Šutka, A., Knite, M.
PVA Hydrogel Electrolyte and Porous Polyisoprene Carbon Nanostructure Composite Based Pressure Sensitive Supercapacitor
(2019) IOP Conference Series: Materials Science and Engineering, 500 (1), art. no. 012018.
DOI: 10.1088/1757-899X/500/1/012018
SNIP (2018)= 0,531

44. **Grigorjeva, L., Grube, J., Bite, I., Zolotarjovs, A., Smits, K., Millers, D.,** Rodnyi, P., Chernenko, K.
Sub-nanosecond excitonic luminescence in ZnO:In nanocrystals
(2019) Radiation Measurements, 123, pp. 69-73.
DOI: 10.1016/j.radmeas.2019.02.016
SNIP (2018)= 1,099

45. **Chesnokov, A., Gryaznov, D., Kotomin, E.**
First principles calculations on CeO_2 doped with $Tb.^{3+}$ ions
(2019) Optical Materials, 90, pp. 76-83.
DOI: 10.1016/j.optmat.2019.02.016
SNIP (2018)= 1,009

46. Juhnevica-Radenkova, K., Radenkovs, V., **Kundzins, K.,** Seglina, D.
Effect of ozone treatment on the microstructure, chemical composition and sensory quality of apple fruits
(2019) Food Science and Technology International, 25 (3), pp. 252-267.
DOI: 10.1177/1082013218815285
SNIP (2018)= 0,797

47. Ruduss, A., Traskovskis, K., **Vembris, A., Grzibovskis, R., Pudzs, K., Lielbardis, M.,** Kokars, V.
Synthesis and investigation of charge transport properties in adducts of hole transporting carbazole derivatives and push-pull azobenzenes
(2019) Journal of Physics and Chemistry of Solids, 127, pp. 178-185.
DOI: 10.1016/j.jpcs.2018.12.019
SNIP (2018)= 0,955

48. Malina, I., Traskovskis, K., **Lesina, N.**, **Vembris, A.**
Eu^{3+} ternary and tetrakis complexes with carbazole and methyl group substituted dibenzoylmethane derivatives: Induction of aggregation enhanced emission
(2019) Dyes and Pigments, 163, pp. 257-266.
DOI: 10.1016/j.dyepig.2018.11.060
SNIP (2018)= 0,909

49. Zarins, E., Siltane, K., **Pervenecka, J., Vembris,** A., Kokars, V.
Glass-forming derivatives of 2-cyano-2-(4H-pyran-4-ylidene) acetate for light-amplification systems
(2019) Dyes and Pigments, 163, pp. 62-70.
DOI: 10.1016/j.dyepig.2018.11.041
SNIP (2018)= 0,909

50. Traskovskis, K., Kokars, V., Belyakov, S., **Lesina, N., Mihailovs, I., Vembris, A.**
Emission Enhancement by Intramolecular Stacking between Heteroleptic Iridium(III) Complex and Flexibly Bridged Aromatic Pendant Group
(2019) Inorganic Chemistry, 58 (7), pp. 4214-4222.
DOI: 10.1021/acs.inorgchem.8b03273
SNIP (2018)= 1,092

51. **Mironova-Ulmane, N., Kuzmin, A.,** Sildos, I., Puust, L., Grabis, J.
Magnon and Phonon Excitations in Nanosized NiO
(2019) Latvian Journal of Physics and Technical Sciences, 56 (2), pp. 61-72.
DOI: 10.2478/lpts-2019-0014
SNIP (2018)= 0,325

52. Korzhik, M., Alenkov, V., Buzanov, O., Fedorov, A., Dosovitskiy, G., Grigorjeva, L., Mechinsky, V., Sokolov, P., Tratsiak, Y., **Zolotarjovs, A.,** Dormenev, V., Dosovitskiy, A., Agrawal, D., Anniyev, T., Vasilyev, M., Khabashesku, V.
Nanoengineered Gd 3 Al 2 Ga 3 O 12 Scintillation Materials with Disordered Garnet Structure for Novel Detectors of Ionizing Radiation
(2019) Crystal Research and Technology, 54 (4), art. no. 1800172.
DOI: 10.1002/crat.201800172
SNIP (2018)= 0,612

53. Grigorjeva, L., Zolotarjovs, A., Bite, I., Grube, J., Millers, D.
Electronic processes in doped ZnO nanopowders
(2019) IOP Conference Series: Materials Science and Engineering, 503 (1), art. no. 012017.
DOI: 10.1088/1757-899X/503/1/012017
SNIP (2018)= 0,531

54. Lukosevics, I., **Lesnicenoks, P., Kleperis, J.**
Synthesis and studying of reduced few-layered graphene coatings in gas sensor applications
(2019) IOP Conference Series: Materials Science and Engineering, 503 (1), art. no. 012013.
DOI: 10.1088/1757-899X/503/1/012013
SNIP (2018)= 0,531

55. **Knoks, A., Lesnicenoks, P., Kleperis, J., Grinberga, L., Hodakovska, J., Klavins, J., Cikvaidze, G., Lukosevics, I.**
Electro-catalytic and photo-catalytic reformation of CO_2-reactions and efficiencies processes (Review)
(2019) IOP Conference Series: Materials Science and Engineering, 503 (1), art. no. 012009.
DOI: 10.1088/1757-899X/503/1/012009
SNIP (2018)= 0,531

56. **Skvortsova, V., Zubkins, M., Kalendarev, R., Arslan, H., Purans, J.**
Optical properties of zinc-iridium oxide thin films
(2019) IOP Conference Series: Materials Science and Engineering, 503 (1), art. no. 012016.
DOI: 10.1088/1757-899X/503/1/012016
SNIP (2018)= 0,531

57. **Fedorenko, D., Vaivars, G.**
Different approaches in sulfonated poly (ether ether ketone) conductivity measurements
(2019) IOP Conference Series: Materials Science and Engineering, 503 (1), art. no. 012030.
DOI: 10.1088/1757-899X/503/1/012030
SNIP (2018)= 0,531

58. **Bocharov, D.,** Rafalskij, Y., Krack, M., **Putnina, M., Kuzmin, A.**
Negative thermal expansion of ScF3: First principles vs empirical molecular dynamics
(2019) IOP Conference Series: Materials Science and Engineering, 503 (1), art. no. 012001.
DOI: 10.1088/1757-899X/503/1/012001
SNIP (2018)= 0,531

59. **Lozkins, S., Hodakovska, J., Kleperis, J.,** Merijs-Meri, R.
Nafion® and polyaniline composite modification with Li and Mg ions
(2019) IOP Conference Series: Materials Science and Engineering, 503 (1), art. no. 012031.
DOI: 10.1088/1757-899X/503/1/012031
SNIP (2018)= 0,531

60. **Zhukovskii, Y.F., Piskunov, S.,** Evarestov, R.A.
First principles evaluation on photocatalytic suitability of 2H structured and [0001] oriented WS_2 nanosheets and nanotubes
(2019) IOP Conference Series: Materials Science and Engineering, 503 (1), art. no. 012002.
DOI: 10.1088/1757-899X/503/1/012002
SNIP (2018)= 0,531

61. **Pentjuss, E., Balodis, J.,** Vdovicenko, M., **Gabrusenoks, J., Bajars, G.,** Petersone, L., **Kleperis, J.**
Mass recovery of carbonated fabrics of glass fibres after isothermal heating
(2019) IOP Conference Series: Materials Science and Engineering, 503 (1), art. no. 012027.
DOI: 10.1088/1757-899X/503/1/012027
SNIP (2018)= 0,531

62. Naidoo, S., Thage, L., Ying, Q., Vallie, S., **Vaivars, G.**
Optimization of the enzyme power source for a nano drug delivery system fuelled by glucose in blood plasma
(2019) IOP Conference Series: Materials Science and Engineering, 503 (1), art. no. 012026.
DOI: 10.1088/1757-899X/503/1/012026
SNIP (2018)= 0,531

63. **Jonane, I., Anspoks, A.,** Nataf, L., Baudelet, F., Irifune, T., **Kuzmin, A.**
Pressure-induced structural changes in α-MoO_3 probed by X-ray absorption spectroscopy
(2019) IOP Conference Series: Materials Science and Engineering, 503 (1), art. no. 012018.
DOI: 10.1088/1757-899X/503/1/012018
SNIP (2018)= 0,531

64. Prieditis, G., Feldbach, E., Kudryavtseva, I., **Popov, A.I.,** Shablonin, E., Lushchik, A.
Luminescence characteristics of magnesium aluminate spinel crystals of different stoichiometry
(2019) IOP Conference Series: Materials Science and Engineering, 503 (1), art. no. 012021.
DOI: 10.1088/1757-899X/503/1/012021
SNIP (2018)= 0,531

65. Klym, H., Ingram, A., Hadzaman, I., Karbovnyk, I., Vasylchyshyn, I., **Popov, A.I.**
Nanoporous characterization of modified humidity-sensitive $MgO-Al_2O_3$ ceramics by positron annihilation lifetime spectroscopy method
(2019) IOP Conference Series: Materials Science and Engineering, 503 (1), art. no. 012019.
DOI: 10.1088/1757-899X/503/1/012019
SNIP (2018)= 0,531

66. Klym, H., Shpotyuk, O., Karbovnyk, I., Calvez, L., **Popov, A.I.**
Structural investigation of crystallized Ge-Ga-Se chalcogenide glasses
(2019) IOP Conference Series: Materials Science and Engineering, 503 (1), art. no. 012020.
DOI: 10.1088/1757-899X/503/1/012020
SNIP (2018)= 0,531

67. Laipniece, L., Kampars, V., Belyakov, S., **Tokmakovs, A., Nitiss, E., Rutkis, M.**
Dendronized azochromophores with aromatic and perfluoroaromatic fragments: Synthesis and properties demonstrating Ar–ArF interactions
(2019) Dyes and Pigments, 162, pp. 394-404.
DOI: 10.1016/j.dyepig.2018.10.035
SNIP (2018)= 0,909

68. Rucins, M., Dimitrijevs, P., Pajuste, K., Petrichenko, O., Jackevica, L., Gulbe, A., Kibilda, S., **Smits, K.,** Plotniece, M., Tirzite, D., Pajuste, K., Sobolev, A., Liepins, J., Domracheva, I., Plotniece, A.
Contribution of molecular structure to self-assembling and biological properties of bifunctional lipid-like 4-(N-alkylpyridinium)-1,4-Dihydropyridines
(2019) Pharmaceutics, 11 (3), art. no. 115.
DOI: 10.3390/pharmaceutics11030115
SNIP (2018)= 1,435

69. Luchechko, A., Vasyltsiv, V., Kostyk, L., Tsvetkova, O., **Popov, A.I.**
Shallow and deep trap levels in X-ray irradiated β-Ga_2O_3 : Mg
(2019) Nuclear Instruments and Methods in Physics Research, Section B: Beam Interactions with Materials and Atoms, 441, pp. 12-17.
DOI: 10.1016/j.nimb.2018.12.045
SNIP (2018)= 0,777

70. **Eglitis, R.I.**
Ab initio calculations of $CaZrO_3$, $BaZrO_3$, $PbTiO_3$ and $SrTiO_3$ (001), (011) and (111) surfaces as well as their (001) interfaces
(2019) Integrated Ferroelectrics, 196 (1), pp. 7-15.
DOI: 10.1080/10584587.2019.1591976
SNIP (2018)= 0,379

71. **Sternberg, A., Grinberga, L.**
Guest Editorial
(2019) Integrated Ferroelectrics, 196 (1), pp. vii-viii.
DOI: 10.1080/10584587.2019.1591953
SNIP (2018)= 0,379

72. **Eglite, L., Antonova, M., Birks, E., Knite, M., Livinsh, M.**
Grain growth in $Na0.5Bi0.5TiO_3$-based solid solutions
(2019) Integrated Ferroelectrics, 196 (1), pp. 112-119.
DOI: 10.1080/10584587.2019.1591971
SNIP (2018)= 0,379

73. Sidorov,N.V., Shuvalova,A.M., Yanichev,A.A., Teplyakova,N.A., Palatnikov,M.N., **Bormanis, K.**
Photoelectric fields in doped lithium niobate crystals
(2019) Integrated Ferroelectrics, 196 (1), pp. 43-46.
DOI: 10.1080/10584587.2019.1591984
SNIP (2018)= 0,379

74. Sugak, D., Yakhnevych, U., Syvorotka, I.I., Buryy, O., **Popov, A.I.,** Ubizskii, S.
Optical investigation of the OH− groups in the $LiNbO_3$ doped by copper
(2019) Integrated Ferroelectrics, 196 (1), pp. 32-38.
DOI: 10.1080/10584587.2019.1591981
SNIP (2018)= 0,379

75. Garbarz-Glos, B., Bąk, W., **Kalvane, A., Antonova, M.,** Klimkowski, G.
Effects of CuO doping on structure, microstructure and dielectric properties of $BaTiO_3$–$PbTiO_3$ solid solution
(2019) Integrated Ferroelectrics, 196 (1), pp. 70-77.
DOI: 10.1080/10584587.2019.1591961
SNIP (2018)= 0,379

76. Sitko, D., Dziubaniuk, M., Suchanicz, J., Kluczewska, K., Konieczny, K., **Kalvane,** A., Nowakowska-Malczyk, M.
Effect of Cu doping on $Ba0.95Pb0.05TiO_3$ electrical properties studied by means of electrical impedance spectroscopy
(2019) Integrated Ferroelectrics, 196 (1), pp. 78-86.
DOI: 10.1080/10584587.2019.1591962
SNIP (2018)= 0,379

77. Sidorov, N.V., Palatnikov, M.N., Teplyakova, N.A., Titov, R.A., **Bormanis, K.**
Optical properties and structure particularities of $LiNbO_3$ crystals grown from a boron-doped melt
(2019) Integrated Ferroelectrics, 196 (1), pp. 39-42.
DOI: 10.1080/10584587.2019.1591983
SNIP (2018)= 0,379

78. Garbarz-Glos, B., Klimkowski, G., Śmiga, W., **Antonova, M., Kalvane, A.**
Preparation and dielectric properties of $(Na0.5K0.5)NbO_3$ ceramics with ZnO and CdO addition
(2019) Integrated Ferroelectrics, 196 (1), pp. 87-93.
DOI: 10.1080/10584587.2019.1591964
SNIP (2018)= 0,379

79. Sadykov, S.A., Kallaev, S.N., Alikhanov, N.M.R., **Bormanis, K., Kalvane, A.**
Dielectric properties and ac conductivities of $Bi1−xSmxFeO_3$ ceramics
(2019) Integrated Ferroelectrics, 196 (1), pp. 100-104.
DOI: 10.1080/10584587.2019.1591968
SNIP (2018)= 0,379

80. Gorev, M.V., Flerov, I.N., **Bormanis, K., Kalvane, A.**
Thermal expansion and polarization of (1-x)PNN-xPT solid solutions
(2019) Integrated Ferroelectrics, 196 (1), pp. 60-63.
DOI: 10.1080/10584587.2019.1591957
SNIP (2018)= 0,379

81. Kallaev, S.N., Omarov, Z.M., Mitarov, R.G., Sadykov, S.A., Khasbulatov, S.V., Reznichenko, L.A., **Bormanis, K., Kundzinsh, M.**
Heat capacity and thermal conductivity of multiferroics $Bi1\text{-}xPrxFeO_3$
(2019) Integrated Ferroelectrics, 196 (1), pp. 120-126.
DOI: 10.1080/10584587.2019.1591973
SNIP (2018)= 0,379

82. Afanassyev, D., Ubizskii, S., Zhydachevskyy, Y., Luchechko, A., **Popov, A.I.,** Suchocki, A.
Time-resolved pulsed OSL of ceramic YAP:Mn phosphors
(2019) Integrated Ferroelectrics, 196 (1), pp. 24-31.
DOI: 10.1080/10584587.2019.1591980
SNIP (2018)= 0,379

83. **Trukhin, A., Antuzevics, A.**
Photoluminescence and Electron Spin Resonance of Silicon Dioxide Crystal with Rutile Structure (Stishovite)
(2019) Physica Status Solidi (A) Applications and Materials Science, 216 (3), art. no. 1800457.
DOI: 10.1002/pssa.201800457
SNIP (2018)= 0,671

84. **Klotins, E.**
Electronic Processes in Solid State: Dirac Framework
(2019) Latvian Journal of Physics and Technical Sciences, 56 (1), pp. 60-69.
DOI: 10.2478/lpts-2019-0006
SNIP (2018)= 0,325

85. Bezvikonnyi, O., **Gudeika, D.,** Volyniuk, D., Mimaite, V., Sebastine, B.R., Grazulevicius, J.V.
Effect of donor substituents on thermally activated delayed fluorescence of diphenylsulfone derivatives
(2019) Journal of Luminescence, 206, pp. 250-259.
DOI: 10.1016/j.jlumin.2018.10.018
SNIP (2018)= 1,048

86. **Skuja, L.,** Ollier, N., Kajihara, K., **Smits, K.**
Creation of glass-characteristic point defects in crystalline SiO_2 by 2.5 MeV electrons and by fast neutrons
(2019) Journal of Non-Crystalline Solids, 505, pp. 252-259.
DOI: 10.1016/j.jnoncrysol.2018.11.014
SNIP (2018)= 1,177

87. **Pankratov, V.,** Pärna, R., Kirm, M., Nagirnyi, V., Nõmmiste, E., Omelkov, S., Vielhauer, S., Chernenko, K., Reisberg, L., Turunen, P., Kivimäki, A., Kukk, E., Valden, M., Huttula, M.
Progress in development of a new luminescence setup at the FinEstBeAMS beamline of the MAX IV laboratory
(2019) Radiation Measurements, 121, pp. 91-98.
DOI: 10.1016/j.radmeas.2018.12.011
SNIP (2018)= 1,099

88. **Rusevich, L.L., Zvejnieks, G., Kotomin, E.A.,** Kržmanc, M.M., Meden, A., Kunej, Š., Vlaicu, I.D.
Theoretical and Experimental Study of (Ba,Sr)TiO_3 Perovskite Solid Solutions and $BaTiO_3$ /$SrTiO_3$ Heterostructures
(2019) Journal of Physical Chemistry C, 123 (4), pp. 2031-2036.
DOI: 10.1021/acs.jpcc.8b09750
SNIP (2018)= 1,083

89. Kenmoe, S., **Lisovski, O., Piskunov, S., Zhukovskii, Y.F.,** Spohr, E.
Electronic and optical properties of pristine, N- and S-doped water-covered TiO_2 nanotube surfaces
(2019) Journal of Chemical Physics, 150 (4), art. no. 041714.
DOI: 10.1063/1.5050090
SNIP (2018)= 0,969

90. Andzane, J., Buks, K., **Zubkins, M.,** Bechelany, M., Marnauza, M., Baitimirova, M., Erts, D.
Structure-determined thermoelectric properties of Bi2Se3 thin films deposited by vapour-solid technique
(2019) Proceedings of the IEEE Conference on Nanotechnology, 2018-July, art. no. 8626225.
DOI: 10.1109/NANO.2018.8626225

91. **Piskunov, S., Lisovski, O., Zhukovskii, Y.F.,** D'Yachkov, P.N., Evarestov, R.A., Kenmoe, S., Spohr, E.
First-Principles Evaluation of the Morphology of WS_2 Nanotubes for Application as Visible-Light-Driven Water-Splitting Photocatalysts
(2019) ACS Omega, 4 (1), pp. 1434-1442.
DOI: 10.1021/acsomega.8b03121
SNIP (2018)= 0,673

92. Traskovskis, K., Ruduss, A., Kokars, V., **Mihailovs, I., Lesina, N., Vembris, A.**
Thiphenylmethane based structural fragments as building blocks towards solution-processable heteroleptic iridium(iii) complexes for OLED use
(2019) New Journal of Chemistry, 43 (1), pp. 37-47.
DOI: 10.1039/c8nj04484h
SNIP (2018)= 0,724

93. **Bormanis, K., Kalvane, A.,** Burkhanov, A.I., Eglite, L., Dikov, R.V.
Dielectric and acoustic properties of modified barium titanate ceramics
(2019) Ferroelectrics, 538 (1), pp. 12-19.
DOI: 10.1080/00150193.2019.1569980
SNIP (2018)= 0,483

94. **Antuzevics, A.**
EPR in glass ceramics
(2019) Experimental Methods in the Physical Sciences, 50, pp. 161-190.
DOI: 10.1016/B978-0-12-814024-6.00008-X
SNIP (2018)= N/A

95. **Vitola, V., Millers, D., Bite, I., Smits, K.,** Spustaka, A.
Recent progress in understanding the persistent luminescence in $SrAl_2O_4$:Eu,Dy
(2019) Materials Science and Technology (United Kingdom), 35 (14), pp. 1661-1677.
DOI: 10.1080/02670836.2019.1649802
SNIP (2018)= 1,038

96. **Eglitis, R.I., Popov, A.I.**
Comparative Ab initio calculations for ABO_3 perovskite (001), (011) and (111) as well as $YAlO_3$ (001) surfaces and F centers
(2019) Journal of Nano- and Electronic Physics, 11 (1), art. no. 01001.
DOI: 10.21272/jnep.11(1).01001
SNIP (2018)= 0,461

97. **Zvejnieks, G., Rusevich, L.L., Gryaznov, D., Kotomin, E.A.**
Interface-induced enhancement of piezoelectricity in the ($SrTiO_3$): M/($BaTiO_3$)M - M superlattice for energy harvesting applications
(2019) Physical Chemistry Chemical Physics, 21 (42), pp. 23541-23551.
DOI: 10.1039/c9cp04086b
SNIP (2018)= 0,981

98. **Zablotsky, D., Kuzovkov, V., Kotomin, E.**
Role of Intrinsic Dipoles in the Evaporation-Driven Assembly of Perovskite Nanocubes into Energy-Harvesting Composites
(2019) Physica Status Solidi (A) Applications and Materials Science, art. no. 1900533.
DOI: 10.1002/pssa.201900533
SNIP (2018)= 0,671

99. Steinberga, I., Sustere, L., **Bikse, J., Bikse, J., Jr., Kleperis, J.**
Traffic flow hypothetical modelling for air quality improvement and planning purposes
(2019) Vide. Tehnologija. Resursi - Environment, Technology, Resources, 1, pp. 283-286.
DOI: 10.17770/etr2019vol1.4155

100. Ruduss, A., Traskovskis, K., **Grzibovskis, R.,** Kokars, V.
Synthesis and photoelectrical properties of 3-(diphenylamino)carbazolyl - Functionalized DMABI derivatives
(2019) Key Engineering Materials, 800 KEM, pp. 280-285.
DOI: 10.4028/www.scientific.net/KEM.800.2800
SNIP (2018)= 0,29

101. Zarins, E., Alksnis, D., **Pervenecka, J**., Paulsone, P., Lazdovica, K., **Vembris, A.,** Kokars, V.
Several derivatives of 6-(tert-butyl)-4H-pyran-4-ylidene malononitrile with different amorphous phase promoting substituents for light-amplification systems
(2019) Key Engineering Materials, 800 KEM, pp. 275-279.
DOI: 10.4028/www.scientific.net/KEM.800.275
SNIP (2018)= 0,29

102. Steinberga, I., Sustere, L., **Bikse, J., Kleperis, J.**
Traffic induced air pollution modeling: Scenario analysis for air quality management in street canyon
(2019) Procedia Computer Science, 149, pp. 384-389.
DOI: 10.1016/j.procs.2019.01.152
SNIP (2018)= 0,883

103. **Bocharov, D., Piskunov, S., Zhukovskii, Y.F.,** Evarestov, R.A.
Ab Initio Calculations on the Electronic Structure and Photocatalytic Properties of Two-Dimensional WS 2 (0001) Nanolayers of Varying Thickness
(2019) Physica Status Solidi - Rapid Research Letters, 13 (1), art. no. 1800253.
DOI: 10.1002/pssr.201800253
SNIP (2018)= 1,017

104. **Vitola, V., Millers, D., Smits, K., Bite, I., Zolotarjovs, A.**
The search for defects in undoped $SrAl_2O_4$ material
(2019) Optical Materials, 87, pp. 48-52.
DOI: 10.1016/j.optmat.2018.06.004
SNIP (2018)= 1,009

105. **Jonane, I., Cintins, A., Kalinko, A.,** Chernikov, R., **Kuzmin, A.**
Low temperature X-ray absorption spectroscopy study of $CuMoO_4$ and $CuMo0.90W0.10O_4$ using reverse Monte-Carlo method
(2019) Radiation Physics and Chemistry, art. no. 108411.
DOI: 10.1016/j.radphyschem.2019.108411
SNIP (2018)= 0,981

106. Xi, J.-Y., Jia, R., Li, W., Wang, J., Bai, F.-Q., **Eglitis, R.I.,** Zhang, H.-X.
How does graphene enhance the photoelectric conversion efficiency of dye sensitized solar cells? An insight from a theoretical perspective
(2019) Journal of Materials Chemistry A, 7 (6), pp. 2730-2740.
DOI: 10.1039/c8ta06872k
SNIP (2018)= 1,575

107. Wang, J., Wang, M.-Y., Yin, G., Jia, R., Wang, J., **Eglitis, R.I.,** Zhang, H.-X.
Nickel-catalyzed carboxylation of aryl zinc reagent with CO_2 : A theoretical and experimental study
(2019) Journal of CO_2 Utilization, 29, pp. 262-270.
DOI: 10.1016/j.jcou.2018.12.007
SNIP (2018)= 1,276

108. Andzane, J., Buks, K., Strakova, M.N., **Zubkins, M.,** Bechelany, M., Marnauza, M., Baitimirova, M., Erts, D.
Structure and Doping Determined Thermoelectric Properties of Bi_2Se_3 Thin Films Deposited by Vapour-Solid Technique
(2019) IEEE Transactions on Nanotechnology, 18, art. no. 8835055, pp. 948-954.
DOI: 10.1109/TNANO.2019.2939862
SNIP (2018)= 1,009

109. **Platonenko, A.,** Gentile, F.S., Pascale, F., Ferrari, A.M., D'Amore, M., Dovesi, R.
Nitrogen substitutional defects in silicon. A quantum mechanical investigation of the structural, electronic and vibrational properties
(2019) Physical Chemistry Chemical Physics, 21 (37), pp. 20939-20950.
DOI: 10.1039/c9cp03185e
SNIP (2018)= 0,981

110. Evarestov, R.A., Senocrate, A., **Kotomin, E.A.,** Maier, J.
First-principles calculations of iodine-related point defects in $CsPbI_3$
(2019) Physical Chemistry Chemical Physics, 21 (15), pp. 7841-7846.
DOI: 10.1039/c9cp00414a
SNIP (2018)= 0,981

111. Xie, M., Hao, L., **Jia, R.,** Wang, J., Bai, F.-Q.
Theoretical study on the influence of electric field direction on the photovoltaic performance of aryl amine organic dyes for dye-sensitized solar cells
(2019) New Journal of Chemistry, 43 (2), pp. 651-661.
DOI: 10.1039/C8NJ04360D
SNIP (2018)= 0,724

112. Ristić, I., Miletić, A., Vukić, N., Marinović-Cincović, M., **Smits, K.,** Cakić, S., Pilić, B.
Characterization of electrospun poly(lactide) composites containing multiwalled carbon nanotubes
(2019) Journal of Thermoplastic Composite Materials.
DOI: 10.1177/0892705719857780
SNIP (2018)= 0,989

113. Paris, P., **Butikova, J.,** Laan, M., Hakola, A., Jõgi, I., Likonen, J., Grigore, E., Ruset, C.
Comparison of LIBS results on ITER-relevant samples obtained by nanosecond and picosecond lasers
(2019) Nuclear Materials and Energy, 18, pp. 1-5.
DOI: 10.1016/j.nme.2018.11.018
SNIP (2018)= 1,021

114. **Heifets, E., Kotomin, E.A.,** Bagaturyants, A.A., Maier, J.
Thermodynamic stability of non-stoichiometric $SrFeO_{3-\delta}$: A hybrid DFT study
(2019) Physical Chemistry Chemical Physics, 21 (7), pp. 3918-3931.
DOI: 10.1039/c8cp07117a
SNIP (2018)= 0,981

115. Luchechko, A., Zhydachevskyy, Y., Ubizskii, S., Kravets, O., **Popov, A.I., Rogulis, U., Elsts,** E., Bulur, E., Suchocki, A.
Afterglow, TL and OSL properties of Mn2+-doped $ZnGa_2O_4$ phosphor
(2019) Scientific Reports, 9 (1), art. no. 9544.
DOI: 10.1038/s41598-019-45869-7
SNIP (2018)= 1,24

116. Usseinov, A.B., Akilbekov, A.T., **Kotomin, E.A., Popov, A.I.,** Seitov, D.D., Nekrasov, K.A., Giniyatova, Sh.G., Karipbayev, Zh.T.
The first principles calculations of CO_2 adsorption on (10 $\bar{1}$ 0) ZnO surface
(2019) AIP Conference Proceedings, 2174, art. no. 020181.
DOI: 10.1063/1.5134332
SNIP (2018)= 0,385

117. **Platonenko, A., Popov, A.I.**
Structural and electronic properties of β-NaYF4 and β-NaYF4:Ce^{3+}
(2019) Optical Materials, art. no. 109529.
DOI: 10.1016/j.optmat.2019.109529
SNIP (2018)= 1,009

118. Bezvikonnyi, O., **Gudeika, D.,** Volyniuk, D., **Rutkis, M.,** Grazulevicius, J.V.
Diphenylsulfone-based hosts for electroluminescent devices: Effect of donor substituents
(2019) Dyes and Pigments, art. no. 108104.
DOI: 10.1016/j.dyepig.2019.108104
SNIP (2018)= 0,909

119. Proyavin, M., **Dumbrajs, O.,** Nusinovich, G., Glyavin, M.
To the Theory of Gyrotrons with Wide Emitters
(2019) Journal of Infrared, Millimeter, and Terahertz Waves.
DOI: 10.1007/s10762-019-00646-5
SNIP (2018)= 1,049

120. Kozlov, M.I., Aslandukov, A.N., Vashchenko, A.A., Medvedko, A.V., Aleksandrov, A.E., **Grzibovskis, R.,** Goloveshkin, A.S., Lepnev, L.S., Tameev, A.R., **Vembris, A.,** Utochnikova, V.V.
On the development of a new approach to the design of lanthanide-based materials for solution-processed OLEDs
(2019) Dalton Transactions, 48 (46), pp. 17298-17309.
DOI: 10.1039/c9dt03823j
SNIP (2018)= 0,9

121. Avotina, L., Conka, D., **Vitins, A.,** Pajuste, E., Baumane, L., Sutka, A., Skute, N., Kizane, G., JET Contributors
Spectrometric analysis of inner divertor materials of JET carbon and ITER-like walls
(2018) Fusion Engineering and Design. Article in Press.
DOI: 10.1016/j.fusengdes.2018.11.037
SNIP (2018)= 1,063

122. Joffrin, E., Abduallev, S., Abhangi, M., Abreu, P., Afanasev, V., Afzal, M., Aggarwal, K.M., Ahlgren, T., Aho-Mantila, L., Aiba, N., Airila, M., Alarcon, T., Albanese, R., Alegre, D., Aleiferis, S., Alessi, E., Aleynikov, P., Alkseev, A., Allinson, M., Alper, B., Alves, E., Ambrosino, G., Ambrosino, R., Amosov, V., M., Vega, J., Ventre, S., Verdoolaege, G., Verona, C., Verona Rinati, G., Veshchev, E., Vianello, N., Vicente, J., Viezzer, E., Villari, S., Villone, F., Vincent, M., Vincenzi, P., Vinyar, I., Viola, B., **Vitins, A.,** Vizvary, Z., Vlad, M., Voitsekhovitch, I., Voltolina, D., Von Toussaint, U., Vondráček, P., Vuksic, M., Wakeling, B., Overview of the JET preparation for deuterium-tritium operation with the ITER like-wall
(2019) Nuclear Fusion, 59 (11), art. no. 112021. Cited 13 times.
DOI: 10.1088/1741-4326/ab2276
SNIP (2018)= 1,739

123. **Sternberg, A., Grinberga, L., Sarakovskis, A., Rutkis, M.**
Preface
(2019) IOP Conference Series: Materials Science and Engineering, 503 (1), art. no. 011001.
DOI: 10.1088/1757-899X/503/1/011001
SNIP (2018)= 0,531

124. **Sprugis, E., Vaivars, G.,** Merijs Meri, R.
A study of mechanical properties of polymer composite membranes with various ionic liquids at elevated temperatures
(2019) Medziagotyra, 25 (1), pp. 66-70.
DOI: 10.5755/j01.ms.25.1.18933
SNIP (2018)= 0,34

125. **Eglitis, R.**, **Purans, J.**, **Popov, A.I.,** Jia, R.
Systematic trends in YAlO3, SrTiO3, BaTiO3, BaZrO3 (001) and (111) surface ab initio calculations
(2019) International Journal of Modern Physics BVolume 33, Issue 32, 30 December 2019, Article number 1950390
DOI: 10.1142/S0217979219503909
SNIP (2018)= 0,413

Other publications in 2019

1. **Grzibovskis, R., Vembris, A.**
   Influence of organic material and sample parameters on the surface potential in Kelvin probe measurements
   (2019) SN APPLIED SCIENCES 1 Issue: 7, UNSP 725
   DOI: 10.1007/s42452-019-0766-z

2. Vlassov, S., Mets, M., **Polyakov, B.,** Bian, J., Dorogin, L.M., Zadin, V.,
   Abrupt elastic-to-plastic transition in pentagonal nanowires under bending
   (2019) BEILSTEIN JOURNAL OF NANOTECHNOLOGY 2019, Volume: 10, Pages: 2468-2476
   DOI: 10.3762/bjnano.10.237
   SNIP (2018)= 0,98

3. **Ozolinsh, M, Pastare, A**
   Spatial Frequency Impact on Onset of Peripheral Illusory Movement Perception
   (2019) PERCEPTION Volume: 48 Issue: 3 Pages: 277-278
   DOI: 10.1177/0301006619828106
   SNIP (2018)= 0,79

4. Nichol T., **Teteris J., Reinfelde M.,** Mitkova M.
   Dual Effect of Light Irradiation for Surface Relief Gratings Formation in Se-rich Ge-Se Thin Films
   Advanced Materials Letters, Volume 10, Issue 12, Pages 868-873, Year 2019
   DOI: 10.5185/amlett.2019.0012
   SNIP (2018)= 0,91

5. **J. Mikelsone, J. Teteris, M. Reinfelde**
   Enhancement of Photosensitivity in Azo-Epoxy Resists for Direct Holographic Recording
   (2019) Optoelectronics and Advanced Materials 13 (11-12), 2019, p.576-579
   Link
   SNIP (2018)= 0,4

6. **Auzins, K.**, **Zolotarjovs, A.**, **Bite, I**., **Laganovska, K.**, **Vitola, V**., **Smits, K.**, **Millers, D.**
   Production of Phosphorescent Coatings on 6082 Aluminum Using Sr0.95Eu0.02Dy0.03Al2O4-δ Powder and Plasma Electrolytic Oxidation
   (2019) Plasma Electrolytic Oxidation (PEO) Coatings 2019, 9(12), 865
   DOI: 10.3390/coatings9120865

7. Oras, S., Vlassov. S.V., **Polyakov. B.**, Antsov, M., Lõhmus, R., Mougin, K.
   The effect of heat-treatment on morphology and mobility of Au nanoparticles
   (2019) Beilstein Archives (1), 68
   DOI: 10.3762/bxiv.2019.68.v1

8. **Kleperis, J.**, **Kristins, A., Veinbergs, J.**, **Gvardina, I.**, Viesturs, D., Rucins, A., Straumite, E., **Sloka, B.**, Bruveris, J.
   Application of ozone in grain drying: autonomous sensor system construction and peculiarities
   (2019) Proceedings of the 9th International Scientific Conference Rural Development, 6 pages
   DOI: 10.15544/RD.2019.029

9. **Muktepavela, F**., **Maniks, J.**, **Zabels, R**., Gorokhova, E.I., Rodnyi, P.
Nanoindentation study of ZnO, ZnO:In, Zn:Ga scintillation ceramics
(2019) Proc. International Conference "Promising materials and technologies", May 27-31, Brest, Belarus, p.532-534
Link

10. **Einbergs, E.**, **Zolotarjovs, A**., **Bite, I.**, **Laganovska, K.**, **Auzins, K.**, **Smits, K., Trinkler, L.**
Usability of Cr-Doped Alumina in Dosimetry
(2019) Ceramics, 2, 525-535
DOI: 10.3390/ceramics2030040

11. **Vembris, A.**, **Pervenecka, J**., Zarins, E., Siltane, K., Kokars, V.
Light Amplification Properties of Pyraniliden 2-cyano-2-(4H-pyran-4-ylidene) Acetate Group Containing Molecular Glasses
(2019) Optics, Photonics and Lasers (OPAL 2019), Page 32-33
Link

12. Paulsone, P., Zarins, E., Lazdovica, K., Kokars, V., **Vembris, A**.
Investigation of Amplified Spontaneous Emission in Neat Thin Films of Glass Forming Pyranyliden Derivatives
(2019) Optics, Photonics and Lasers (OPAL 2019), Page 42-43
Link

13. **Lesina, N.**, Traskovskis, K., Ruduss, A., Kokars, V., **Mihailovs, I., Vembris, A.**
Electroluminescence Properties of Glass Forming Iridium (III) Complexes
(2019) Optics, Photonics and Lasers (OPAL 2019), Page 44-45
Link

14. **Pervenecka, J., Vembris, A.**, E. Zarins, E., Kokars, V.
Investigation of Photoluminescence and Amplified Spontaneous Emission Properties of Cyanoacetic Acid Derivative (KTB) in Polysulfone (PSU) Amorphous Thin Films
(2019) Optics, Photonics and Lasers (OPAL 2019), Page 62-63
Link

15. **Bundulis, A., Rutkis, M**.
Study of Nonlinear Optical Properties of Novel Indandion Derivatives
(2019) Optics, Photonics and Lasers (OPAL 2019), Page 34-36
Link

16. **Berzina. B., Trinklere L., Korsaks V.,** Ruska R., **Krieke G., Sarakovskis A.**
F-center Luminescence and Oxygen Gas Sensing Properties of AlN Nanoparticles
(2019) Sensors & Transducers, 238, 11, pp. 87-93
Link

17. **Karitans, V., Nitiss, E., Tokmakovs, A.**
Wavefront Recovery: Shack-Hartmann Aberrometry vs PhaseLift Using a Single Binary Amplitude Modulating Mask
(2019) Imaging and Applied Optics, JW2A.13
DOI: 10.1364/COSI.2019.JW2A.13

18. **Kuzmin, A.**
Solid state physics: solving the structure of materials with X-ray absorption spectroscopy
(2019) SciTech Europa Quarterly 31, 78-80
Link

19. Comp. **Kleperis, J.**
Nanostructured Composite Materials for Energy Storage and Conversion
(2019) University of Latvia Academic Publishing, pages 157
DOI: 10.22364/ncmesc

Theses 2019

PhD Theses

No.	Author	Title	Supervisor	Degree
1.	Kaspars Pudžs	Study of electrical and thermoelectrical properties of organic thin films with different morphology	Dr. phys. A. Vembris	Dr. phys.
2.	Raitis Gržibovskis	Requirements for energy level determination of organic materials using photoelectron yield spectroscopy and scanning Kelvin probe	Dr. phys . A. Vembris	Dr. phys.
3.	Virgīnija Vītola	Electronic excitations and processes in long lasting luminescence material $SrAl_2O_4$	Dr. phys. K. Šmits	Dr. phys.

M.Sc. Theses

No.	Author	Title	Supervisor	Study programme
1.	Marta Kāne	Stability of sulfonated poly(ether ether ketone) and ionic liquid composite membranes in electrolyte water solutions	Dr. chem. G. Vaivars	chemistry
2.	Deniss Fedorenko	Investigation of properties of SPEEK composite membranes for application in electrochemical CO_2 converters	Dr. chem. G. Vaivars	chemistry
3.	Elza Lina Linina	Poling dynamics of an EO active material using parallel –plate electrodes	Dr. phys M. Rutkis	physics

B.Sc. Theses

No.	Author	Title	Supervisor	Study programme
1.	Jēkabs Cīrulis	Temperature dependent gadolinium ion incorporation in calcium fluoride nano/micro-particles	Dr. phys. A. Antuzēvičs	physics
2.	Normunds Strautnieks	Study of P3HT thin film properties for 3D printed thermoelectric device application	Dr. phys. K. Pudžs	physics
3.	Ernests Einbergs	Usability of chrome doped alumina in dosimetry	M. Sc. A. Zolotarjovs	physics
4.	Krišjānis Roze	Optical properties of fluorine activated and alkali metal doped silicon dioxide	M. Sc. K. Laganovska	physics
5.	Miks Jurjāns	Electromechanical properties of pure and doped sodium bismuth titanate	Dr. phys. Ē. Birks	physics
6.	Edgars Straumanis	Software development for determining elementary processes from experimental data	M. Sc. A. Zolotarjovs	computer science
7.	Madara Leimane	Influence of alkali metals on the optical properties of amorphous silicon dioxide	M. Sc. I. Bite	chemistry
8.	Karīna Taranda	Synthesis of inactivated and F-activated silicon dioxide nanoparticles	M. Sc. I. Bite	chemistry
9.	Viktorija Novikova	The dependence of glass transition temperature of sulfonated polyetheretherketone membranes on zirconia nanoparticle additives	Dr. chem. G. Vaivars	chemistry